

AD-A151 464

AFWAL-TR-84-2104



INFLUENCE OF FUEL PROPERTIES ON GAS TURBINE COMBUSTION PERFORMANCE

A. H. Lefebvre

Combustion Laboratory
Thermal Science and Propulsion Center
School of Mechanical Engineering
Purdue University
West Lafayette, Indiana 47907

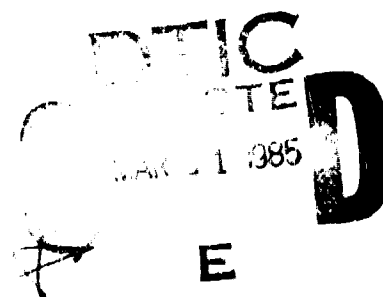
January 1985

Final Report for Period 3 January 1983 - 30 September 1984

Approved for public release; distribution unlimited.

DTIC FILE COPY

**AERO PROPULSION LABORATORY
AIR FORCE WRIGHT AERONAUTICAL LABORATORIES
AIR FORCE SYSTEMS COMMAND
WRIGHT-PATTERSON AFB, OH 45433-6563**



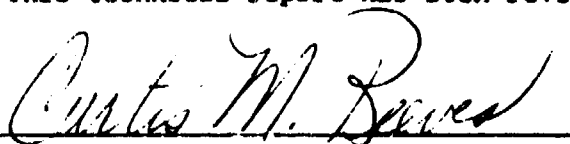
85 03 08 065

NOTICE

When Government drawings, specifications, or other data are used for any purpose other than in connection with a definitely related Government procurement operation the United States Government thereby incurs no responsibility nor any obligation whatsoever; and the fact that the government may have formulated, furnished, or in any way supplied the said drawings, specifications, or other data, is not to be regarded by implication or otherwise as in any manner licensing the holder or any other person or corporation, or conveying any rights or permission to manufacture use, or sell any patented invention that may in any way be related thereto.

This report has been reviewed by the Office of Public Affairs (ASD/PA) and is releasable to the National Technical Information Service (NTIS). At NTIS, it will be available to the general public, including foreign nations.

This technical report has been reviewed and is approved for publication.



CURTIS M. REEVES
Project Engineer
Fuels Branch
Fuels and Lubrication Division



ARTHUR V. CHURCHILL, Chief
Fuels Branch
Fuels and Lubrication Division

FOR THE COMMANDER



ROBERT D. SHERRILL, Chief
Fuels and Lubrication Division
Aero Propulsion Laboratory

"If your address has changed, if you wish to be removed from our mailing list, or if the addressee is no longer employed by your organization please notify AFWAL/POSF, W-PAFB, OH 45433 to help us maintain a current mailing list".

Copies of this report should not be returned unless return is required by security considerations, contractual obligations, or notice on a specific document.

UNCLASSIFIED

SECURITY CLASSIFICATION OF THIS PAGE

REPORT DOCUMENTATION PAGE

1a. REPORT SECURITY CLASSIFICATION UNCLASSIFIED			1b. RESTRICTIVE MARKINGS	
2a. SECURITY CLASSIFICATION AUTHORITY			3. DISTRIBUTION/AVAILABILITY OF REPORT Approved for Public Release; Distribution Unlimited	
2b. DECLASSIFICATION/DOWNGRADING SCHEDULE				
4. PERFORMING ORGANIZATION REPORT NUMBER(S) N/A			5. MONITORING ORGANIZATION REPORT NUMBER(S) AFWAL-TR-84-2104	
6a. NAME OF PERFORMING ORGANIZATION School of Mechanical Engineering, Purdue University		6b. OFFICE SYMBOL (If applicable) N/A		7a. NAME OF MONITORING ORGANIZATION Aero Propulsion Laboratory (AFWAL/PGS) Air Force Wright Aeronautical Laboratories, AFSC
6c. ADDRESS (City, State and ZIP Code) West Lafayette IN 47907			7b. ADDRESS (City, State and ZIP Code) Wright-Patterson Air Force Base OH 45433-6563	
8a. NAME OF FUNDING/SPONSORING ORGANIZATION Aero Propulsion Laboratory USAF		8b. OFFICE SYMBOL (If applicable) AFWAL/POSF		9. PROCUREMENT INSTRUMENT IDENTIFICATION NUMBER F33615-81-C-2067
8c. ADDRESS (City, State and ZIP Code) Wright-Patterson Air Force Base OH 45433-6563			10. SOURCE OF FUNDING NOS.	
			PROGRAM ELEMENT NO 62203F	PROJECT NO 3048
			TASK NO 05	WORK UNIT NO 13
11. TITLE (Include Security Classification) INFLUENCE OF FUEL PROPERTIES ON GAS TURBINE COMBUSTION PERFORMANCE				
12. PERSONAL AUTHOR(S) A.H. Lefebvre				
13a. TYPE OF REPORT Summary Technical Rpt.		13b. TIME COVERED FROM 3Jan83 TO 30Sep84		14. DATE OF REPORT (Yr., Mo., Day) January 1985
15. PAGE COUNT 143				
16. SUPPLEMENTARY NOTATION				
17. COSATI CODES			18. SUBJECT TERMS (Continue on reverse if necessary and identify by block number)	
FIELD	GROUP	SUB GR		
21	02	-	Fuels Exhaust Emissions Lean Blow Out	
21	04	-	Alternative Fuels Fuel Atomization Ignition	
21	04	-	Gas Turbine Comb. Comb. Efficiency Liner Wall Temperature	
19. ABSTRACT (Continue on reverse if necessary and identify by block number)				
<p>Results of an analytical and experimental program to determine the effects of broad variations in fuel properties on the performance, emissions, and durability of several prominent turbojet engine combustion systems, including both tubo-annular and annular configurations, are presented. Measurements of mean drop size conducted at representative engine operating conditions are used to supplement the available experimental data on the effects of combustor design parameters, combustor operating conditions, and fuel type, on combustion efficiency, lean blowout limits, lean lightoff limits, liner wall temperatures, pattern factor, and pollutant emissions.</p> <p>The results of the study indicate that the fuel's physical properties that govern atomization quality and evaporation rates strongly affect combustion efficiency, weak extinction limits, and lean lightoff limits. The influence of fuel chemistry on these performance parameters is quite small.</p> <p>Analysis of the experimental data shows that fuel chemistry has a significant effect</p>				
20. DISTRIBUTION/AVAILABILITY OF ABSTRACT UNCLASSIFIED/UNLIMITED <input checked="" type="checkbox"/> SAME AS RPT <input type="checkbox"/> DTIC USERS <input type="checkbox"/>			21. ABSTRACT SECURITY CLASSIFICATION UNCLASSIFIED	
22a. NAME OF RESPONSIBLE INDIVIDUAL CURTIS M. REEVES			22b. TELEPHONE NUMBER (Include Area Code) (513) 255-3524	22c. OFFICE SYMBOL AFWAL/POSF

DD FORM 1473, 83 APR

EDITION OF 1 JAN 73 IS OBSOLETE

UNCLASSIFIED
SECURITY CLASSIFICATION OF THIS PAGE

UNCLASSIFIED

SECURITY CLASSIFICATION OF THIS PAGE

Block 18 (cont):

Pattern Factor
Sauter Mean Diameter

Block 19 (cont):

on flame emissivity, flame radiation, and liner wall temperature, but its influence on the emissions of carbon monoxide, unburned hydrocarbons, and oxides of nitrogen, is small.

Smoke emissions are found to be strongly dependent on combustion pressure, primary-zone fuel/air ratio, and the mode of fuel injection (pressure atomization or airblast). Fuel chemistry, as indicated by hydrogen content, is also important.

At the high power conditions where the durability of hot section components is of major concern, the influence of fuel type on pattern factor is shown to be negligibly small.

Equations are presented for the correlation and/or prediction of several key aspects of combustion performance, including combustion efficiency, weak extinction limits, lean lightoff limits, pattern factor, and exhaust emissions, in terms of combustor size, combustor geometry, engine operating conditions, fuel spray characteristics, and fuel type.

UNCLASSIFIED

SECURITY CLASSIFICATION OF THIS PAGE

FOREWORD

This final report is submitted by the Combustion Laboratory of the Thermal Science and Propulsion Center, School of Mechanical Engineering, Purdue University. The report documents work conducted under Contract No. F33615-81-C-2067 during the period 3 January 1983 to 30 September 1984. Program sponsorship and guidance were provided by the Fuels Branch of the Aero Propulsion Laboratory (APL), Air Force Wright Aeronautical Laboratories, Wright-Patterson Air Force Base, Ohio. The Air Force Technical Monitor employed on this program was Mr Curtis M. Reeves.

Accession For	
NTIS GRA&I	<input checked="checked" type="checkbox"/>
DTIC TAB	<input type="checkbox"/>
Unannounced	<input type="checkbox"/>
Justification	
By	
Distribution/	
Availability Codes	
Dist	Avail and/or Special
A-1	

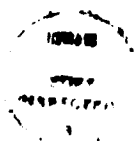


TABLE OF CONTENTS

SECTION	PAGE
I. INTRODUCTION	1
II. FUEL ATOMIZATION	7
III. COMBUSTION EFFICIENCY	25
IV. LEAN BLOWOUT	39
V. IGNITION	53
VI. LINER WALL TEMPERATURE	63
1. Internal Radiation	64
2. External Radiation	65
3. Internal Convection	65
4. External Convection	66
VII. POLLUTANT EMISSIONS	73
1. Oxides of Nitrogen	75
2. Carbon Monoxide	76
3. Unburned Hydrocarbons	94
4. Smoke	95
VIII. PATTERN FACTOR	117
IX. DISCUSSION AND SUMMARY	125
1. Combustion Efficiency	125
2. Lean Blowout	126
3. Lean Lightup	127
4. Liner Wall Temperature	128
5. NO _x Emissions	129
6. CO _x Emissions	129
7. Unburned Hydrocarbons	130
8. Smoke	130
9. Pattern Factor	131
X. CONCLUSIONS	133
XI. REFERENCES	136
XII. LIST OF SYMBOLS	145

LIST OF ILLUSTRATIONS

FIGURE	PAGE
1. Distillation Characteristics of Test Fuels.	5
2. Schematic Diagram of Spray Test Rig.	9
3. Mean Drop Sizes Obtained for J79-17A Fuel Nozzle.	14
4. Mean Drop Sizes Obtained for J79-17C Fuel Nozzle.	15
5. Mean Drop Sizes Obtained for F101 Fuel Nozzle.	16
6. Mean Drop Sizes Obtained for TF39 Fuel Nozzle.	17
7. Mean Drop Sizes Obtained for J85 Fuel Nozzle.	18
8. Mean Drop Sizes Obtained for J85 Fuel Nozzle.	19
9. Influence of Ambient Air Density and Atomizer Air/Fuel Ratio on SMD for F100 Fuel Nozzle.	20
10. Influence of Atomizer Air/Fuel Ratio and Pressure Drop on SMD for F100 Fuel Nozzle.	21
11. Variation of Effective Evaporation Constant with Normal Boiling Point at a Pressure of 100 kPa.	27
12. Variation of Effective Evaporation Constant with Normal Boiling Point at a Pressure of 1000 kPa.	28
13. Variation of Effective Evaporation Constant with Normal Boiling Point at a Pressure of 2000 kPa.	29
14. Comparison of Measured and Predicted Values of Combustion Efficiency for J79-17A Combustor.	31
15. Comparison of Measured and Predicted Values of Combustion Efficiency for J79-17C Combustor.	32
16. Comparison of Measured and Predicted Values of Combustion Efficiency for F101 Combustor.	33
17. Comparison of Measured and Predicted Values of Combustion Efficiency for TF41 Combustor.	34
18. Comparison of Measured and Predicted Values of Combustion Efficiency for TF39 Combustor.	35
19. Comparison of Measured and Predicted Values of Combustion Efficiency for J85 Combustor.	36

20.	Comparison of Measured and Predicted Values of Combustion Efficiency for TF33 Combustor.	37
21.	Comparison of Measured and Predicted Values of Combustion Efficiency for F100 Combustor.	38
22.	Comparison of Measured and Predicted Values of Lean Blowout for J79-17A Combustor.	45
23.	Comparison of Measured and Predicted Values of Lean Blowout for J79-17A Combustor.	46
24.	Comparison of Measured and Predicted Values of Lean Blowout for J79-17C Combustor.	47
25.	Comparison of Measured and Predicted Values of Lean Blowout for J79-17C Combustor.	48
26.	Comparison of Measured and Predicted Values of Lean Blowout for F101 Combustor.	49
27.	Comparison of Measured and Predicted Values of Lean Blowout for TF39 Combustor.	50
28.	Comparison of Measured and Predicted Values of Lean Blowout for J85 Combustor.	51
29.	Comparison of Measured and Predicted Values of Lean Blowout for F100.	52
30.	Comparison of Measured and Predicted Values of Lean Light Off for J79-17A Combustor.	55
31.	Comparison of Measured and Predicted Values of Lean Light Off for J79-17A Combustor.	56
32.	Comparison of Measured and Predicted Values of Lean Light Off for J79-17C Combustor.	57
33.	Comparison of Measured and Predicted Values of Lean Light Off for J79-17C Combustor.	58
34.	Comparison of Measured and Predicted Values of Lean Light Off for F101 Combustor.	59
35.	Comparison of Measured and Predicted Values of Lean Light Off for TF39 Combustor.	60
36.	Comparison of Measured and Predicted Values of Lean Light Off for J85 Combustor.	61
37.	Comparison of Measured and Predicted Values of Lean Light Off for F100 Combustor.	62

38.	Comparison of Measured and Predicted Values on the Effect of H_2 Content on Liner Temperature for J79-17A Combustor.	68
39.	Comparison of Measured and Predicted Values on the Effect of H_2 Content on Liner Temperature for J79-17C Combustor.	69
40.	Comparison of Measured and Predicted Values on the Effect of H_2 Content on Liner Temperature for F101 Combustor.	70
41.	Comparison of Measured and Predicted Values on the Effect of H_2 Content on Liner Temperature for TF41 Combustor.	71
42.	Comparison of Measured and Predicted Values of NO_x Emissions for J79-17A Combustor.	77
43.	Comparison of Measured and Predicted Values of NO_x Emissions for J79-17A Combustor.	78
44.	Comparison of Measured and Predicted Values of NO_x Emissions for J79-17C Combustor.	79
45.	Comparison of Measured and Predicted Values of NO_x Emissions for J79-17C Combustor.	80
46.	Comparison of Measured and Predicted Values of NO_x Emissions for F101 Combustor.	81
47.	Comparison of Measured and Predicted Values of NO_x Emissions for F101 Combustor.	82
48.	Comparison of Measured and Predicted Values of NO_x Emissions for TF41 Combustor.	83
49.	Comparison of Measured and Predicted Values of NO_x Emissions for TF41 Combustor.	84
50.	Comparison of Measured and Predicted Values of NO_x Emissions for TF39 Combustor.	85
51.	Comparison of Measured and Predicted Values of NO_x Emissions for TF33 Combustor.	86
52.	Comparison of Measured and Predicted Values of NO_x Emissions for F100 Combustor.	87
53.	Comparison of Measured and Predicted Values of CO Emissions for J79-17A Combustor.	89
54.	Comparison of Measured and Predicted Values of CO	90

Emissions for J79-17C Combustor.

55.	Comparison of Measured and Predicted Values of CO Emissions for F101 Combustor.	91
56.	Comparison of Measured and Predicted Values of CO Emissions for TF41 Combustor.	92
57.	Comparison of Measured and Predicted Values of CO Emission for F100 Combustor.	93
58.	Comparison of Measured and Predicted Values of Unburned Hydrocarbons Emissions for J79-17A Combustor.	96
59.	Comparison of Measured and Predicted Values of Unburned Hydrocarbons Emissions for J79-17C Combustor.	97
60.	Comparison of Measured and Predicted Values of Unburned Hydrocarbons Emissions for J79-17C Combustor.	98
61.	Comparison of Measured and Predicted Values of Unburned Hydrocarbons Emissions for F101 Combustor.	99
62.	Comparison of Measured and Predicted Values of Unburned Hydrocarbons Emissions for TF41 Combustor.	100
63.	Comparison of Measured and Predicted Values of Unburned Hydrocarbons Emissions for TF41 Combustor.	101
64.	Graphs Illustrating Influence of Hydrogen Content and Engine Operating Conditions on Soot Emissions for J79-17A Combustor.	106
65.	Graphs Illustrating Influence of Hydrogen Content and Engine Operating Conditions on Soot Emissions for J79-17C Combustor.	107
66.	Graphs Illustrating Influence of Hydrogen Content and Engine Operating Conditions on Soot Emissions for F101 Combustor.	108
67.	Graphs Illustrating Influence of Hydrogen Content and Engine Operating Conditions on Soot Emissions for TF41 Combustor.	109
68.	Graphs Illustrating Influence of Hydrogen Content and Engine Operating Conditions on Soot Emissions for TF39 Combustor.	110
69.	Graphs Illustrating Influence of Hydrogen Content and Engine Operating Conditions on Soot Emissions for J85 Combustor.	111

70.	Graphs Illustrating Influence of Hydrogen Content and Engine Operating Conditions on Soot Emissions for TF33 Combustor.	112
71.	Graphs Illustrating Influence of Hydrogen Content and Engine Operating Conditions on Soot Emissions for F100 Combustor.	113
72.	Comparison of Measured and Predicted Values of Pattern Factor for J79-17A Combustor.	120
73.	Comparison of Measured and Predicted Values of Pattern Factor for J79-17C Combustor.	121
74.	Comparison of Measured and Predicted Values of Pattern Factor for TF41 Combustor.	122

LIST OF TABLES

TABLE	PAGE
1. Test Fuel Chemical and Physical Properties.	4
2. Values of A and B Employed in Equations (16) and (17).	43
3. Values of C_3 and C_4 Employed in Equation (34).	114

SECTION I

INTRODUCTION

For the gas turbine and, in fact, for most other forms of heat engines, the most important fuel issues of today are those of cost and availability. The measures now being taken to ensure future supplies of fuels for gas turbines, in addition to various forms of fuel conservation, include the exploitation of alternative fuel sources and the acceptance of a broader specification for aviation fuels. These developments highlight the need for prediction techniques that will allow the impact of any change in fuel specification on hardware durability and combustion performance to be estimated accurately in the combustor design stage. Unfortunately, the effect of a change in fuel properties is not constant for all combustors but varies between one combustor and another, due to differences in operating conditions and differences in design. An additional complicating factor is that the various properties and characteristics of petroleum fuels are so closely interrelated that it is virtually impossible to change any one property without affecting many others. However, there are several mitigating factors that help to ease the situation. One is that atomization quality is influenced only by the physical properties of the fuel; namely, viscosity and surface tension, both of which are easily measured by standard laboratory techniques. Evaporation rates are also closely linked to the physical properties of the fuel, for example, fuel density provides a useful indication of fuel volatility.

Further simplifications are possible because chemical reaction rates vary only slightly among the various hydrocarbon fuels of interest for the aircraft gas turbine. This is partly because these fuels exhibit only slight differences in adiabatic flame temperature, and also because before entering the true reaction zone, all the fuels are largely pyrolyzed to methane, other 1-2 carbon atom hydrocarbons, and hydrogen. Hence, the gas composition in the reaction zone is substantially independent of the parent fuel. Thus, provided the discussion is restricted to the anticipated range of aircraft fuels, any differences that occur in ignition performance, lean-blowout limits, and combustion efficiency, will be caused mainly by differences in the physical properties of the fuel insofar as they control the quality of atomization and the ensuing rate of evaporation.

During the past decade, the U.S. Air Force, Army, and Navy, along with NASA and the major engine manufacturers, have initiated a number of programs to determine the effects of anticipated future fuels on existing engines. As a result of these studies [1-6] a substantial body of data has become available that yields useful insights into fuel property effects on combustion performance.

In addition to a considerable body of evidence on the effects of fuel property variations on the combustion performance and durability characteristics of the combustors investigated, references 1 thru 6 also contain detailed information on all the relevant chemical and physical properties of the fuels employed.

These fuels were supplied by the U.S. Air Force for combustion system evaluation. They include normal JP4 and JP8, five blends of the JP4, five blends of the JP8 and, in some cases, a No. 2 diesel fuel. The blends were intended to achieve three different levels of hydrogen content; i.e. 12, 13, and 14 percent by mass. The key chemical and physical properties of these fuels are listed in Table 1. Additional information on the distillation characteristics of the test fuels is contained in Fig. 1.

A major drawback to the data contained in references 1 thru 6 is that they include very little information on fuel spray characteristics; in particular, no measurements were made of mean drop size (SMD) for any of the combustors employed in the investigation. In the absence of actual measured values of SMD, previous analytical studies of these data [7-9] had to rely on values of SMD as calculated from standard equations for the mean drop sizes produced by pressure-swirl and airblast atomizers [10]. A main objective of the present investigation was to remedy this deficiency by measuring the drop sizes produced by all the fuel nozzles employed in references 1 thru 6, simulating as far as possible the actual engine conditions of primary-zone gas density and fuel flow rate. While making these measurements, equipment problems prevented the acquisition of drop-size data for all the fuel nozzles of interest. However, sufficient measurements were made on several different types of fuel nozzles to provide the input needed to validate the analytically-derived equations for the correlation and prediction of experimental data

TABLE 1. Test Fuel Chemical and Physical Properties.

Reference				Fuel Components		Hydrogen Content H Weight %	Heating Value (net) MJ/kg	Density ρ 300 K kg/m ³	Viscosity ν 300 K mm ² /s	Surface Tension σ 300 K mN/m	Vapor Pressure P 300 K kPa
1	2	3	4	5	Base Fuel	Blending Agents					
1	1	1	1	1B, 1C	JP-4	-	43.603	752.7	0.924	23.27	12.04
2	2	7	2	2B1	JP-8	-	43.210	799.5	1.849	25.85	2.15
3	3	12	3	-	JP-8	Gulf Mineral Seal Oil	43.189	801.2	2.071	25.92	1.97
4	4	8	4	-	JP-8	2040 Solvent	41.947	852.3	1.809	27.62	1.16
5	5	11	5	-	JP-8	Xylene Bottoms	42.724	813.4	1.428	26.38	1.48
6	6	10	6	-	JP-8	Xylene Bottoms	42.129	827.6	1.160	26.66	1.33
7	7	9	7	-	JP-8	2040	42.556	825.2	1.804	26.42	1.38
8	8	2	8	8B, 8C	JP-4	2040	42.203	829.7	1.141	25.22	7.38
9	9	3	9	9B, 9C	JP-4	2040	42.629	796.3	1.028	23.75	8.61
10	10	4	10	-	JP-4	Xylene	42.196	808.0	0.830	25.21	6.17
11	11	5	11	-	JP-4	Xylene	42.682	786.5	0.835	24.20	9.06
12	12	6	12	-	JP-4	Xylene & GMSO	43.366	796.6	1.057	23.45	10.25
13	13	13	13	13B1, 13C	2-D	-	42.691	837.2	3.245	27.35	1.59

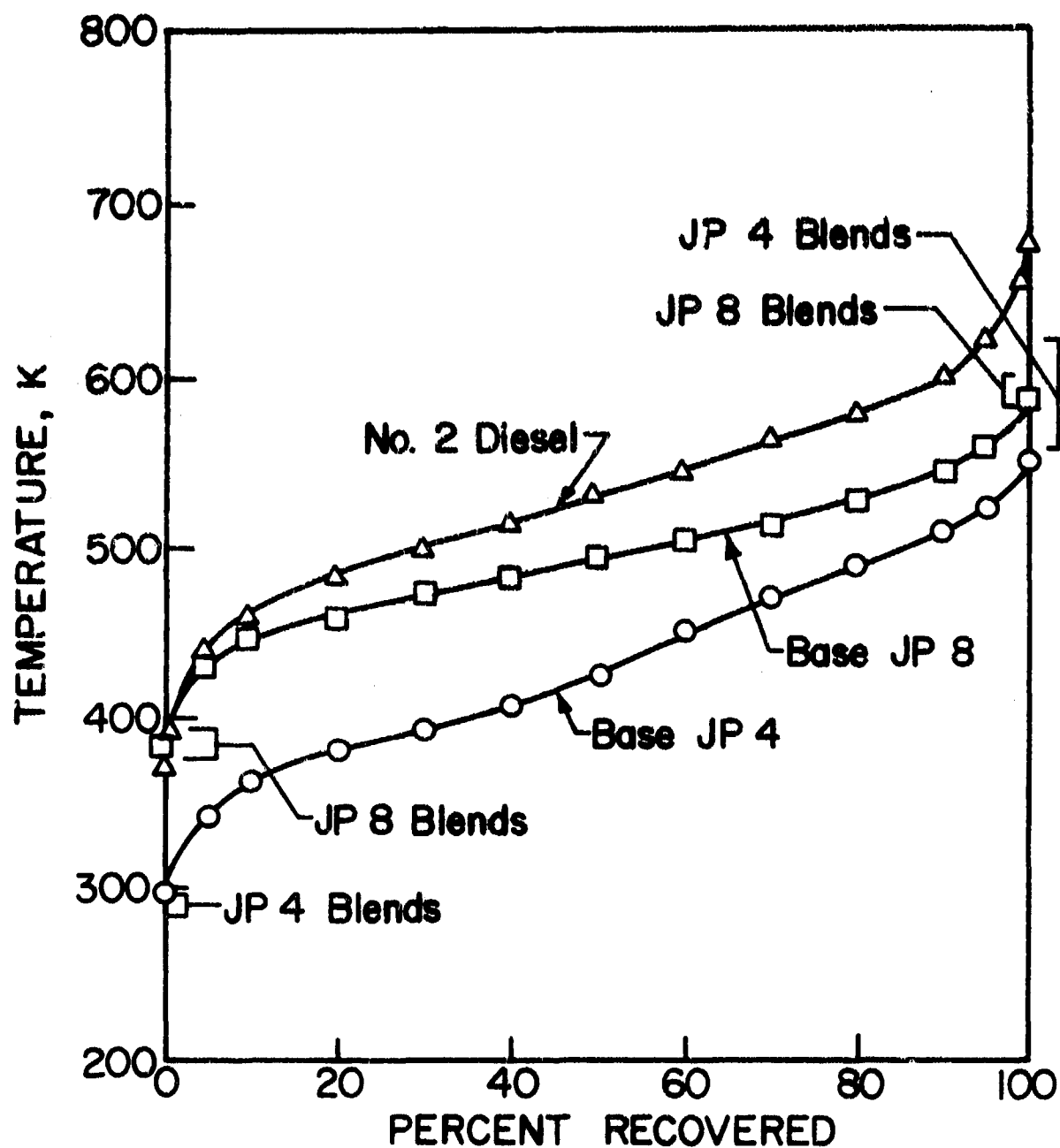


Figure 1. Distillation Characteristics of Test Fuels (Ref. 2).

on all the key aspects of gas turbine combustion performance.

The method used to measure spray characteristics and the results obtained are described in the next section. In subsequent sections the main combustor performance parameters are discussed in turn, following the style of presentation employed in reference 7. In each case, a brief outline is given of the methods employed in identifying the basic relationships between the relevant fuel properties and each individual aspect of performance. As liner wall temperatures and the emissions of oxides of nitrogen are not materially affected by spray characteristics the findings in regard to these remain unchanged from reference 7, and are included herein for completeness in a suitably reduced form.

For each performance parameter, the general approach has been either to enhance existing correlations or to replace them with new correlations that are based on a firmer scientific footing. It is hoped that the relationships developed in this program will make a useful contribution to future combustor designs.

SECTION II

FUEL ATOMIZATION

The quality of the experimental data contained in references 1 thru 6 is generally high. Although the main liner dimensions and airflow distribution are not always precisely defined, it is usually possible to deduce these parameters to an acceptable level of accuracy. Reliable information is lacking only in the area of fuel atomization. In a previous study [7] an attempt was made to overcome this deficiency by calculating SMD values using one of the following two expressions [8]:

For airblast atomizers

$$\frac{SMD}{D_h} = \left[1 + \frac{m_F}{m_A} \right] \left[0.33 \left[\frac{\sigma_F}{\rho_A U_A^2 D_p} \right]^{0.6} \left[\frac{\rho_F}{\rho_A} \right]^{0.1} + 0.068 \left[\frac{\mu_F^2}{\rho_F \sigma_F D_p} \right]^{0.5} \right] \quad (1)$$

For pressure swirl atomizers

$$SMD = 7.1 \times 10^4 \sigma_F^{0.25} \nu_F^{0.25} m_F^{0.25} \Delta P_F^{-0.5} \rho_g^{-0.25} \quad (2)$$

These equations take full account of variations in fuel properties (σ_F , ρ_F , ν_F , μ_F), air properties (ρ_A and U_A), and atomizer geometry (D_p and D_h). However, they do have certain defects. For example, Eq. (2), and all other published SMD equations for pressure swirl nozzles, are based almost entirely on measurements carried out in quiescent air at normal atmospheric pressure and temperature. For airblast atomizers the prefilmer diameter, D_p , and the hydraulic mean diameter of the air discharge orifice, D_h ,

are often difficult to measure and, in some cases, difficult to define. Usually they can only be established for any given atomizer by carrying out measurements of SMD at some convenient test condition. After inserting these values into Eq. (1) it can then be used to predict values of mean drop size at other operating conditions.

The lack of measured SMD values in references 1 thru 6 is rendered more serious by the fact that in many performance equations, for example the equations for predicting lean lightoff and lean blowout limits, the mean drop size appears as SMD squared. Thus, the magnitude of any errors in the estimation of SMD are effectively squared. In a previous study [7] these errors were minimized by replacing the absolute values of SMD in these equations with values expressed relative to the drop sizes obtained with the baseline fuel, JP4. This helped to compensate for the lack of information on nozzle characteristic dimensions, but it also diminished the practical utility of the resulting equations. In order to remedy this deficiency it was decided at the outset of the present study to measure the drop sizes produced by all the fuel nozzles described in references 1 thru 6. The apparatus employed for drop-size measurement is shown schematically in Fig. 2. The main component is a cylindrical pressure vessel which is mounted on a stand with its axis in the vertical position. It is 120 cm long and 75 cm in diameter. The atomizer under test is located centrally at the top of the cylinder and sprays downward into the vessel which is pressurized to the desired level using

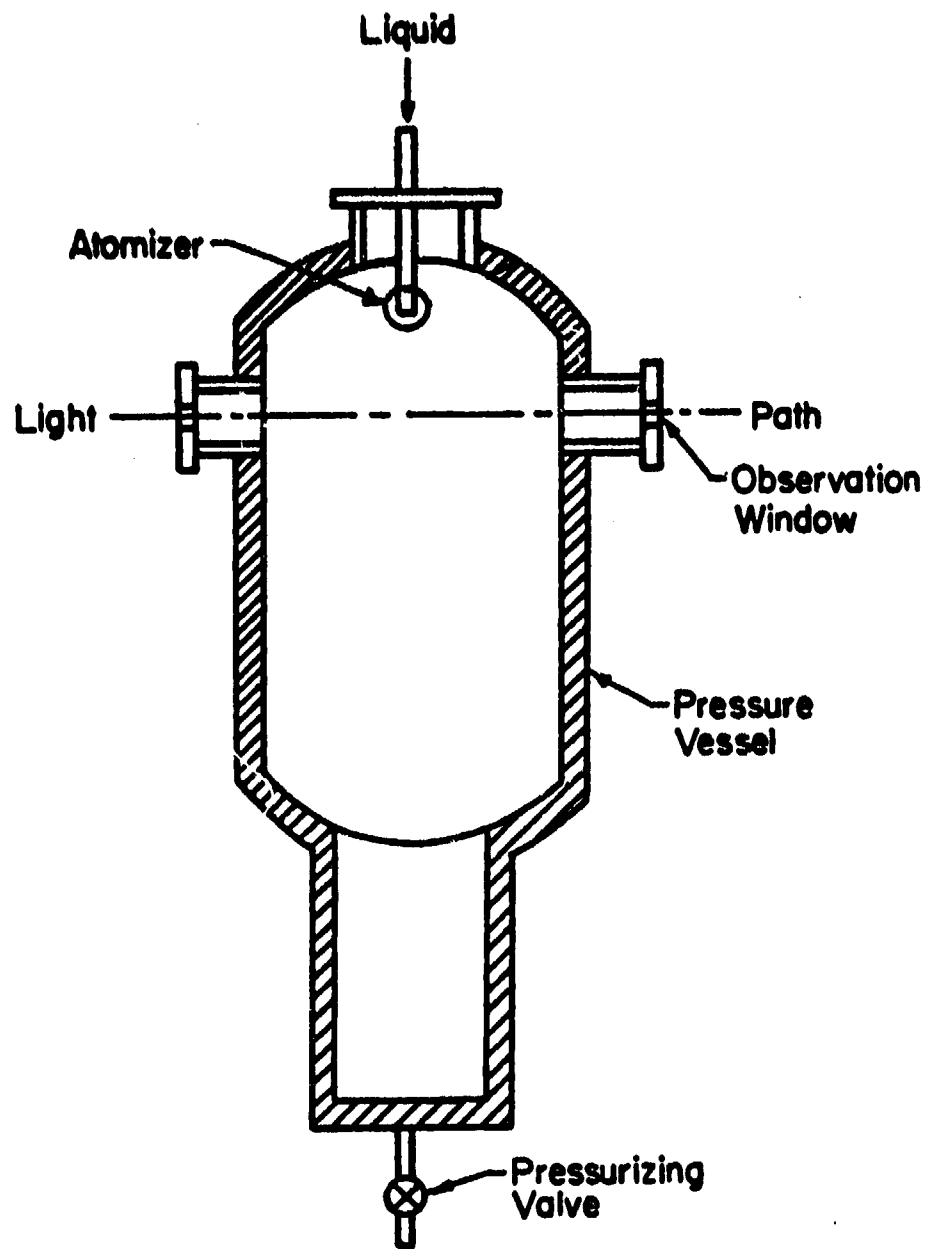


Figure 2. Schematic Diagram of Spray Test Rig.

gaseous nitrogen that is tapped from a large liquid nitrogen storage/evaporator system. The reason for using nitrogen instead of air is to avoid the risk of explosion at high pressures. As the physical properties of nitrogen are very similar to those of air the results obtained with nitrogen are considered valid for systems using air. The droplets produced by atomization gravitate into a collection tank at the bottom of the chamber, from whence the fuel is returned to the storage tank. The objective is to conserve fuel and to avoid potential pollution of the atmosphere due to escaping fuel droplets.

In addition to the nitrogen supplies for atomization and tank pressurization two extra nitrogen lines are connected to the tank. One line is used to protect the windows from any contamination by fuel drops or mist, while the other line is connected to a manifold located at the top of the tank which provides a gentle downdraft of nitrogen through a large number of holes. By this means the problem of droplet recirculation is kept to a minimum.

Drop sizes were measured using the light-scattering technique first proposed by Dobbins, Crocco, and Glassman [11] and later developed at Cranfield [12]. It is based on a direct measurement of the scattered light intensity profile after a monochromatic light beam has passed through the spray. The SMD is obtained directly from measurement of intensity versus radius in the focal plane of the receiving lens. In practice, this is

accomplished by measuring the traverse distance (r) between the optical axis and a point on the profile at which the light intensity is equal to one-tenth of the normalized intensity in the scattered profile. The SMD of the spray can then be determined using the relationship between r and SMD as derived by Roberts and Webb [13].

When using the light-scattering technique or, in fact, any other optical technique for drop-size measurement, it is important not to attempt measurements of mean drop size too close to the nozzle. This is because although all the drops leave the nozzle with approximately the same velocity, the smaller drops tend to lose momentum faster than the larger drops, due to air resistance, which leads to over-representation of the fine drops in the sampling volume. Further away from the nozzle, where all the drops are moving at roughly the same velocity as the down-draft of nitrogen, the measurements indicate larger values of SMD which are more representative of the actual spray. However, it is equally important not to attempt to measure drop sizes too far downstream of the nozzle as this could introduce errors due to fuel spray evaporation. Calculations indicate an ideal distance of 15 cm for the conditions of the present experiments, and this is the value actually used.

Due to the considerable time and effort that would be required to make detailed measurements of spray characteristics for all nozzles and all fuels, it was decided to conduct all measurements using one fuel only, and then to use these measured

values to estimate the corresponding mean drop sizes for all other fuels. The fuel selected for detailed study was aviation kerosine (Jet A), which has the following physical properties.

$$\sigma = 0.02767 \text{ kg/s}^2, \mu = 0.00129 \text{ kg/ms}, \rho = 784 \text{ kg/m}^3$$

As fuel density has only a very slight effect on atomization quality, consideration need be given only to surface tension and viscosity. For pressure atomizers Eq. (2) suggests that SMD is proportional to $\mu^{0.25}$, but some preliminary measurements of SMD carried out on JP4 and DF2 fuels (representing the two extremes of viscosity) indicated a slightly lower viscosity dependence so that for pressure atomizers we have

$$\text{SMD} \propto \sigma^{0.25} \mu^{0.20} \quad (3)$$

For airblast atomizers, which are characterized by a slightly higher dependence on surface tension and a lower dependence on viscosity [10], it is found that changes in SMD arising from variations in fuel type can be expressed to a sufficient degree of accuracy by the relationship

$$\text{SMD} \propto \sigma^{0.35} \mu^{0.05} \quad (4)$$

Thus, for any given atomizer, if measured values of SMD are available for one fuel, then Eqs. (3) and (4) allow mean drop sizes to be calculated for any other fuel, provided of course its physical properties of surface tension and viscosity are known. For the fuels of interest to the present study, mean drop sizes for all operating conditions of fuel flow rate and ambient air

density were obtained using the measured values of SMD for Jet A fuel, in conjunction with one of the following two expressions.

For pressure-swirl atomizers

$$SMD_F = SMD_{\text{Jet A}} (\sigma_F / \sigma_{\text{Jet A}})^{0.25} (\mu_F / \mu_{\text{Jet A}})^{0.20} \quad (5)$$

For airblast atomizers

$$SMD_F = SMD_{\text{Jet A}} (\sigma_F / \sigma_{\text{Jet A}})^{0.35} (\mu_F / \mu_{\text{Jet A}})^{0.05} \quad (6)$$

The SMD data obtained for the J79-17A, J79-17C, F101, TF39, J85 and F100 fuel nozzles, using Jet A fuel, are shown plotted in Figs. 3 thru 10. Due to the difficulties encountered in the procurement of an F101 fuel nozzle of the type employed in the F101 combustion program [2], it was decided to substitute a more recent version for the atomization tests. As these two types of nozzles differ mainly in regard to fuel distribution characteristics rather than atomization quality, it is believed that no significant error was introduced by this substitution. Due to equipment problems and time restraints, no results were obtained for the TF41 and TF33 fuel nozzles. Thus for these nozzles, SMD values were calculated using Eq. (2).

The SMD data contained in Figs. 3 thru 10 are presented mainly as plots of SMD versus fuel flow rate, \dot{m}_F , for various values of ambient air density, ρ_A , but for the F100 nozzle the SMD values are plotted against AFR in order to demonstrate the effects of air/fuel ratio and liner pressure drop on mean drop size. Not surprisingly, Fig. 10 indicates that atomization

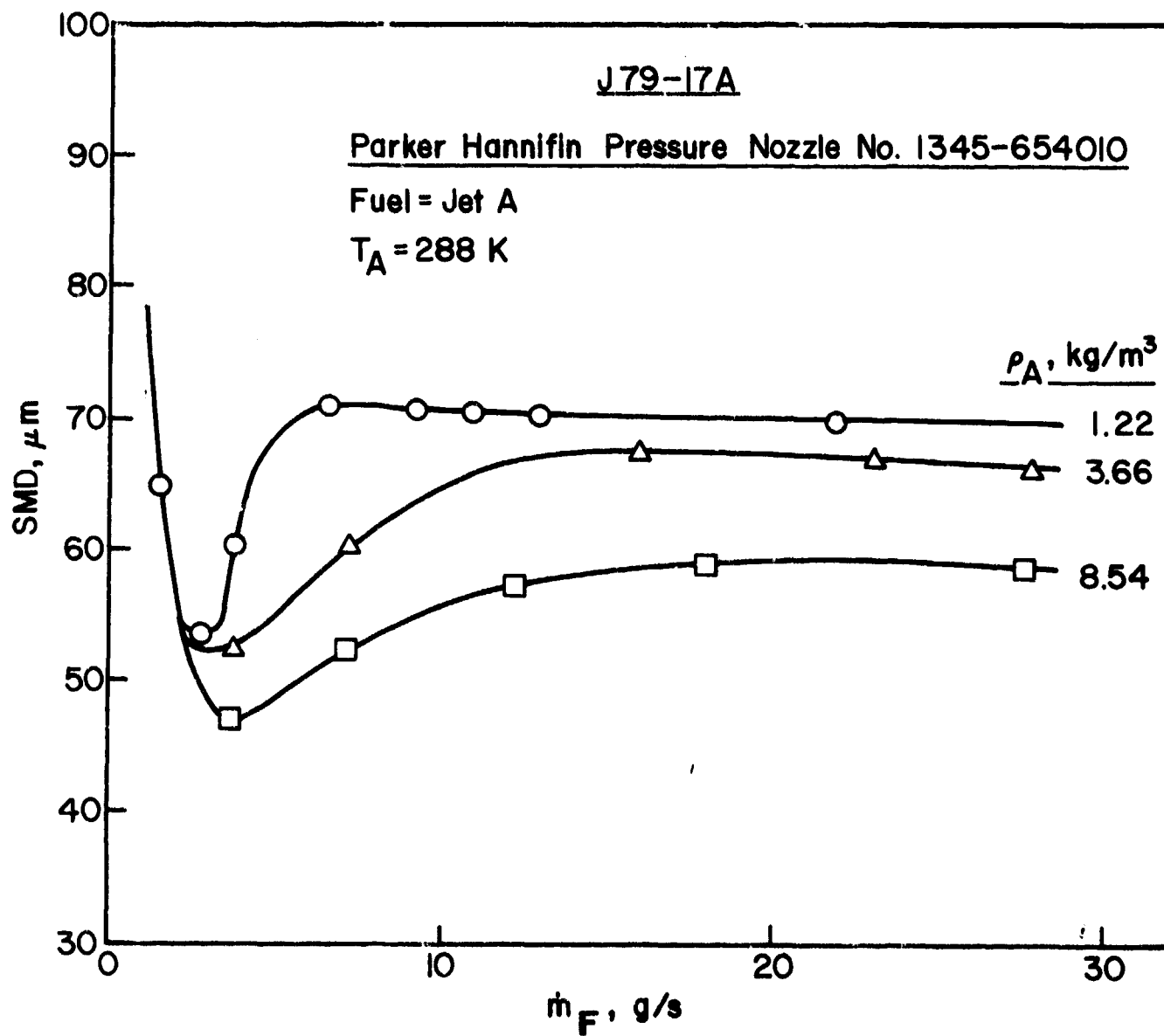


Figure 3. Mean Drop Sizes obtained for J79-17A Fuel Nozzle.

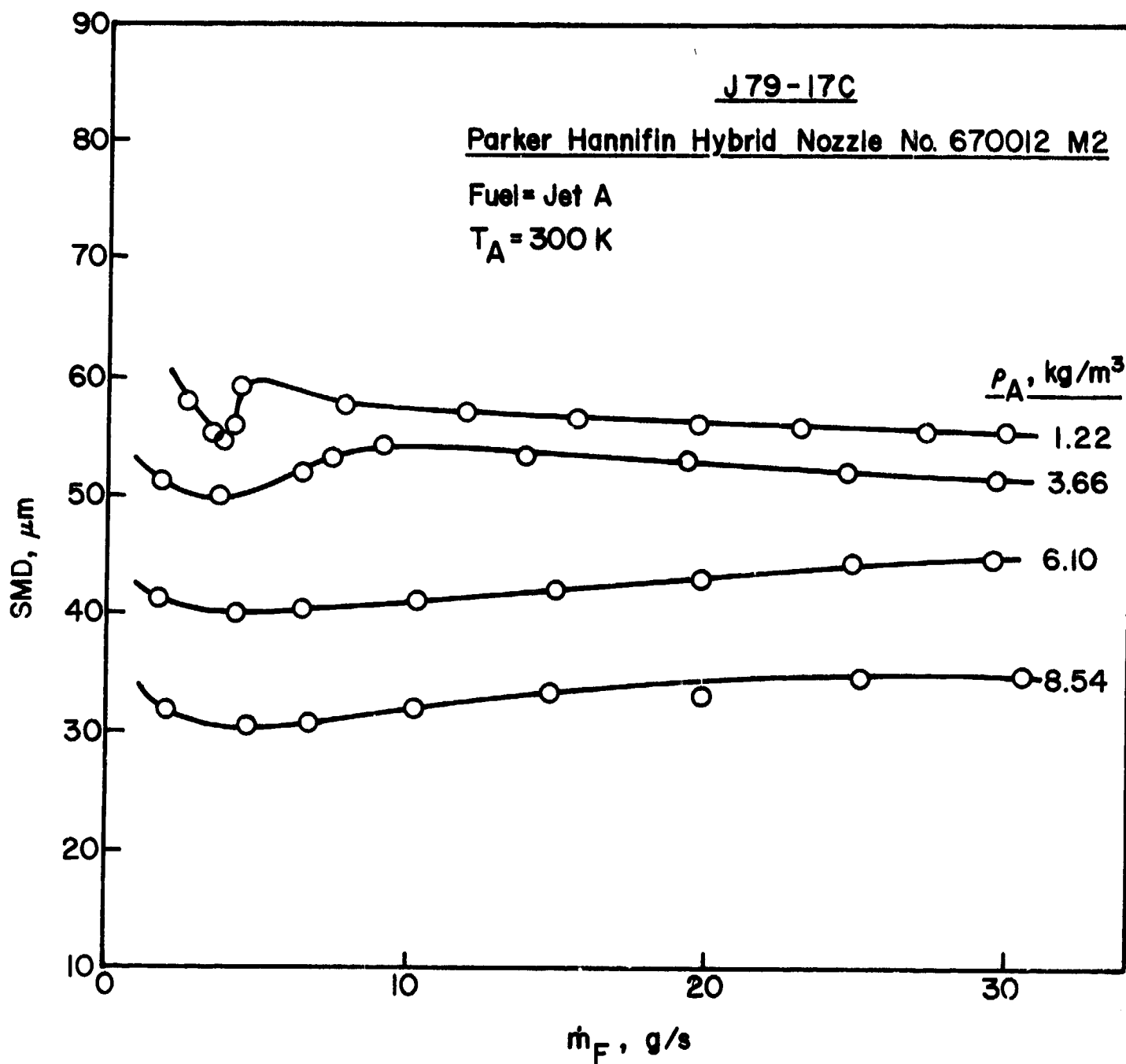


Figure 4. Mean Drop Sizes obtained for J79-17C Fuel Nozzle.

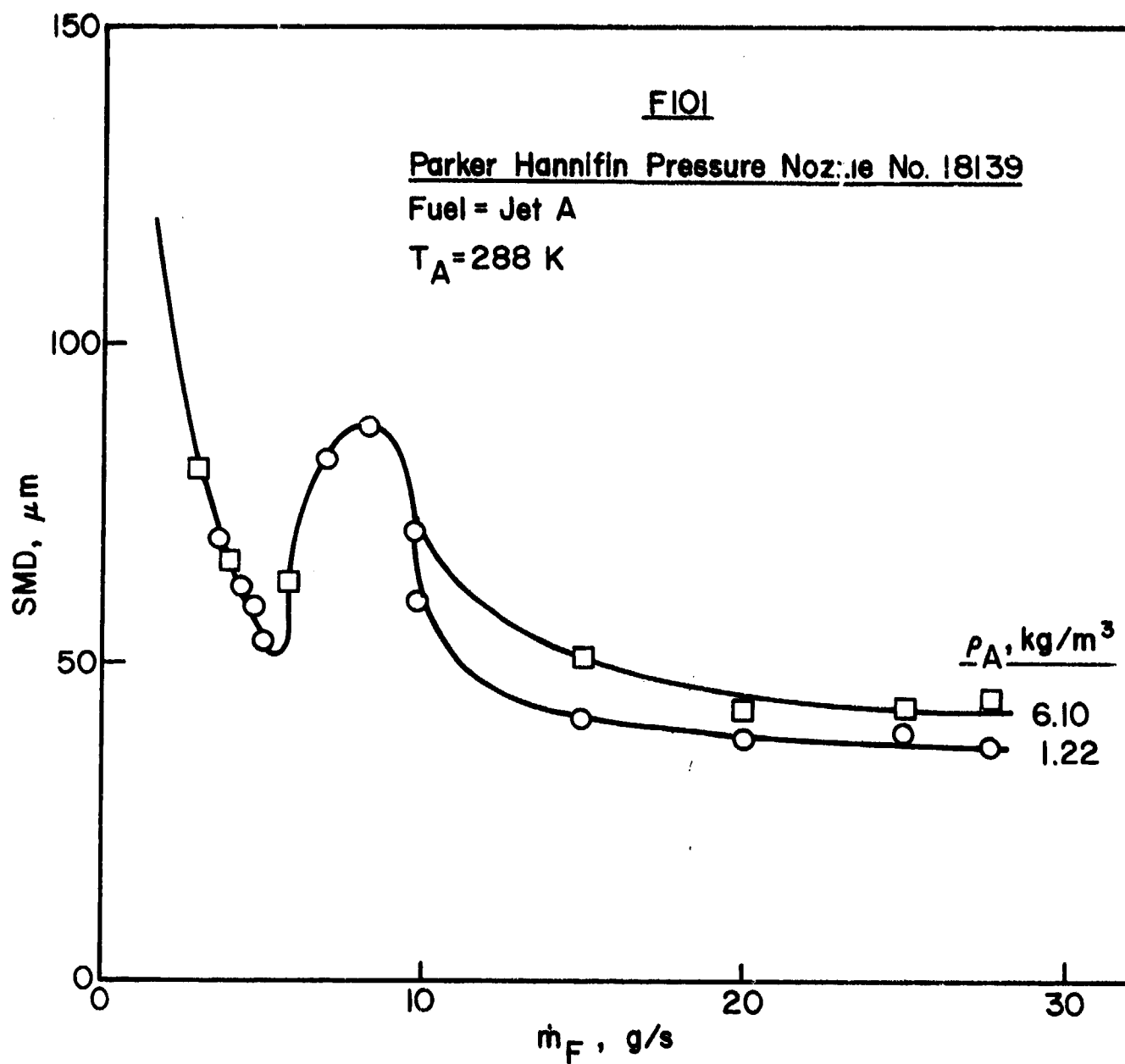


Figure 5. Mean Drop Sizes obtained for F101 Fuel Nozzle.

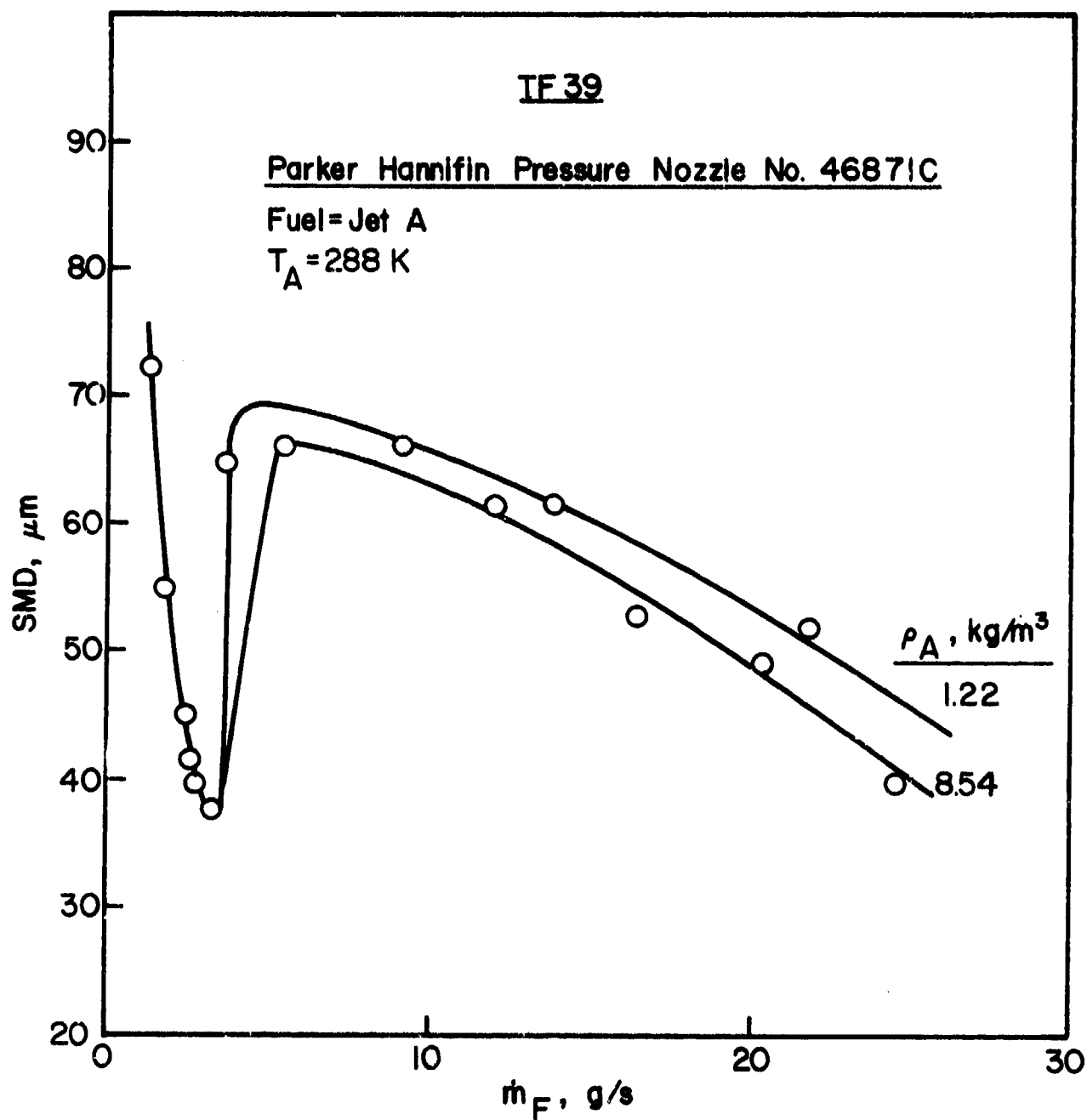


Figure 6. Mean Drop Sizes obtained for TF39 Fuel Nozzle.

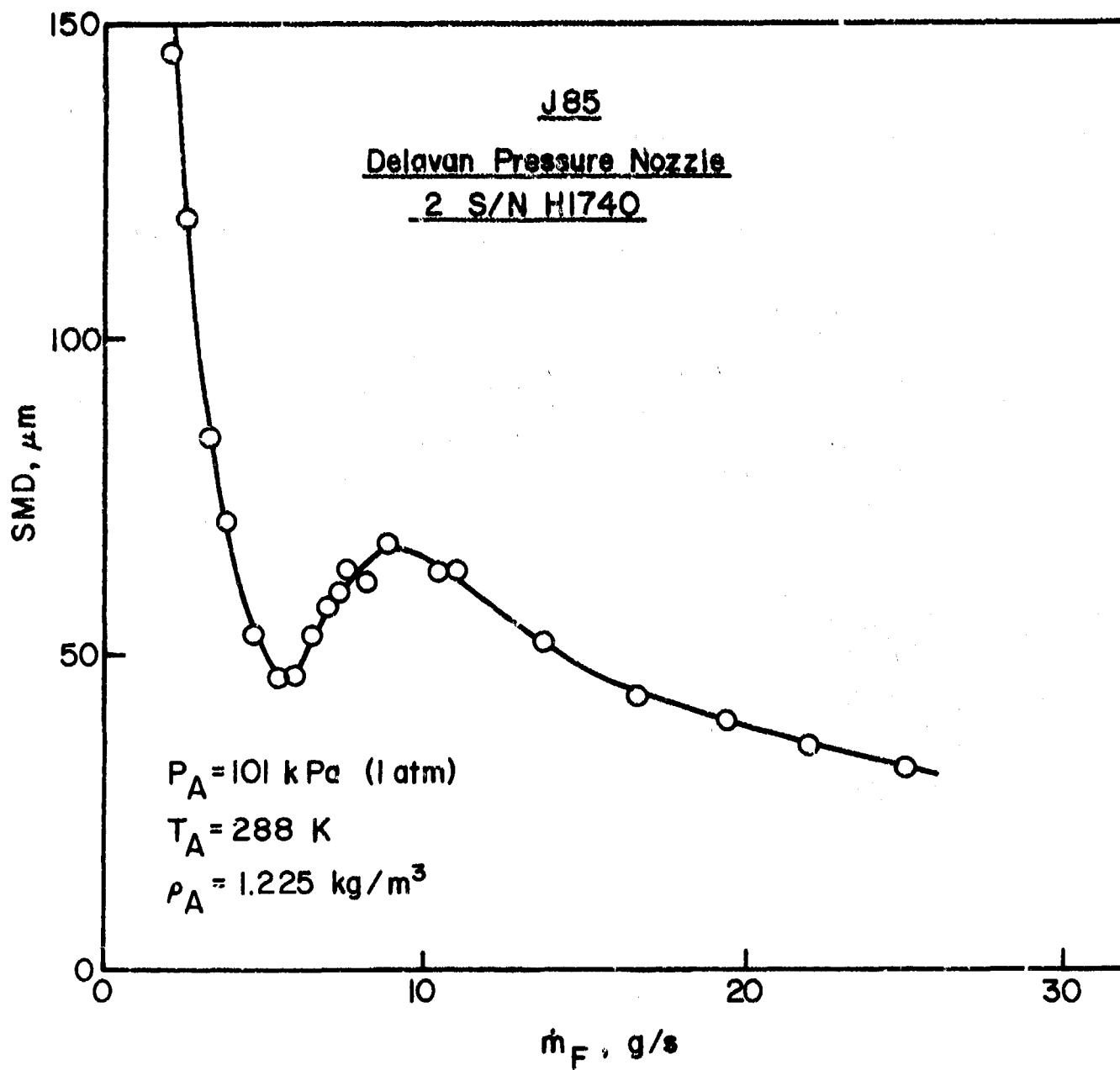


Figure 7. Mean Drop Sizes obtained for J85 Fuel Nozzle.

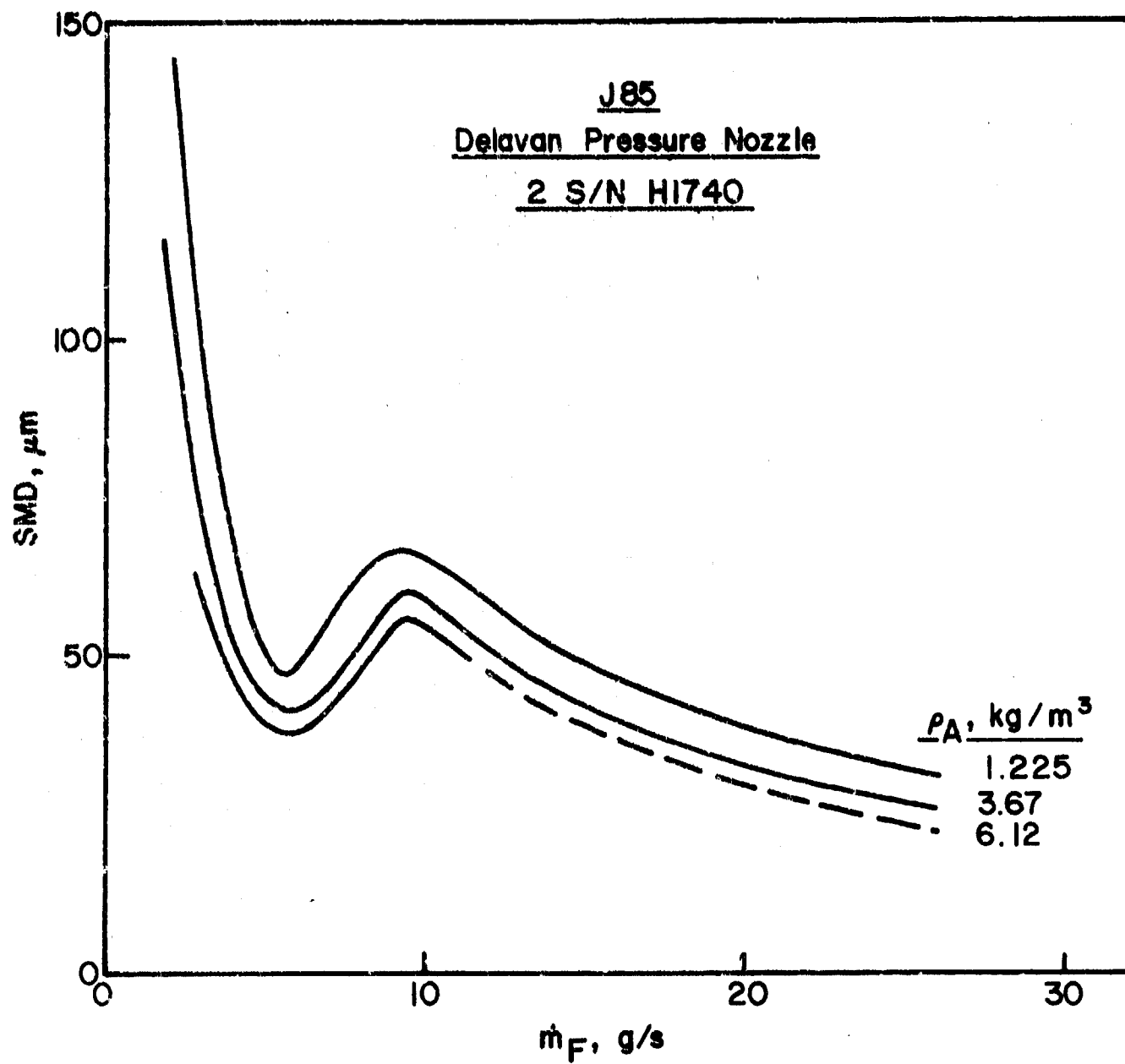


Figure 8. Mean Drop Sizes obtained for J85 Fuel Nozzle.

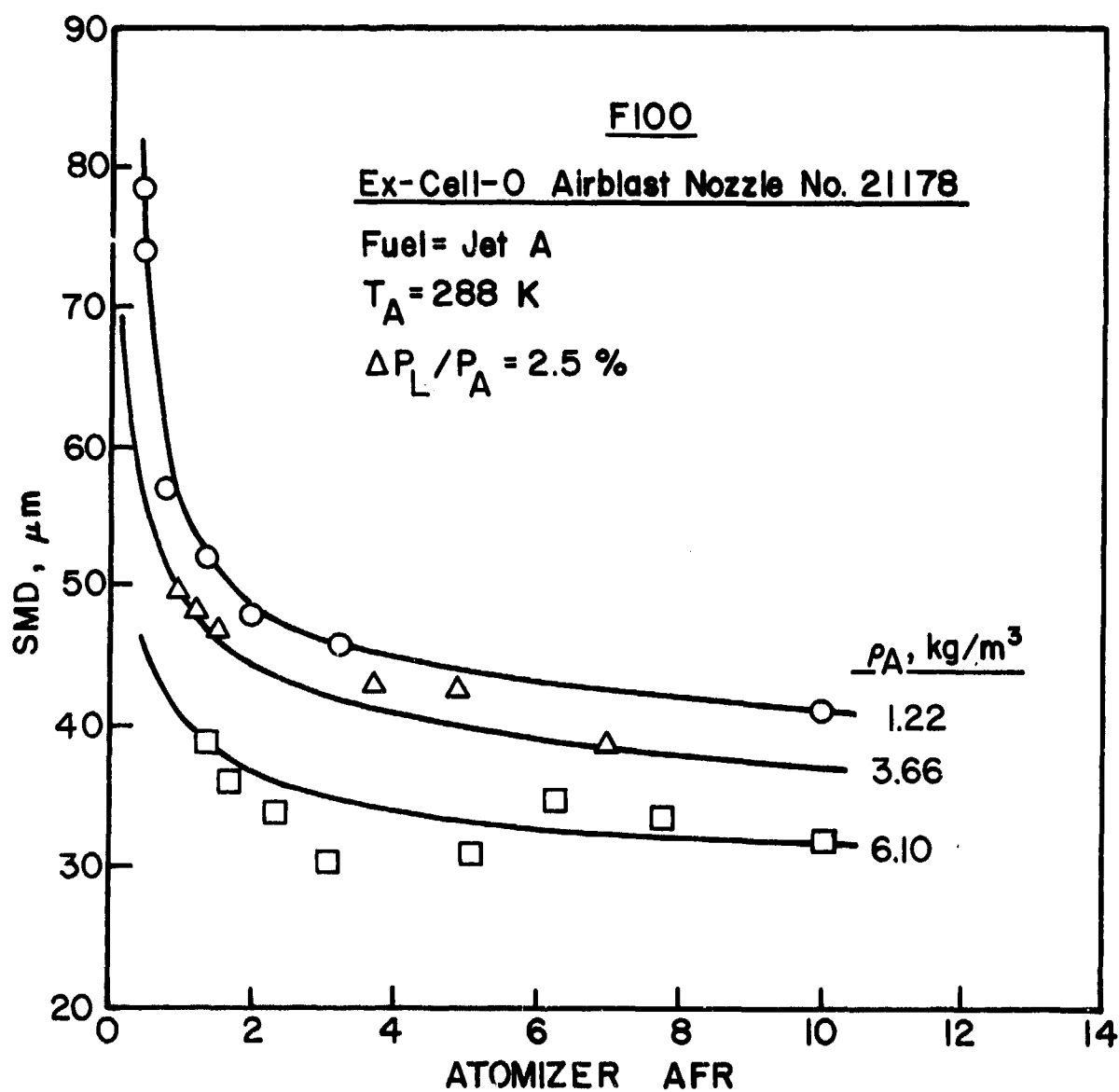


Figure 9. Influence of Ambient Air Density and Atomizer Air/Fuel Ratio on SMD for F100 Fuel Nozzle.

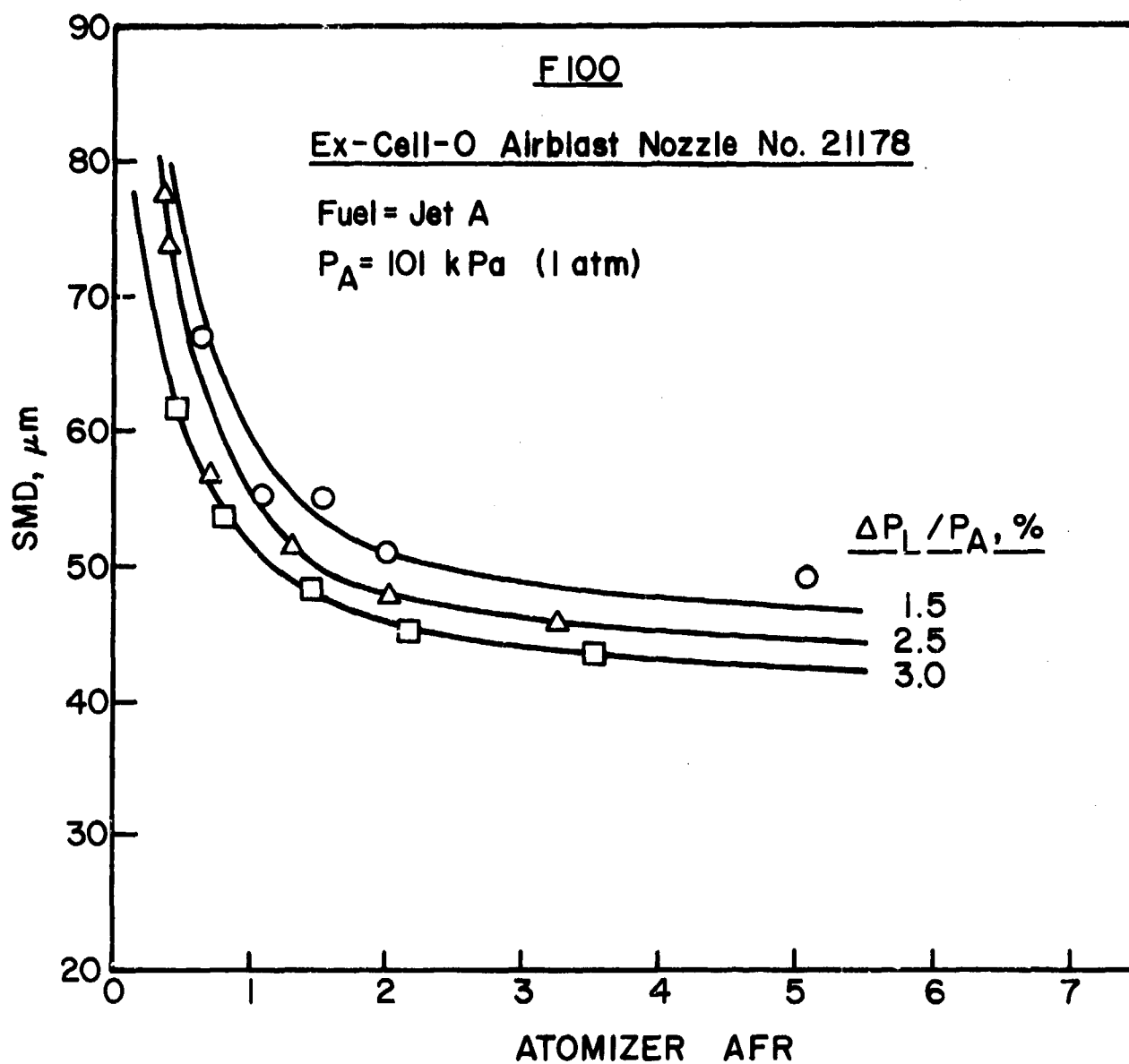


Figure 10. Influence of Atomizer Air/Fuel Ratio and Pressure Drop on SMD for F100 Fuel Nozzle.

quality improves with increase in liner pressure drop. The results obtained with a value of $\Delta P_L/P_A$ of 2.5 percent were selected for use in this study, as this is considered to best represent the liner pressure drop in the dome region.

The variations in SMD with fuel flow rate exhibited by the curves drawn in Figs. 3, 5, , 7 and 8 are characteristic of dual-orifice atomizers. Thus it is observed that atomization quality improves with increase in fuel flow rate up to a certain level, beyond which SMD values start to rise again. The point of minimum SMD coincides with the opening of the pressurizing valve which admits fuel into the main nozzle. As this fuel enters the nozzle at relatively low pressure its atomization quality is poor. With further increase in fuel flow, the main fuel pressure increases and atomization quality starts to improve. For the airblast atomizer it is seen (Figs. 9 and 10) that atomization quality improves continuously with decrease in fuel flow rate, i.e. with increase in AFR. For the hybrid nozzle, as illustrated in Fig. 4, the characteristic shapes of the SMD curves lie somewhere between those of the pressure nozzle and the pure airblast atomizer, so that SMD remains sensibly independent of fuel flow rate, at least over the range of fuel flows tested.

The steep temperature rise that accompanies combustion in the primary zone causes a reduction in gas density that largely offsets the increase in density experienced by the air during its passage through the compressor. In consequence, at low power settings where atomization quality is most limiting to combustion

performance, the density of the gas into which the fuel is sprayed is roughly the same as that of air at normal atmospheric pressure and temperature. For the results contained in Figs. 3 thru 10 the variation in ambient air density was obtained by changing air pressure while maintaining the air temperature constant at around 15°C. Inspection of Figs. 3 thru 10 reveals that atomization quality is generally improved by increases in ambient air density, except for the F101 nozzle which exhibits a slight deterioration in atomization quality with increase in ρ_A .

With appropriate interpolations, the results contained in Figs. 3 thru 10 can be used to establish formulae based on absolute values of mean drop size for the prediction of combustion efficiency, lean blowout limits, lean lightoff limits, pattern factor, and pollutant emissions, including unburned hydrocarbons and smoke. These various aspects of combustion performance are discussed in the following sections.

SECTION III

COMBUSTION EFFICIENCY

The separate effects on combustion of fuel evaporation, fuel-air mixing, and chemical reaction rates, have been fully described elsewhere [7,9]. For the aircraft gas turbine the main factors affecting the level of combustion efficiency are evaporation rates and chemical reaction rates. Mixing rates tend to be limiting to performance only at operating conditions where the level of combustion efficiency is so close to 100 percent that deficiencies in performance due to inadequate mixing are difficult to discern.

Three separate ranges of operating conditions may be defined, one in which combustion efficiency is governed solely by reaction rates, another in which combustion inefficiency is due entirely to low evaporation rates, and a third region in which the level of combustion efficiency depends on both reaction rates and evaporation rates. For all three regions the combustion efficiency is obtained as the product of the reaction rate efficiency, η_{c_θ} , and the evaporation efficiency, η_{c_e} , i.e.

$$\eta_c = \eta_{c_\theta} \times \eta_{c_e} \quad (7)$$

The second term on the right hand side of Eq. (7) represents the fraction of the fuel that is vaporized within the combustion zone. For $\eta_{c_e} = 1$, $\eta_c = \eta_{c_\theta}$, and Eq. (7) reverts to the θ parameter which denotes the fraction of fuel vapor that is converted

into combustion products by chemical reaction.

From analysis of the available experimental data on combustion efficiency, the following expressions for η_{c_θ} and η_{c_e} were derived [7].

$$\eta_{c_\theta} = 1 - \exp \left[- \frac{0.022 P_3^{1.3} V_c \exp (T_c/400)}{f_c m_A} \right] \quad (8)$$

$$\text{and } \eta_{c_e} = 1 - \exp \left[- \frac{36 \times 10^6 P_3 V_c \lambda_{eff}}{T_c D_o^2 f_c m_A} \right] \quad (9)$$

In Eq. (8) the temperature dependence is expressed in terms of T_c , which is the adiabatic flame temperature in the combustion zone, assuming complete combustion of the fuel. It is calculated from the expression

$$T_c = T_3 + \Delta T_c \quad (10)$$

where ΔT_c is obtained from standard temperature rise charts for the fuel in question, using appropriate values of P_3 , T_3 and q_c ($=q_{ov}/f_c$).

Equations (8) and (9) relate combustion efficiency to combustor dimensions (via V_c), combustor operating conditions (via m_A , P_3 and T_c), fuel nozzle characteristics (via D_o) and fuel type (via λ_{eff}).

Values of λ_{eff} are shown plotted in Figs. 11, 12 and 13. These figures contain plots of λ_{eff} versus T_{bn} at three levels of

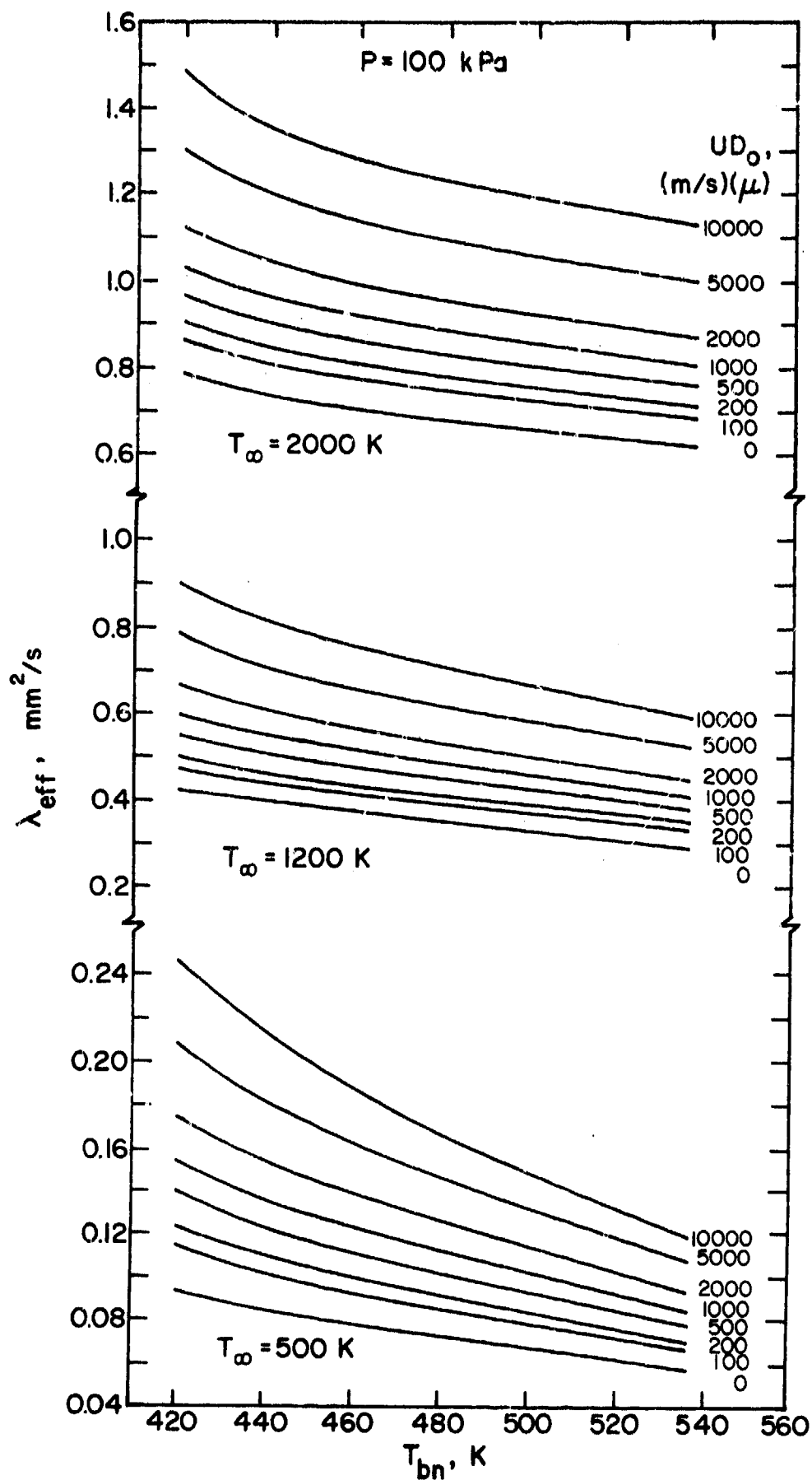


Figure 11. Variation of Effective Evaporation Constant with Normal Boiling Point at a Pressure of 100 kPa.

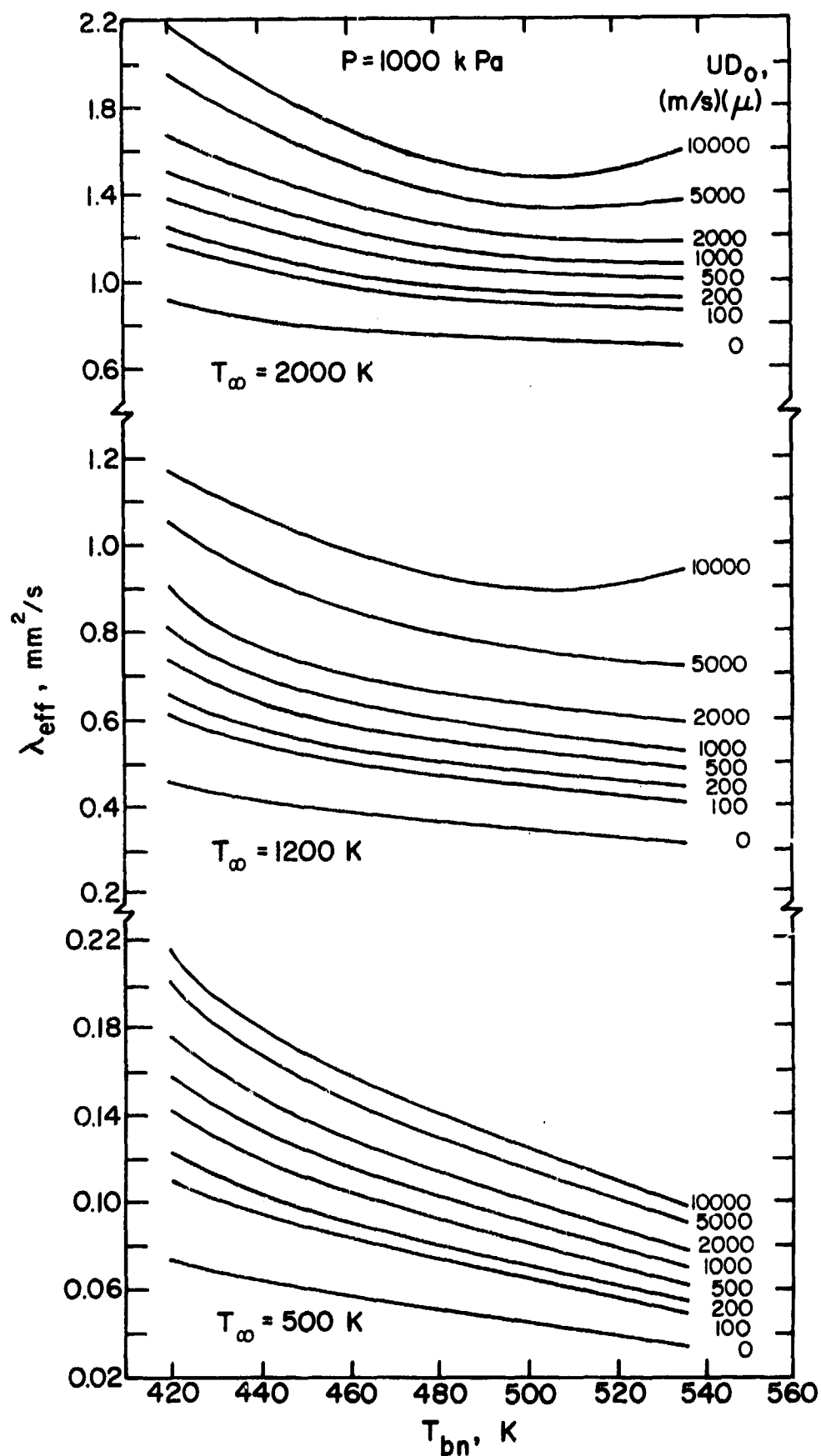


Figure 12. Variation of Effective Evaporation Constant with Normal Boiling Point at a Pressure of 1000 kPa.

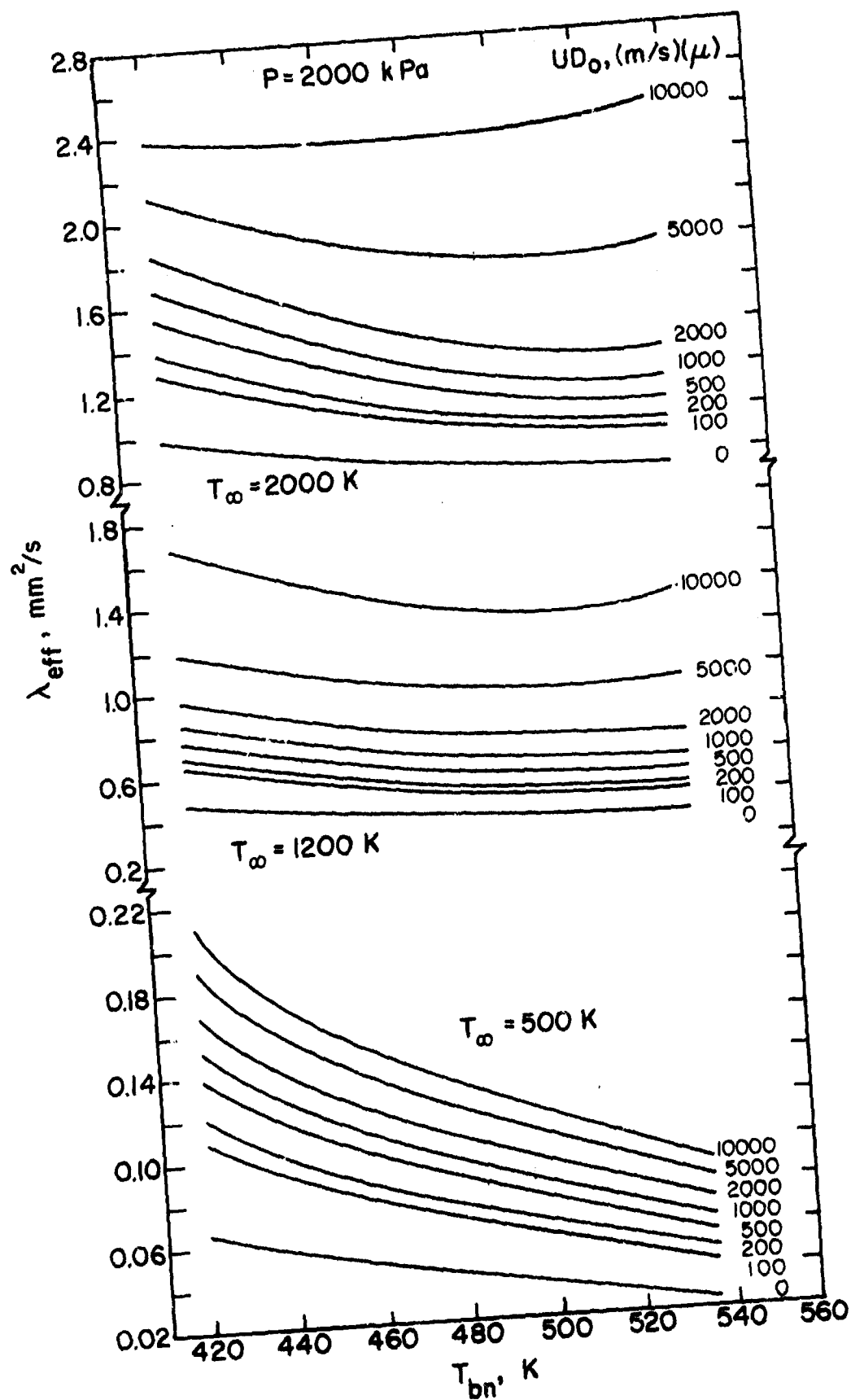


Figure 13. Variation of Effective Evaporation Constant with Normal Boiling Point at a Pressure of 2000 kPa.

pressure, namely 100, 1000 and 2000 kPa, and three levels of ambient temperature, namely 500, 1200 and 2000K. For each value of temperature several lines are drawn to represent different values of UD_0 , where U is the relative velocity between the fuel drop and the surrounding gas, and D_0 is the initial drop diameter.

From a practical standpoint the concept of λ_{eff} has considerable advantages since it takes into account the reduced rate of evaporation that occurs during the initial droplet heat-up period, as well as the enhancement of fuel evaporation rates due to the effects of forced convection [14]. Thus plots of λ_{eff} of the type shown in Figs. 11 thru 13 greatly simplify calculations on rates of spray evaporation and drop lifetimes.

The very satisfactory correlation of combustion efficiency data provided by Eq. (7) is demonstrated in Figs. 14 thru 21, which include all the relevant data on combustion efficiency contained in references 1 thru 6.

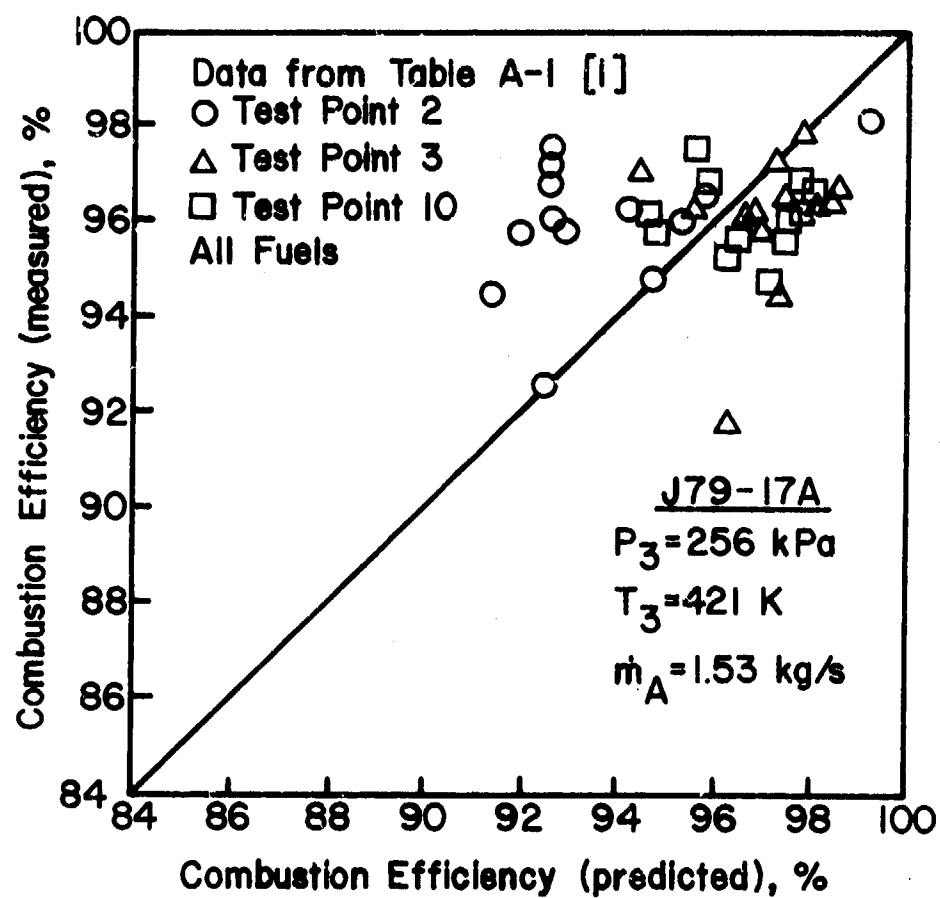


Figure 14. Comparison of Measured and Predicted Values of Combustion Efficiency for J79-17A Combustor.

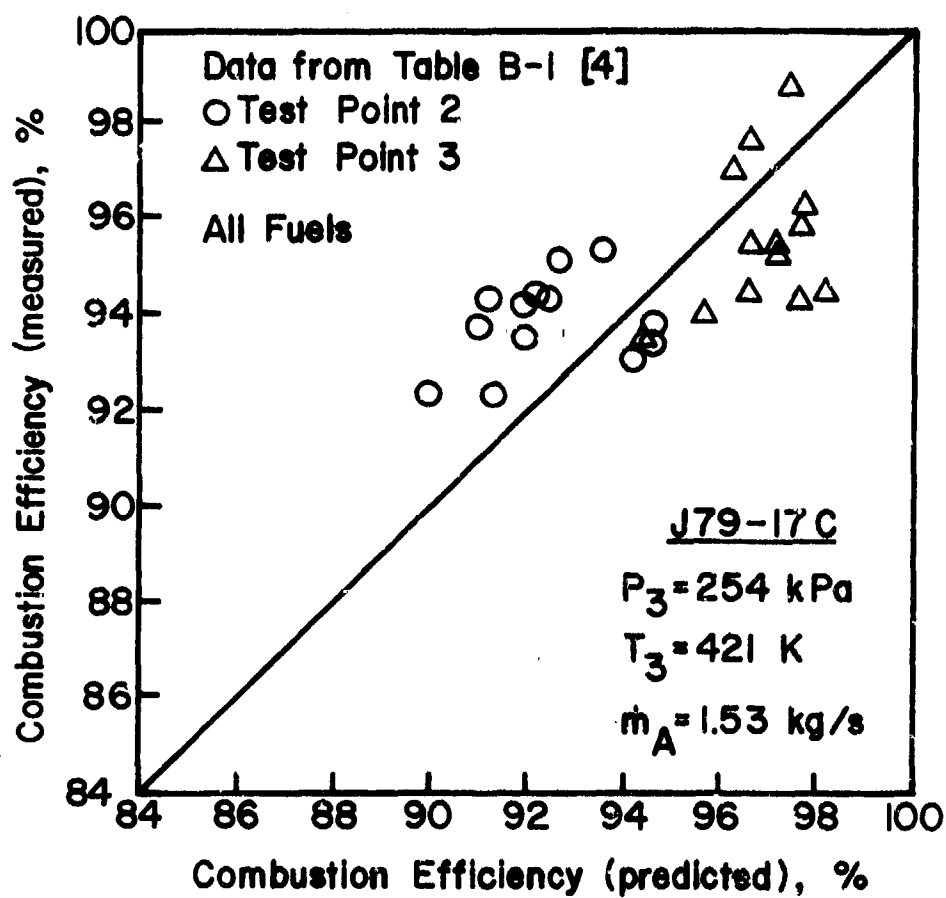


Figure 15. Comparison of Measured and Predicted Values of Combustion Efficiency for J79-17C Combustor.

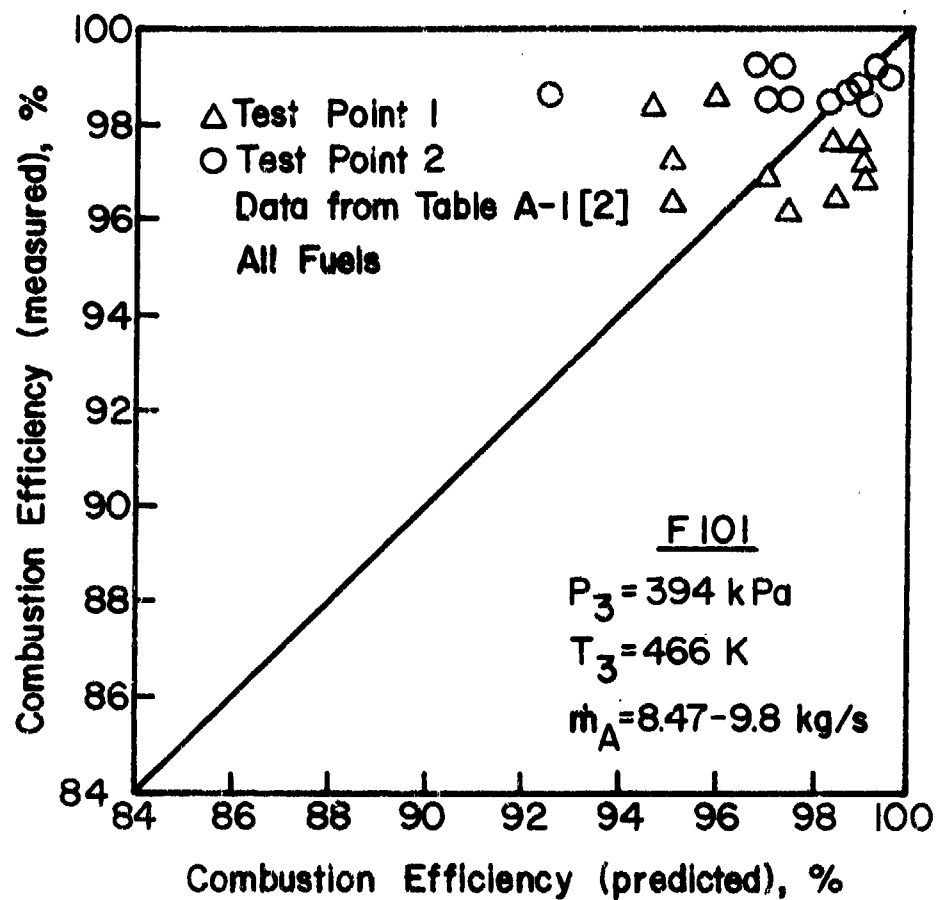


Figure 16. Comparison of Measured and Predicted Values of Combustion Efficiency for F101 Combustor.

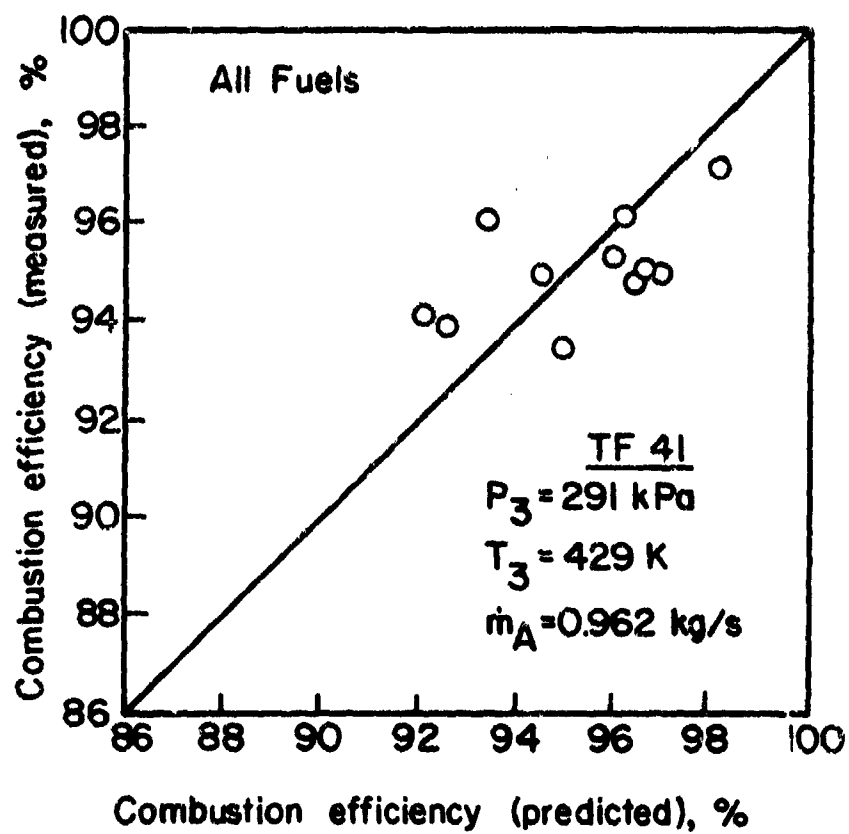


Figure 17. Comparison of Measured and Predicted Values of Combustion Efficiency for TF41 Combustor.

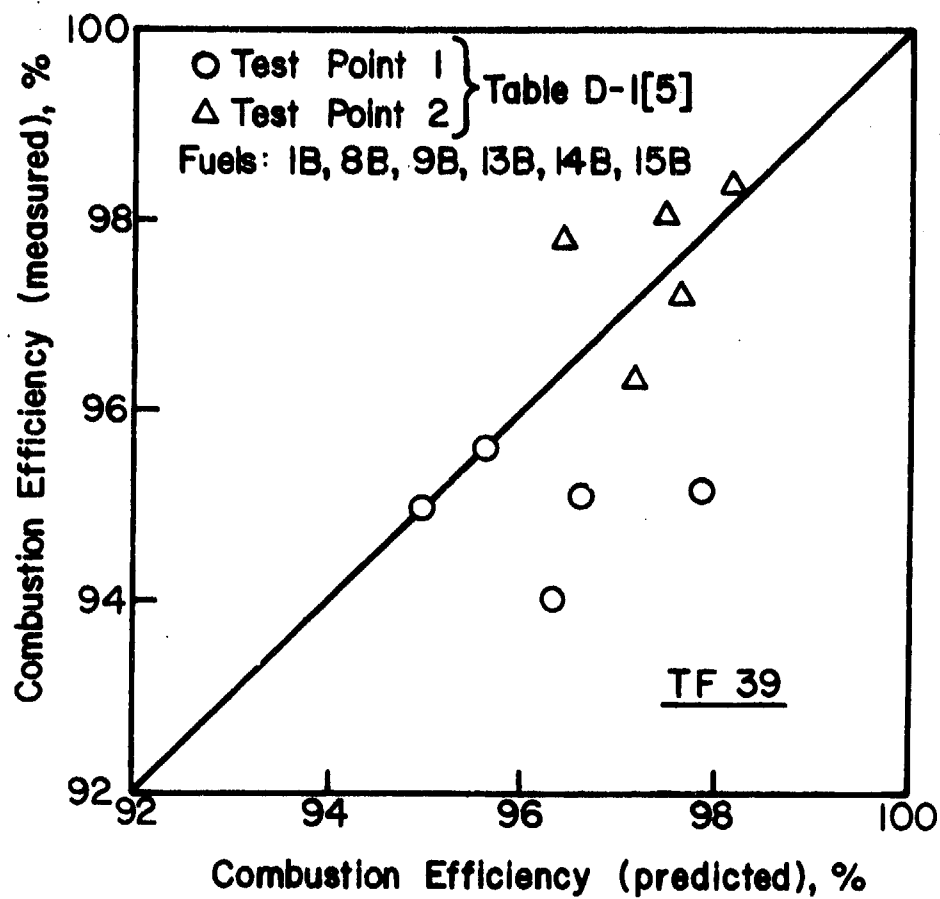


Figure 18. Comparison of Measured and Predicted Values of Combustion Efficiency for TF39 Combustor.

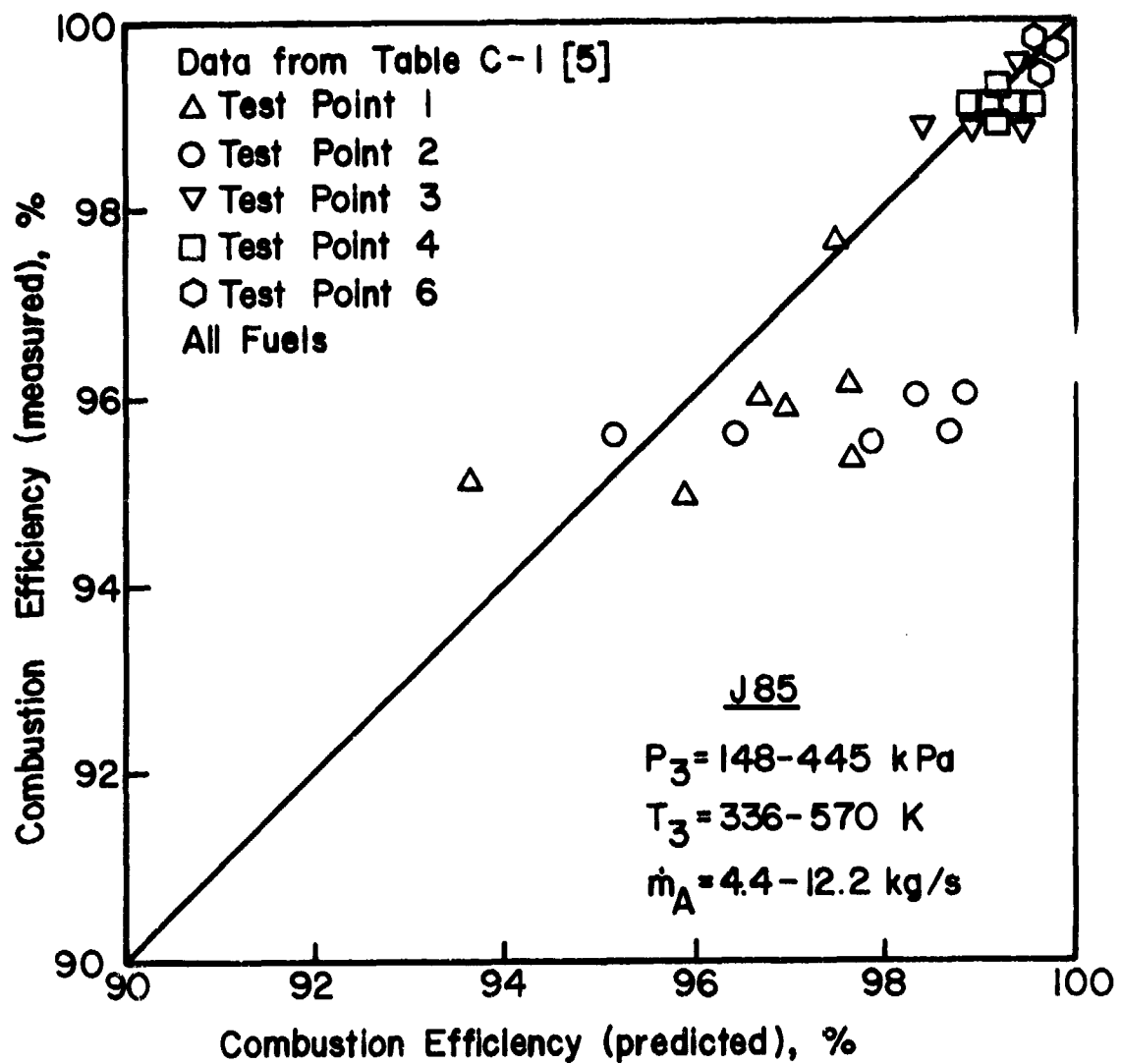


Figure 19. Comparison of Measured and Predicted Values of Combustion Efficiency for J85 Combustor.

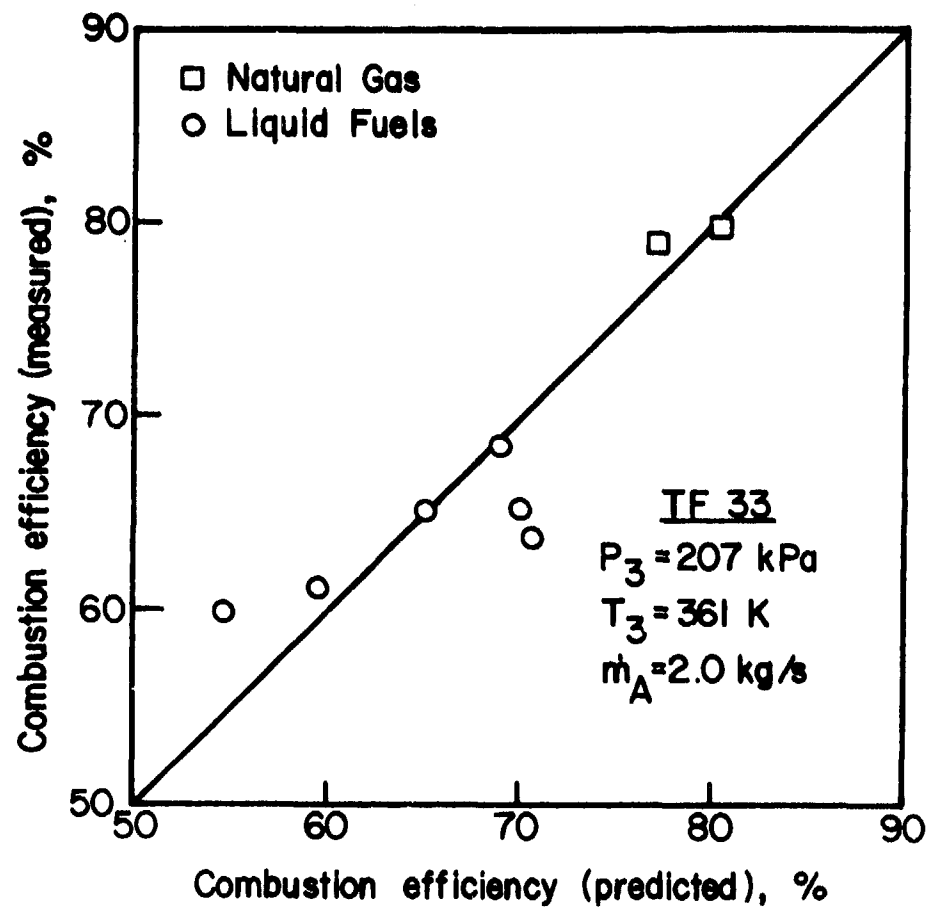


Figure 20. Comparison of Measured and Predicted Values of Combustion Efficiency for TF33 Combustor.

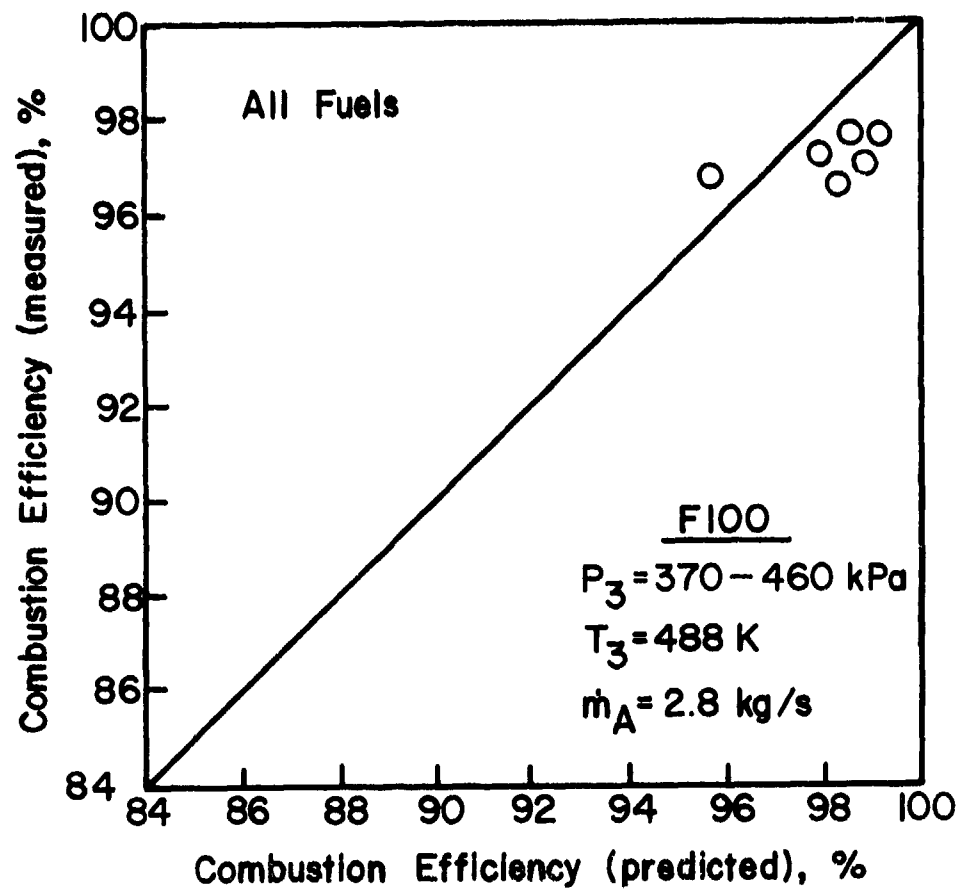


Figure 21. Comparison of Measured and Predicted Values of Combustion Efficiency for F100 Combustor.

SECTION IV

LEAN BLOWOUT

The problem of lean blowout has not loomed very large in the past, due mainly to the widespread use of pressure swirl atomizers. The poor mixing characteristics of these atomizers allow combustion to occur at mixture strengths that are well below the normal weak limit of flammability. In fact, lean blowout limits of around 1000 air/fuel ratio (AFR), based on overall combustor values of air and fuel flow rates, used to be quite commonplace. In recent years the continuing trend toward improved primary-zone fuel-air mixing for the reduction of pollutant emissions and flame radiation has led to a narrowing of stability limits and to increasing concern over the attainment of satisfactory lean blowout performance.

For homogeneous fuel-air mixtures, flame blowout occurs when the rate of heat liberation in the primary zone becomes insufficient to heat the incoming fresh mixture up to the required reaction temperature. The lean blowout fuel/air ratio depends on the inlet air velocity, pressure, and temperature, and on the size of the primary zone. The relationship is of the form [15]

$$q_{LBO} \propto \left[\frac{\dot{m}_A}{v_{pz} p_3^n \exp(T_3/b)} \right]^x \quad (11)$$

Equation (11) may also be used to predict the lean blowout limits of combustion chambers supplied with heterogeneous fuel-air mixtures, provided that the rate of fuel evaporation is

sufficiently high to ensure that all the fuel is fully vaporized within the primary combustion zone. If the fuel does not fully vaporize, then clearly the "effective" fuel/air ratio will be lower than the nominal value. However, if the fraction of fuel that is vaporized is known, or can be calculated, it can then be combined with Eq. (11) to yield the fuel/air ratio at lean blowout, i.e.,

$$q_{LBO(\text{heterogeneous})} = q_{LBO(\text{homogeneous})} \times f_f^{-1} \quad (12)$$

where f_f is the fraction of fuel that is vaporized within the primary combustion zone.

From analysis of the factors governing the rate of evaporation of a fuel spray [14], it was found that

$$f_f = 10^6 \rho_g V_{pz} \lambda_{eff} / f_{pz} \dot{m}_A D_o^2 \quad (13)$$

It should be noted that Eq. (13) allows f_f to exceed unity. When this occurs it simply means that the time available for fuel evaporation exceeds the time required, so that the fuel is fully vaporized within the recirculation zone. In these circumstances f_f should be assigned a value of unity.

Substitution of $q_{LBO(\text{hom})}$ from Eq. (11) and f_f from Eq. (13) into Eq. (12) leads to

$$q_{LBO} \propto \left[\frac{f_{pz}}{V_{pz}^{(1+x)}} \right] \left[\frac{\dot{m}_A^{(1+x)}}{P_3^{(1+n)} \exp(T_3/b)} \right] \left[\frac{D_o^2}{\lambda_{eff} LCV} \right] \quad (14)$$

The first term on the right hand side of Equation 14 is a function of combustor design. The second term represents the combustor operating conditions. The third term embodies the relevant fuel-dependent properties, including the lower calorific value of the fuel. This property is included because lean blowout occurs at roughly the same temperature for all fuels, so that fuels having a higher heat content are capable of burning at lower mixture strengths [10].

Analysis of the experimental data for all engines indicates optimum values for b , n , and x of 300, 0.3 and 0, respectively. Insertion of these values into Eq. (14) gives

$$q_{LBO} = A' \left[\frac{f_{pz}}{v_{pz}} \right] \left[\frac{\dot{m}_A}{P_3^{1.3} \exp(T_3/300)} \right] \left[\frac{D_o^2}{\lambda_{eff} LCV} \right] \quad (15)$$

where A' is a constant whose value depends on the geometry and mixing characteristics of the combustion zone. Having determined the value of A' at any convenient test condition, Eq. (15) may then be used to predict the lean blowout fuel/air ratio at any other operating condition.

A difficulty that arises with Eq. (15) is that of assigning appropriate values to v_{pz} , since for many combustors the primary-zone volume is not clearly defined. To surmount this problem it was decided to substitute the pre-dilution zone, V_c , into Eq. (15), instead of v_{pz} . This may be justified on the grounds that V_c is easier to define and measure; also, values of V_c have already been used in the correlation of combustion

efficiency data. Furthermore, as the ratio of primary-zone volume to pre-dilution volume tends to be fairly constant for most conventional combustion chambers, using V_c instead of V_{pz} has the virtue of consistency without loss of accuracy. With this modification Eq. (15) becomes

$$q_{LBO} = A \left[\frac{f_{pz}}{V_c} \right] \left[\frac{\dot{m}_A}{P_3^{1.3} \exp(T_3/300)} \right] \left[\frac{D_o^2}{\lambda_{eff} LCV} \right] \left[\frac{D_o \text{ at } T_F}{D_o \text{ at } 277.5K} \right]^2 \text{ g/kg (16)}$$

The term $(D_o \text{ at } T_F)^2 / (D_o \text{ at } 277.5)^2$ is introduced into the above equation to take into account the variation in drop size arising from a change in fuel temperature from the initial baseline value, which is taken as 277.5K. For lean blowout limits, λ_{eff} should be evaluated at an air temperature of 1400K, since this approximates the weak extinction temperature for all fuels.

For each combustor a value of A was chosen for insertion into Eq. (16) that would provide the best fit to the experimental data. These values of A are given in Table 2. It would clearly be advantageous if similar types of primary zones yielded similar values of A, since this would facilitate the prediction of lean blowout limits for new combustor designs. Although the variation in the values of A listed in Table 2 virtually prohibits such extrapolation, it should be borne in mind that these values embody all the errors incurred in the estimates of combustion volume and the fraction of air involved in primary combustion, as well as in the measurements of mean drop size. By combining A with f_{pz} the deviation is reduced, as illustrated in Table 2.

Table 2. Values of A and B employed in equations (16) and (17).

Engine	A	Af_{pz}	B	Bf_{pz}
J79-17A	0.95	0.22	0.477	0.109
J79-17C	0.70	0.22	0.544	0.103
F101	0.54	0.22	0.700	0.287
TF39	0.60	0.18	0.360	0.108
J85	1.00	0.30	0.335	0.104
F100	0.45	0.16	0.508	0.178

As discussed in reference 7, the initial value of Af_{pz} calculated for the F101 combustor was exceptionally high, and this was attributed to an error in recording either the fuel flow rate or air flow rate when testing on a 54° segment of an annular combustor. Dividing the reported values of q_{LBO} contained in reference 2 by $(360/54)$ not only gives more sensible values of q_{LBO} , but also reduces Af_{pz} to 0.22, which is fully consistent with the results obtained for the other combustors.

The correlations of lean blowout limits provided by Eq. (16), using appropriate values of A , are illustrated in Figs. 22 thru 29 for the J79-17A, J79-17C, F101, TF39, J85, and F100 combustors, respectively. The close agreement exhibited between the predicted and the measured values of lean blowout fuel/air ratio is clearly very satisfactory.

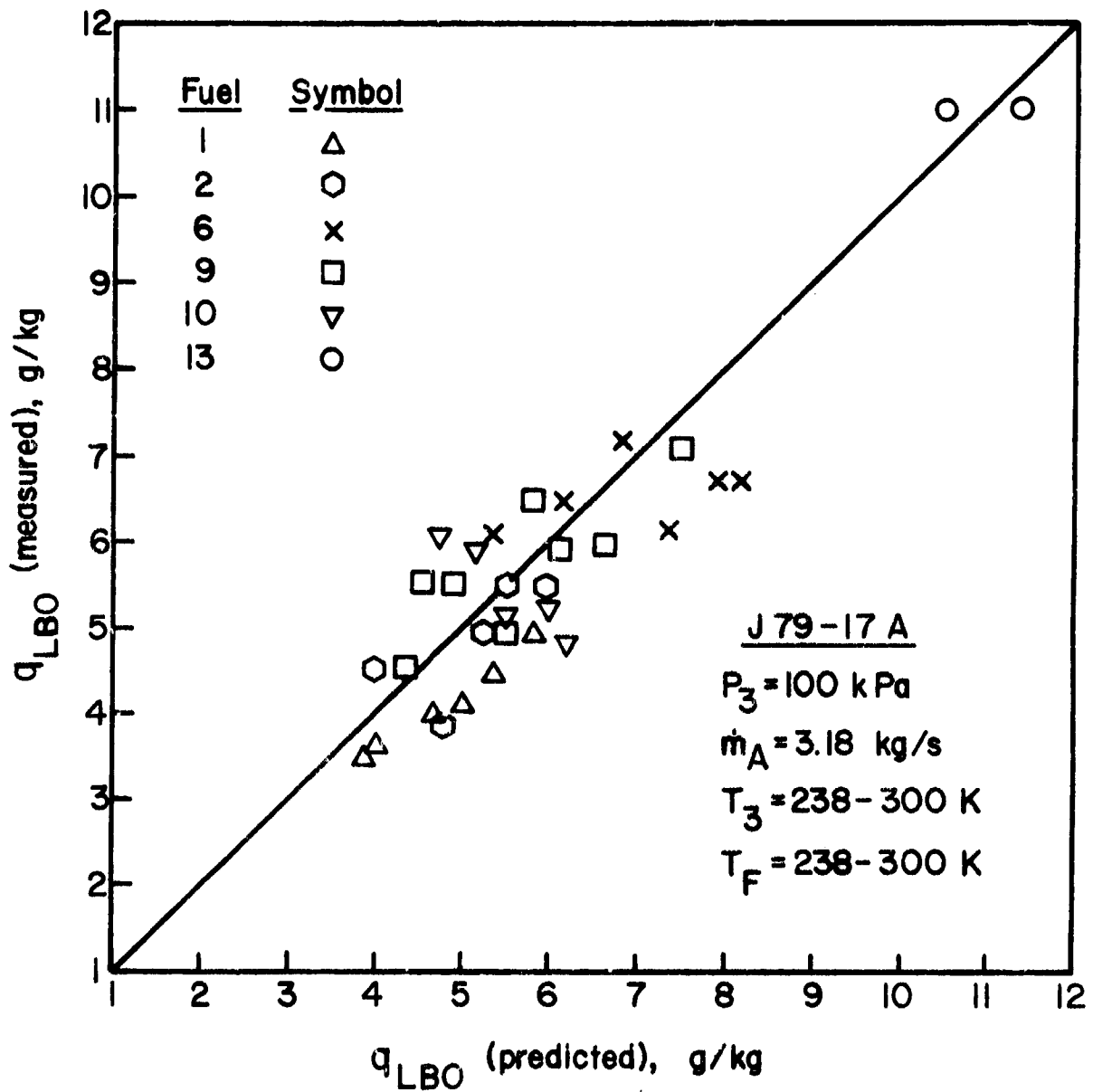


Figure 22. Comparison of Measured and Predicted Values of Lean Blowout for J79-17A Combustor.

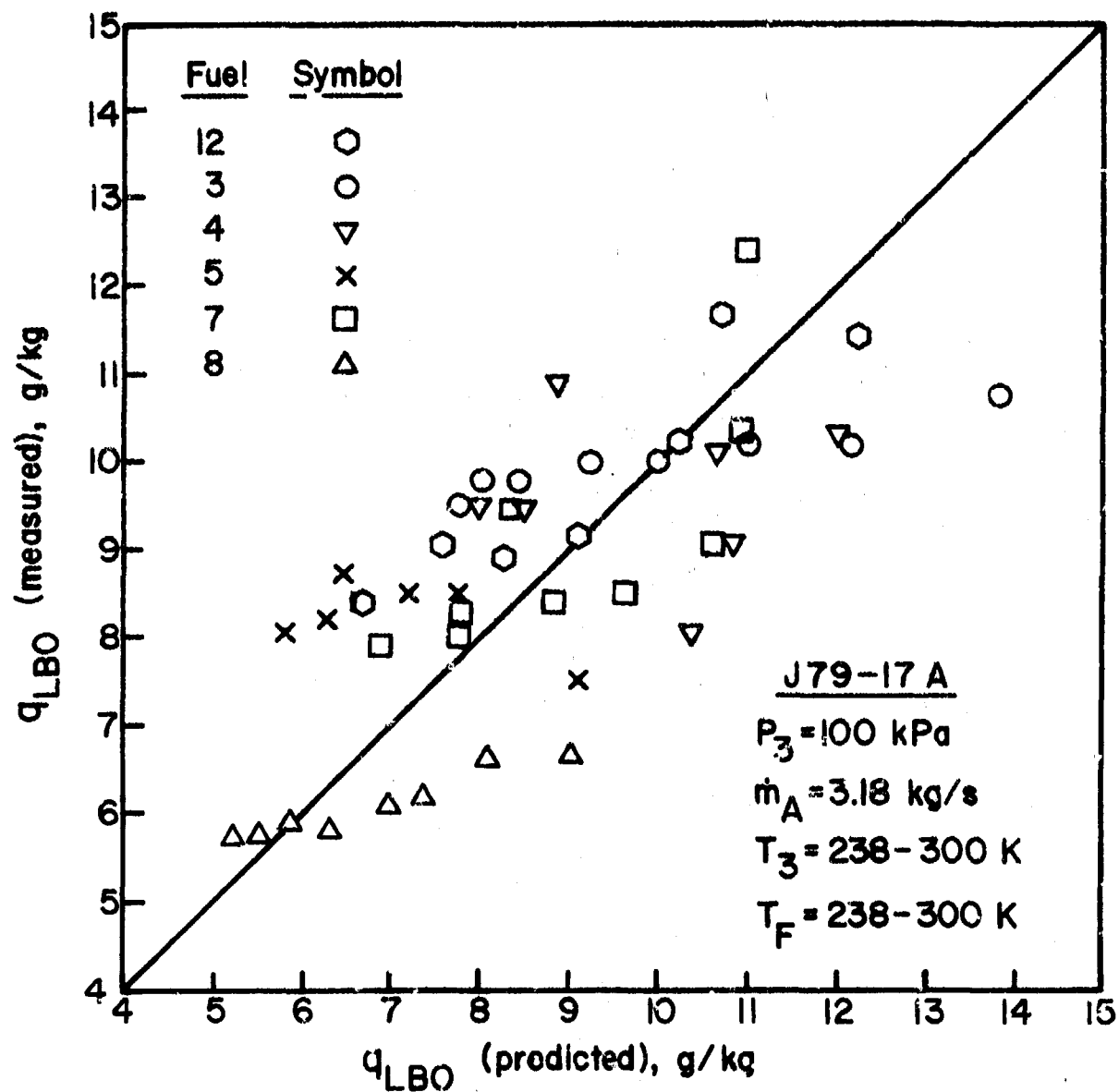


Figure 23. Comparison of Measured and Predicted Values of Lean Blowout for J79-17A Combustor.

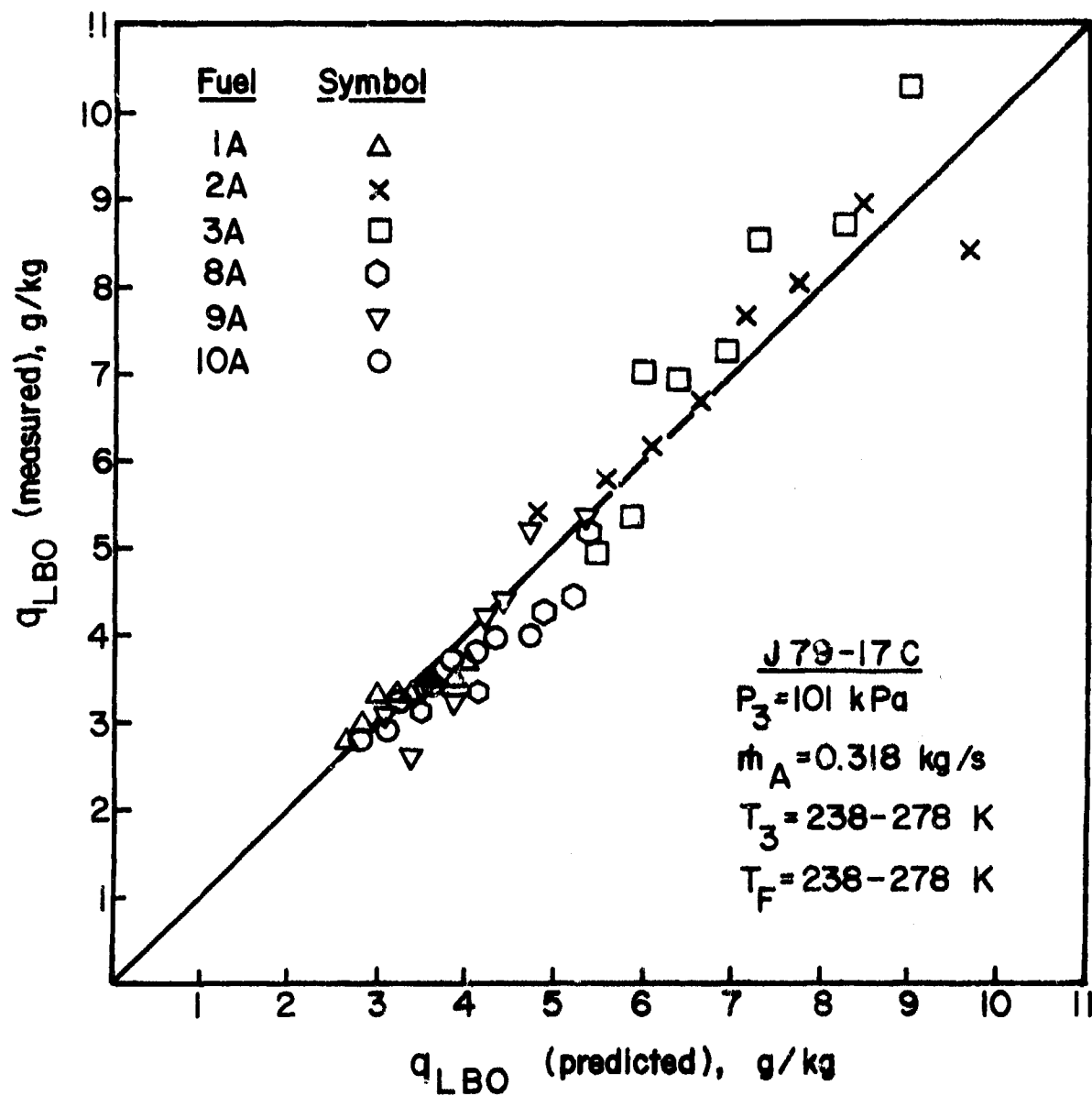


Figure 24. Comparison of Measured and Predicted Values of Lean Blowout for J79-17C Combustor.

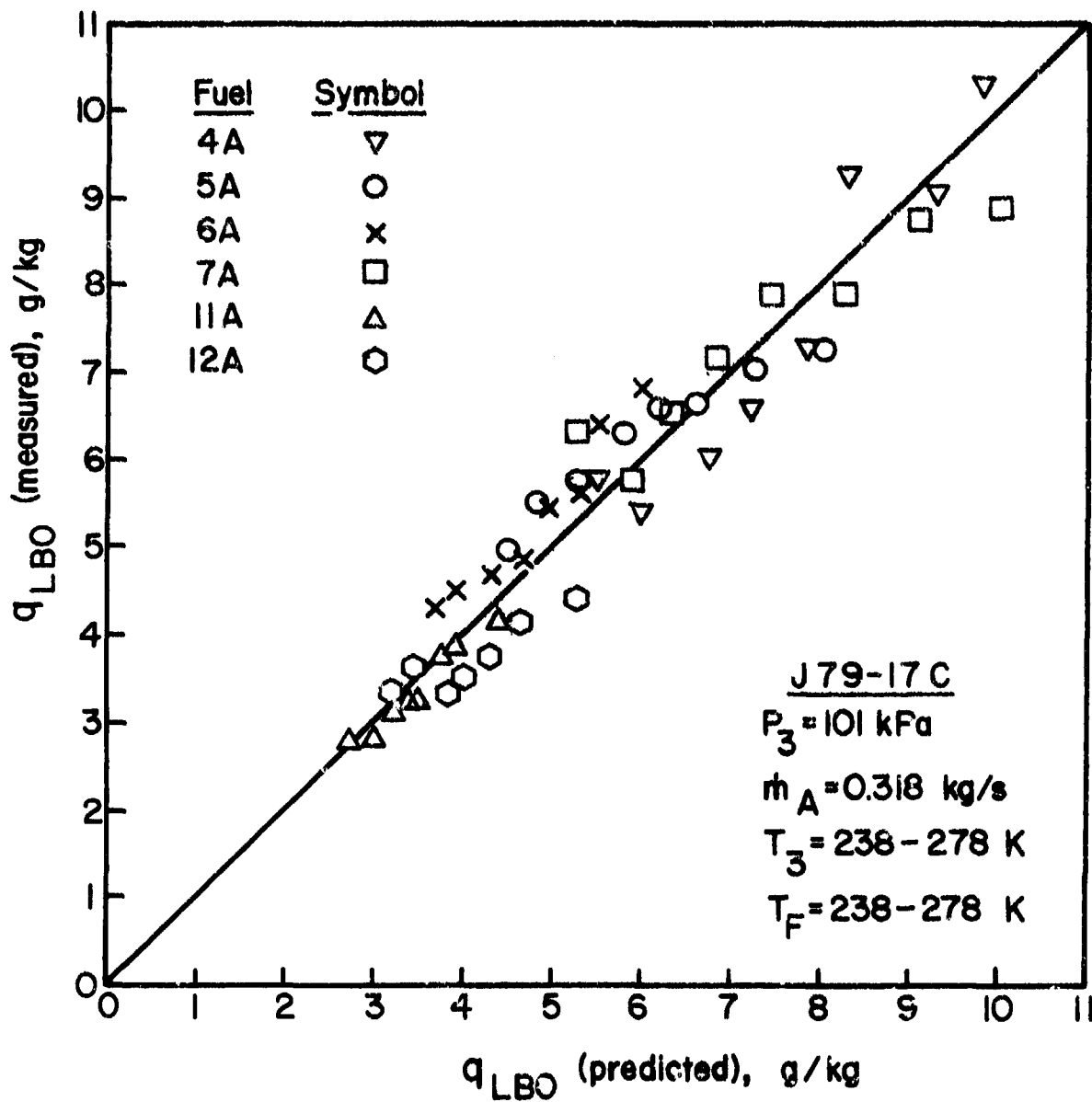


Figure 25. Comparison of Measured and Predicted Values of Lean Blowout for J79-17C Combustor.

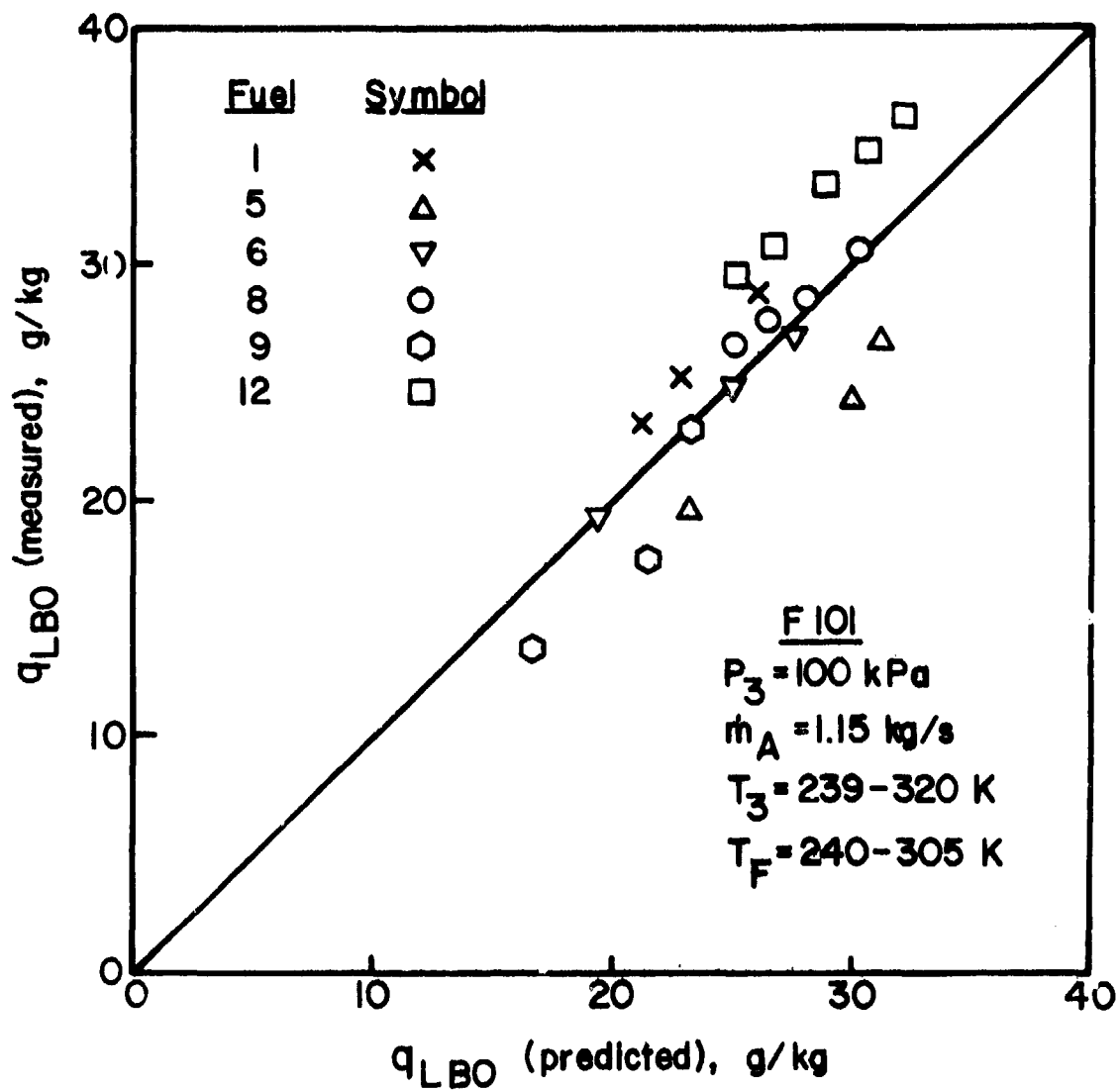


Figure 26. Comparison of Measured and Predicted Values of Lean Blowout for F101 Combustor.

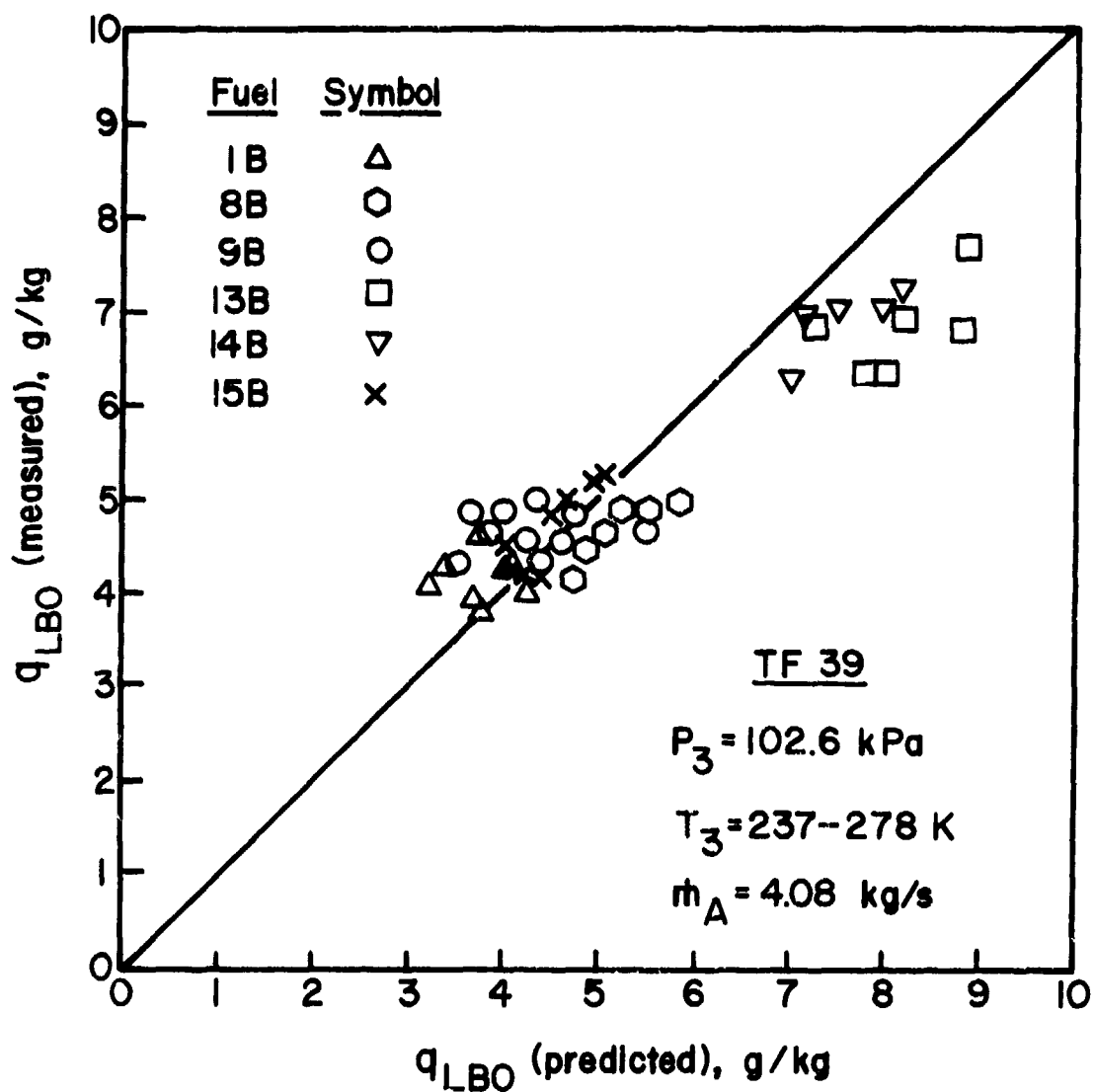


Figure 27. Comparison of Measured and Predicted Values of Lean Blowout for TF39 Combustor.

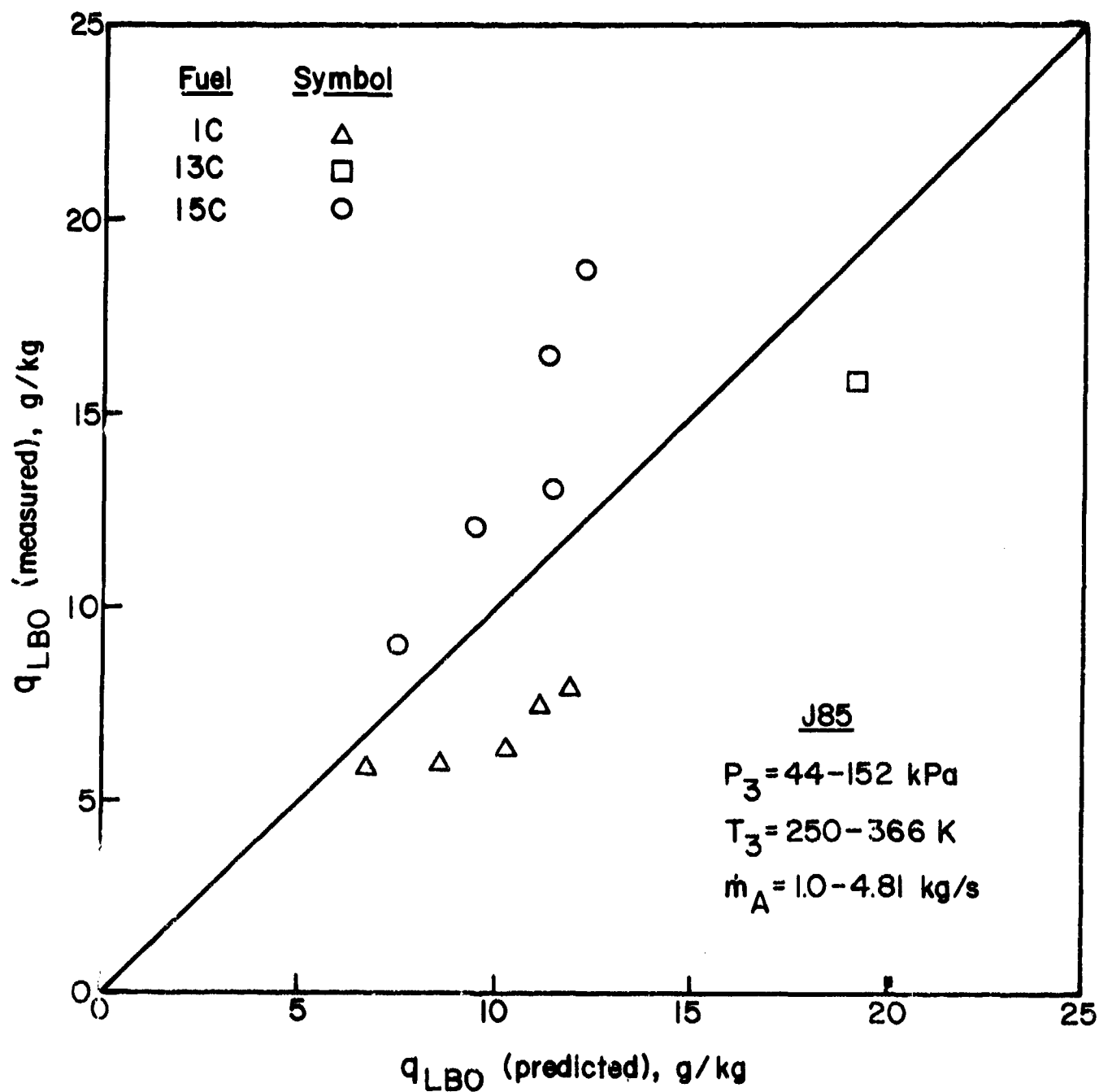


Figure 28. Comparison of Measured and Predicted Values of Lean Blowout for J85 Combustor.

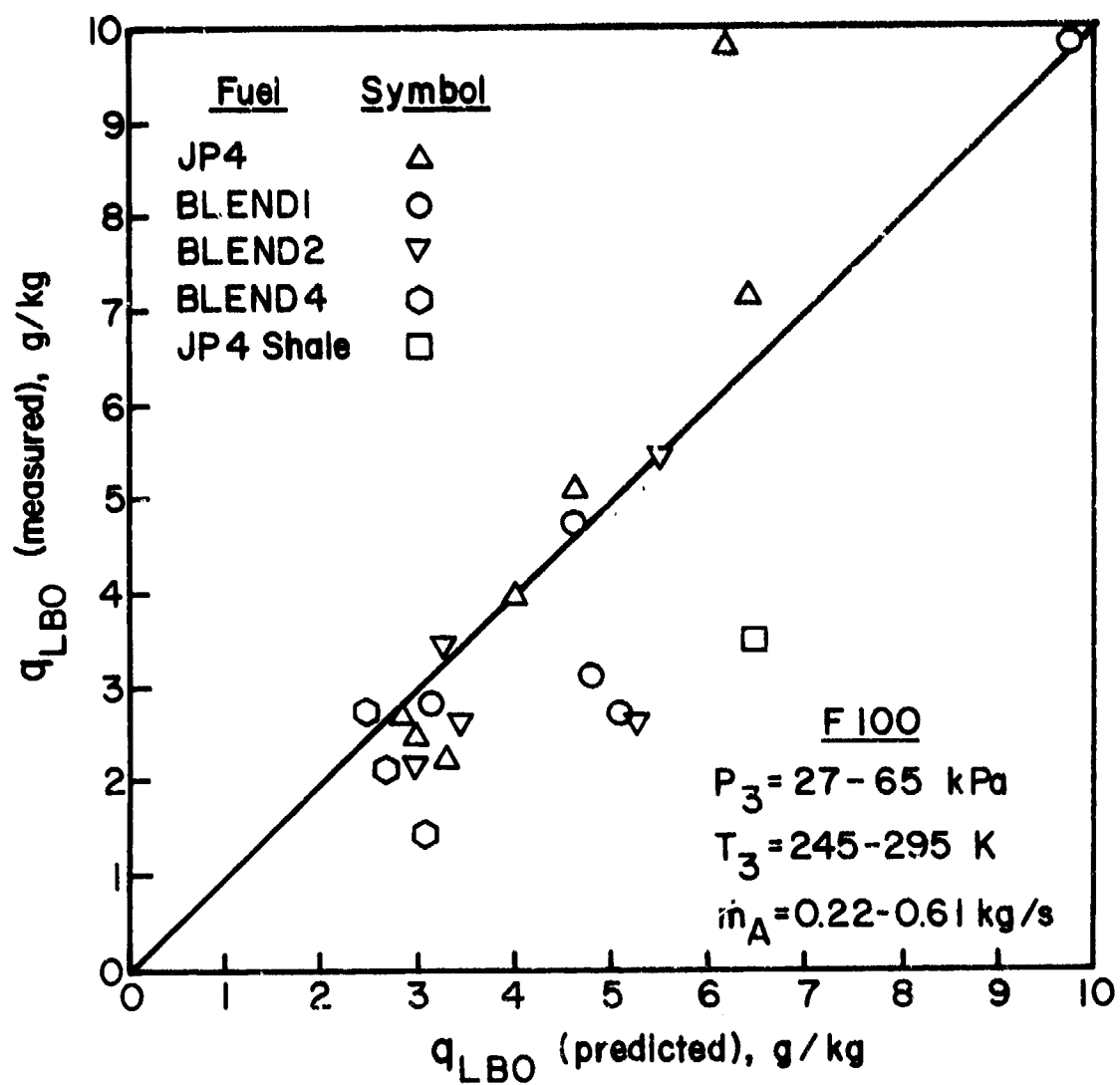


Figure 29. Comparison of Measured and Predicted Values of Lean Blowout for F100.

SECTION V

IGNITION

It is well-established that ignition is made easier by increases in pressure, temperature, and spark energy, and is impeded by increases in velocity and turbulence intensity. Ignition performance is also markedly affected by fuel properties through the way in which they influence the concentration of fuel vapor in the spark region. These influences arise mainly from the effect of volatility on evaporation rates, and also from the effects of surface tension and viscosity on mean fuel drop size. The amount of energy required for ignition is very much larger than the values normally associated with gaseous fuels at stoichiometric fuel/air ratio. Much of this extra energy is absorbed in the evaporation of fuel drops, the actual amount depending on the distribution of fuel throughout the primary zone and on the quality of atomization.

Application of the theoretical concepts developed in references 16 and 17 to the ignition data contained in references 1 thru 6 leads to the following equation for lean lightoff fuel/air ratio.

$$q_{LLO} = B \left[\frac{f_{pz}}{v_c} \right] \left[\frac{\dot{m}_A}{P_3^{1.5} \exp(T_3/300)} \right] \left[\frac{D_o^2}{\lambda_{eff} LCV} \right] \left[\frac{D_o \text{ at } T_F}{D_o \text{ at } 277.5K} \right]^2 \text{ g/kg (17)}$$

This equation is virtually identical to Eq. (16) except for a higher pressure dependence; namely $P_3^{1.5}$ instead of $P_3^{1.3}$. Another minor difference is that λ_{eff} is evaluated at the combustor inlet

air temperature, T_3 .

The correlation of lightup data obtained with Eq. (17) is illustrated in Figs. 30 thru 37 for the J79-17A, J79-17C, F101, TF39, J85, and F100 combustors, respectively. The level of agreement between predicted and experimental values is considered satisfactory, especially in view of the well-known lack of consistency that usually characterizes ignition data. Values of B and Bf_{pz} for all combustors are listed in Table 2.

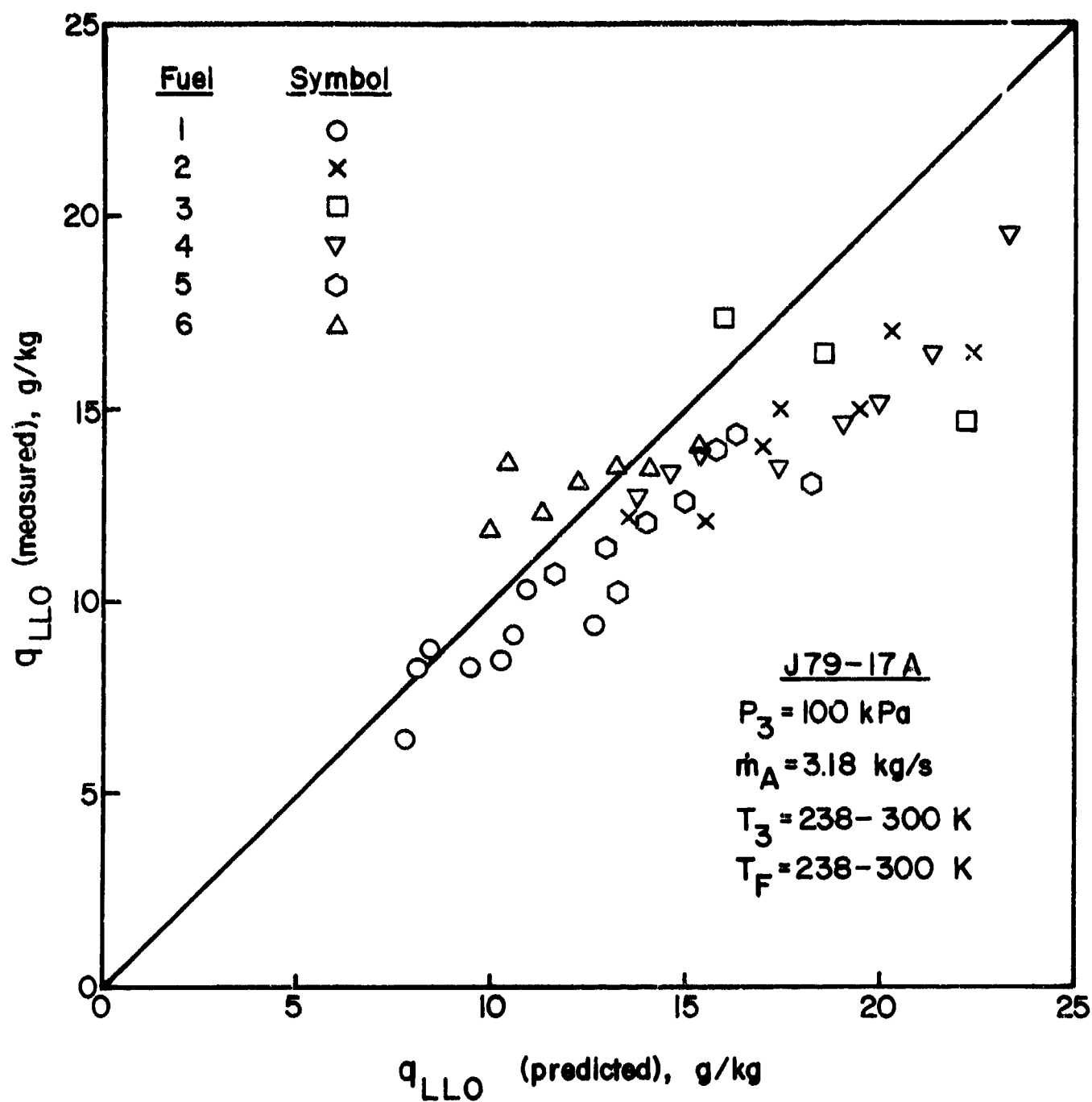


Figure 30. Comparison of Measured and Predicted Values of Lean Light Off for J79-17A Combustor.

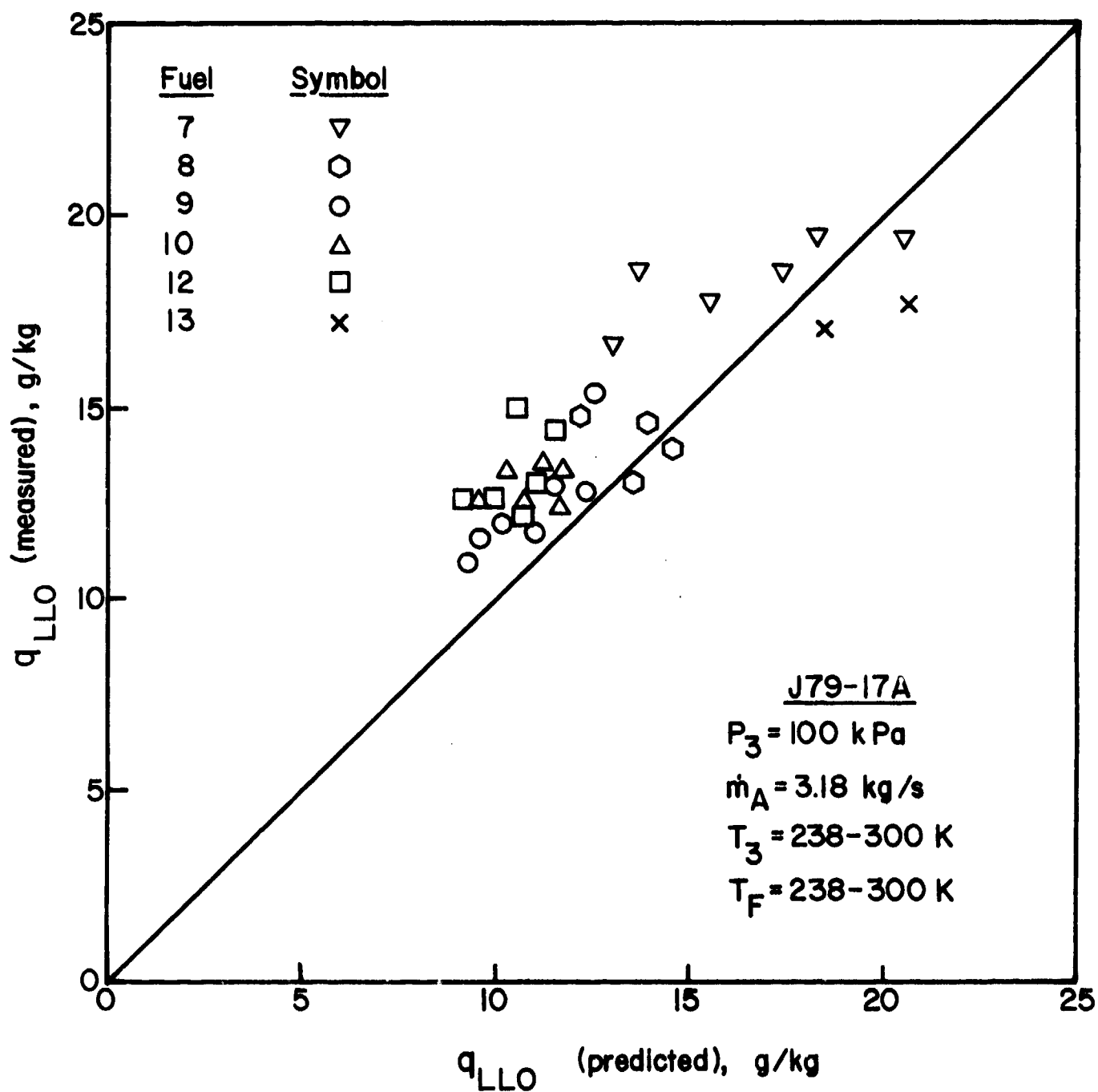


Figure 31. Comparison of Measured and Predicted Values of Lean Light Off for J79-17A Combustor.

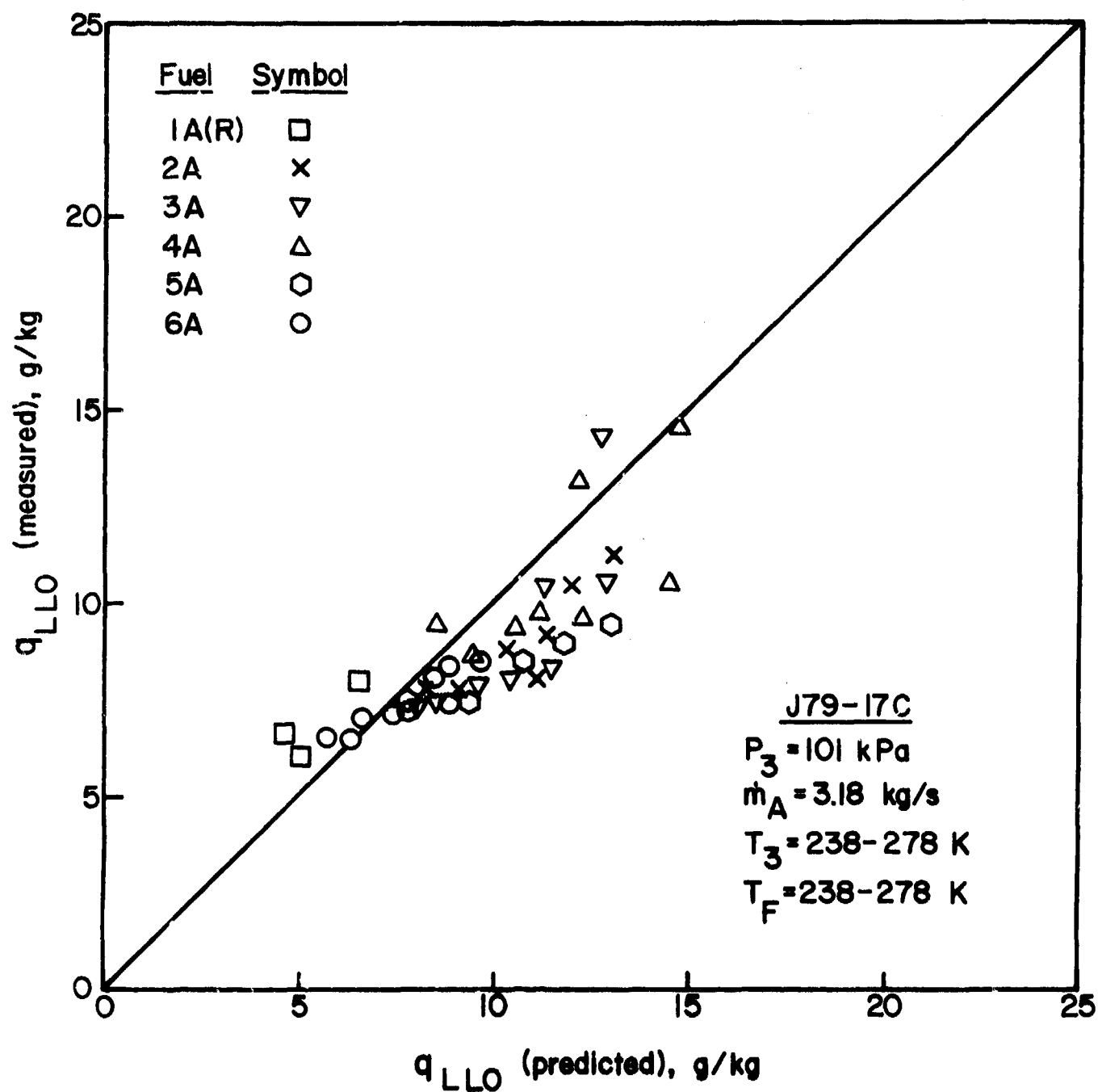


Figure 32. Comparison of Measured and Predicted Values of Lean Light Off for J79-17C Combustor.

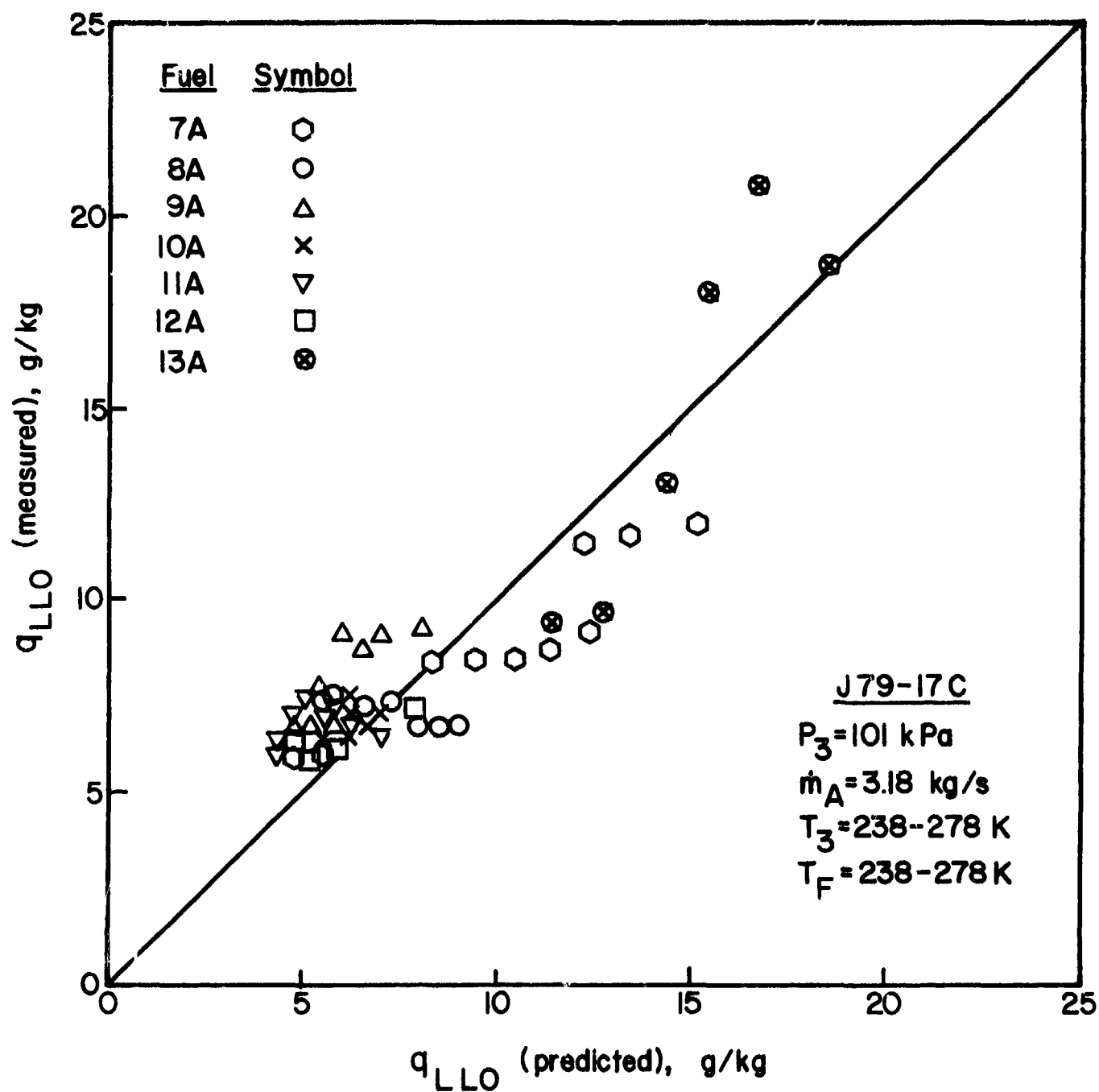


Figure 33. Comparison of Measured and Predicted Values of Lean Light Off for J79-17C Combustor.

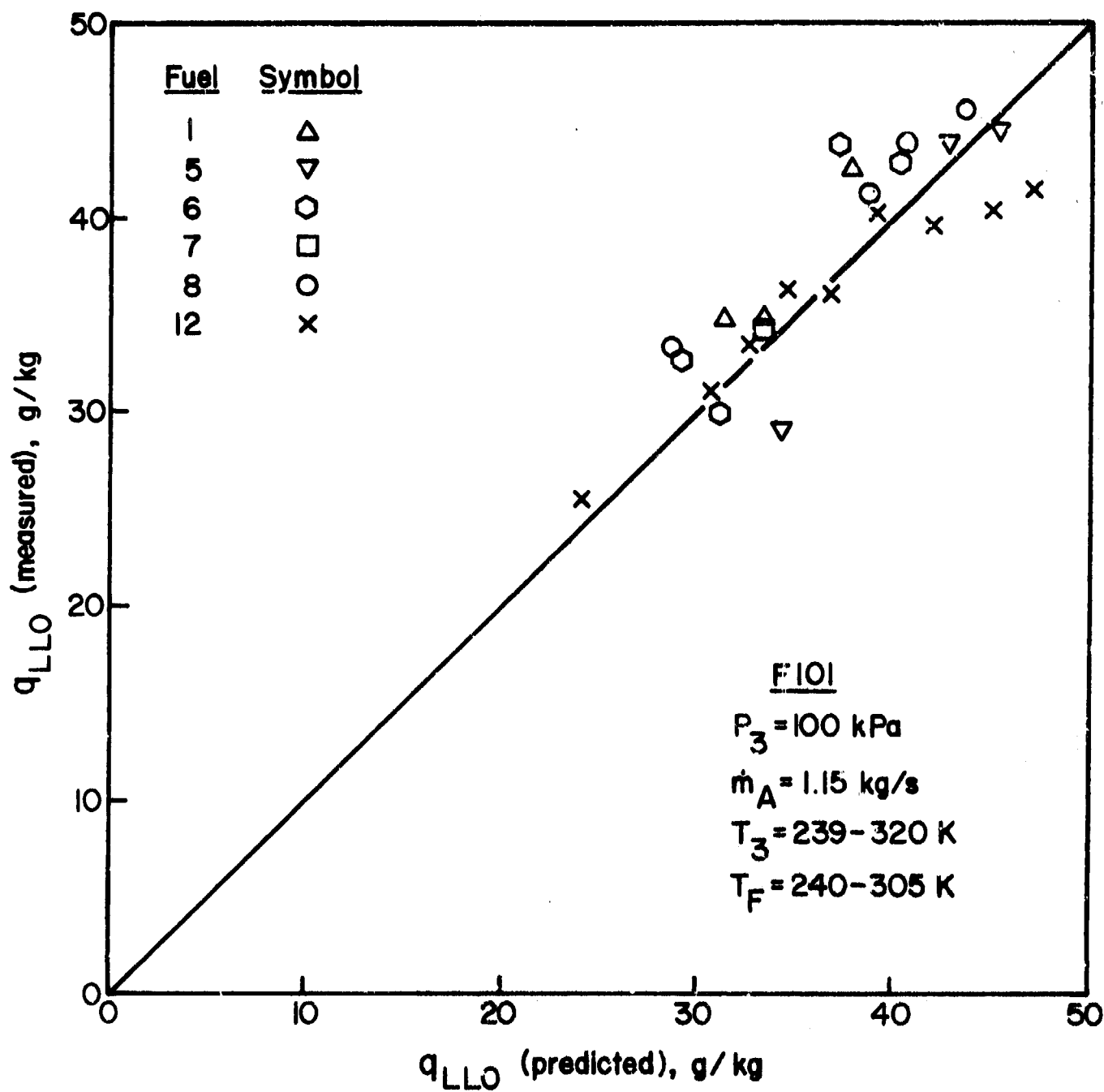


Figure 34. Comparison of Measured and Predicted Values of Lean Light Off for F101 Combustor.

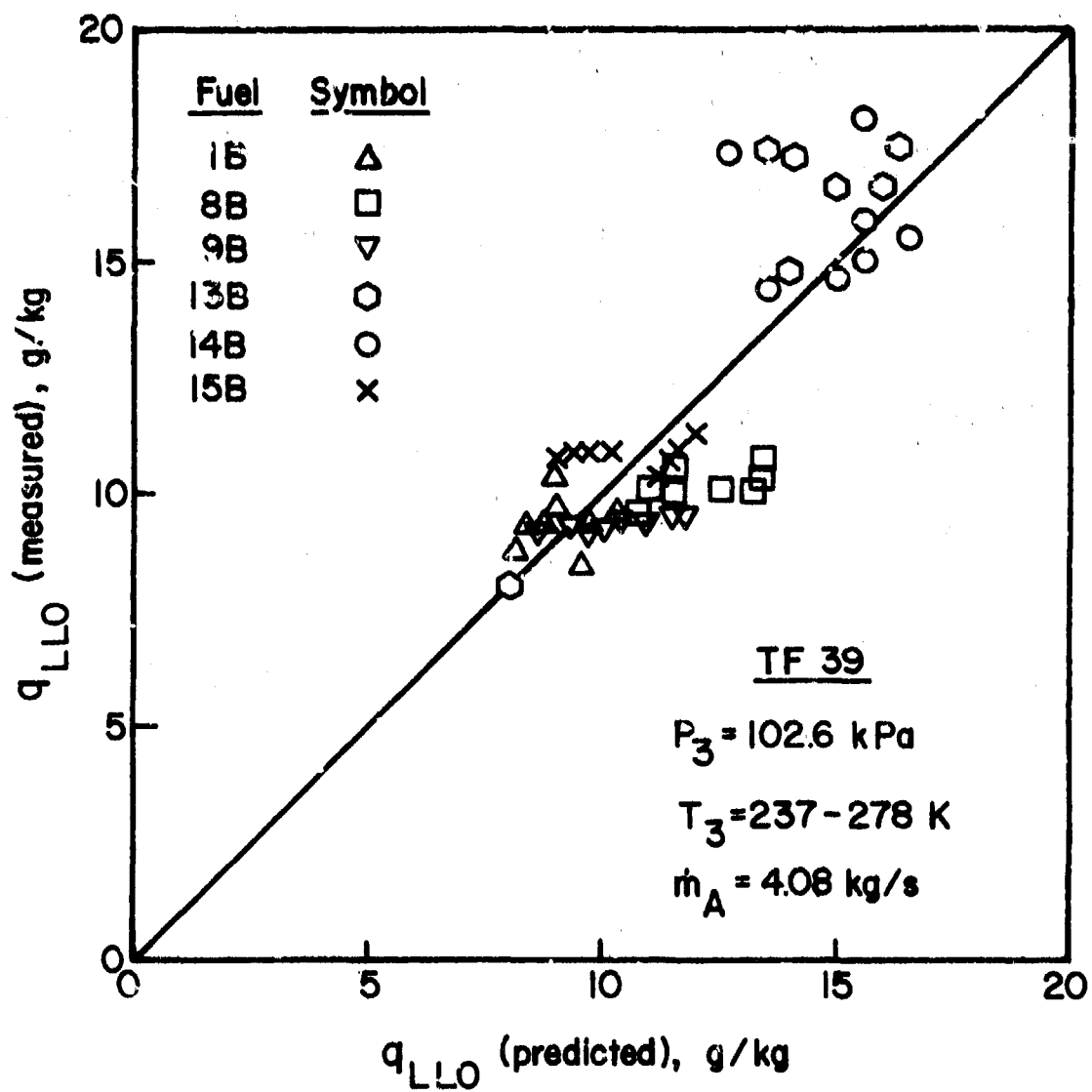


Figure 35. Comparison of Measured and Predicted Values of Lean Light Off for TF39 Combustor.

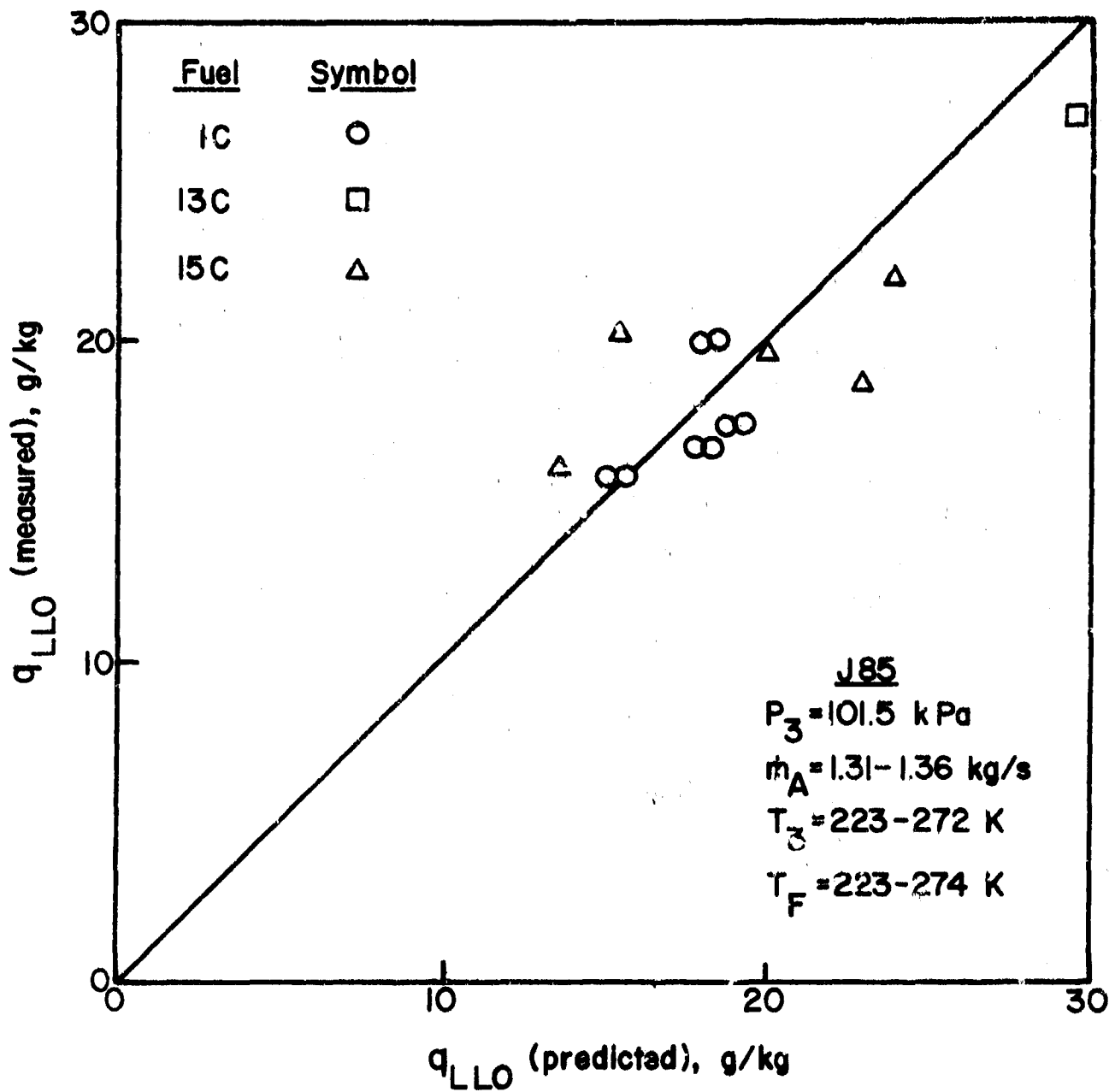


Figure 36. Comparison of Measured and Predicted Values of Lean Light Off for J85 Combustor.

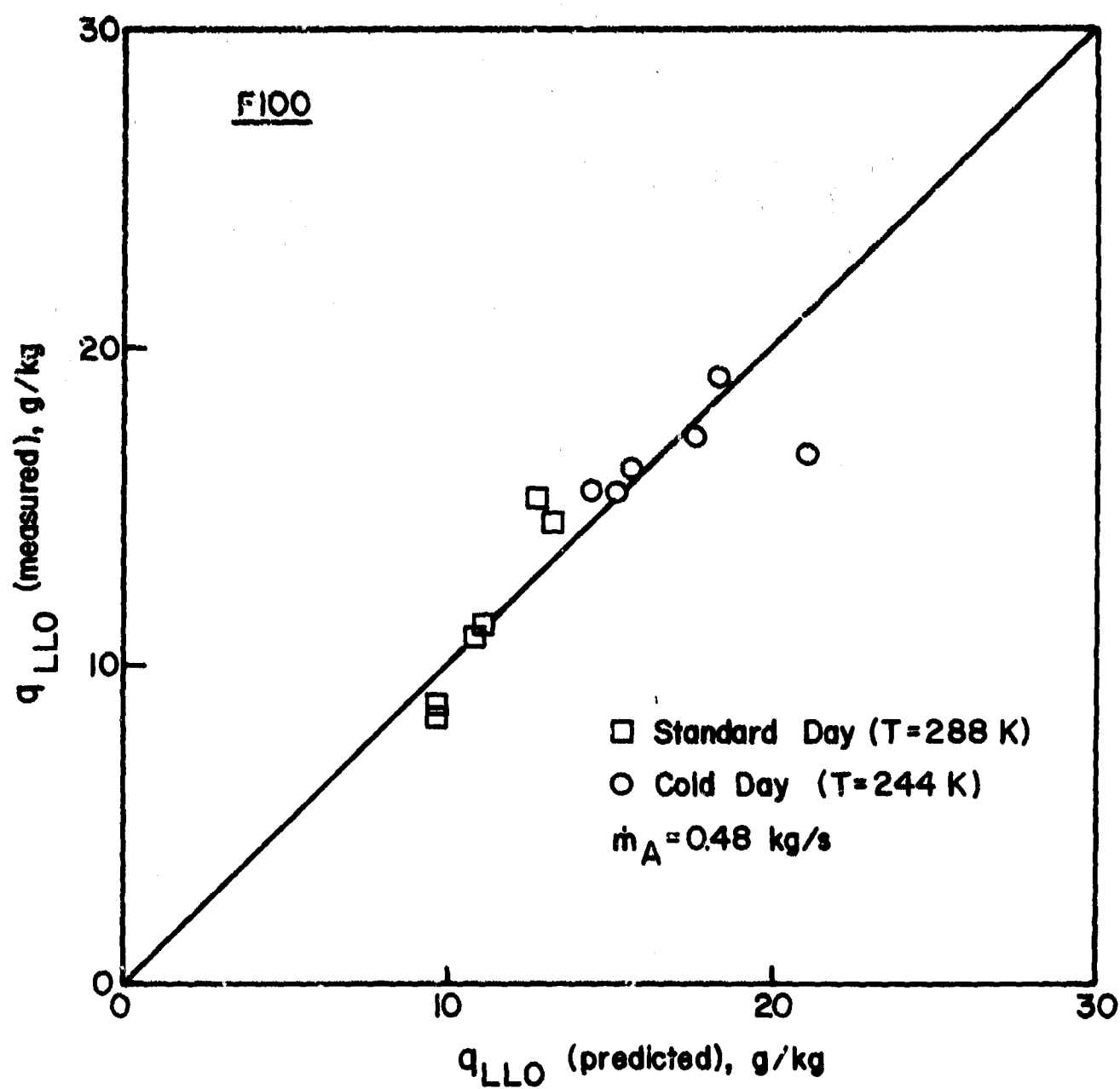


Figure 37. Comparison of Measured and Predicted Values of Lean Light Off for F100 Combustor.

SECTION VI

LINER WALL TEMPERATURE

For the purpose of analysis a liner may be regarded as a container of hot flowing gases surrounded by a casing in which air is flowing between the container and the casing. Broadly, the liner is heated by radiation and convection from the hot gases inside it, and is cooled by radiation to the outer casing and by convection to the annulus air. The relative proportions of the radiation and convection components depend upon the geometry and operating conditions of the system. Under equilibrium conditions the liner temperature is such that the internal and external heat fluxes at any point are just equal. Loss of heat by conduction along the liner wall is comparatively small and usually may be neglected. Under steady-state conditions, the rate of heat transfer into the wall must be balanced by the rate of heat transfer out. Under steady-state conditions

$$R_1 + C_1 = R_2 + C_2 \quad (18)$$

The derivations of suitable equations for R_1 , C_1 , R_2 and C_2 are fully described in reference 10. As these equations contain no drop-size terms they are unaffected by the results of the present investigation. Hence, the following discussion will be confined to summarizing the key features of the calculation procedures for estimating liner wall temperature, along with a comparison of measured and predicted values of T_w for various types of combustors.

1. Internal Radiation

This is the component of heat transfer that is most affected by a change in fuel type. It is given by [18]

$$R_1 = 0.5 \sigma (1 + \epsilon_w) \epsilon_g T_g^{1.5} (T_g^{2.5} - T_w^{2.5}) \quad (19)$$

where σ = Stefan Boltzmann constant

ϵ_w = liner wall emissivity

ϵ_g = gas emissivity

T_g = gas temperature

T_w = wall temperature

The 'bulk' or mean gas temperature, T_g , is obtained as the sum of the chamber entry temperature, T_3 , and the temperature rise due to combustion, ΔT_{comb} .

Thus:

$$T_g = T_3 + \Delta T_{\text{comb}} \quad (20)$$

ΔT_{comb} may be read off standard temperature rise curves. The appropriate value of fuel/air ratio is the product of the local fuel/air ratio and the local level of combustion efficiency. Most heat transfer calculations are carried out at high pressure conditions where it is reasonable to assume a combustion efficiency of 100 percent.

For the luminous flames associated with the combustion of heterogeneous fuel-air mixtures, the value of ϵ_g for insertion in Eq. (19) is obtained as [18]

$$\epsilon_g = 1 - \exp[-290 P_3 L (q l_b)^{0.5} T_g^{-1.5}] \quad (21)$$

where q is the local fuel/air ratio and l_b is the 'beam length' of the radiating gas. The luminosity factor, L , is an empirical correction introduced to obtain reasonable agreement between experimental data on gas radiation and predictions from Eq. (21). Analysis of the experimental data contained in references 1 thru 6 led to the following expression for L . [7]

$$L = 336/(\text{percent hydrogen})^2 \quad (22)$$

Substitution of this value of L into Eq. (21) allows calculations of flame radiation to be carried out for all fuels over the entire range of test conditions.

2. External Radiation

The radiation heat transfer from the liner wall to the outer casing, R_2 , can be estimated only approximately due to lack of accurate information on wall emissivities. For this reason it is sufficient to use the cooling-air temperature, T_3 , in place of the unknown temperature of the outer air casing. Also, for radiation across a long annular space, the geometric shape factor can be assumed equal to unity, and the expression for net radiation flux then reduces to

$$R_2 = 0.4 \sigma (T_w^4 - T_3^4) \quad (23)$$

3. Internal Convection

Of the four heat transfer processes which together determine

the liner temperature, this component is the most difficult to estimate accurately. In the primary zone, the gases involved are at high temperature and undergoing rapid physical and chemical change. Further difficulty is introduced by the existence within the primary zone of steep gradients of temperature, velocity, and composition. Uncertainties regarding the airflow pattern, the state of the boundary-layer development and the effective gas temperature make the choice of a realistic model almost arbitrary.

In the absence of more exact data it is reasonable to assume that some form of the classical heat-transfer relation for straight pipes will hold for conditions inside a liner, using a Reynolds number index consistent with established practice for conditions of extreme turbulence. This leads to an expression of the form [18]

$$C_1 = 0.017 \left[\frac{k_g}{D_L^{0.2}} \right] \left[\frac{\dot{m}_{gz}}{A_L \mu_g} \right]^{0.8} (T_g - T_w) \quad (24)$$

4. External Convection

This is obtained as [18]

$$C_2 = 0.020 \left[\frac{k_A}{D_{an}^{0.2}} \right] \left[\frac{\dot{m}_{an}}{A_{an} \mu_A} \right]^{0.8} (T_w - T_3) \quad (25)$$

The fluid properties are evaluated at the annulus air temperature, T_3 . In practice, the cooling air temperature increases

during its passage downstream, but normally this amounts to no more than a few degrees and can reasonably be neglected.

For equilibrium

$$R_1 + C_1 = R_2 + C_2 \quad (18)$$

Solution of this equation yields the wall temperature, T_w .

The value of T_w as determined by the method outlined above represents the liner wall temperature that would be obtained in the absence of internal wall cooling. As references 1 thru 6 do not contain the detailed information needed to estimate film cooling effects on T_w , it was decided to calculate 'uncooled' wall temperatures for four combustors only, namely J79-17A, J79-17C, F101 and TF41, in order to ascertain if the results obtained reflected anticipated trends in regard to the effect of fuel hydrogen content on liner wall temperature. The results of these calculations are shown in Figs. 38 thru 41 for all fuels as plots of T_w versus hydrogen content.

It may be noted in Figs. 38 thru 41 that the calculated values of T_w are generally higher than the corresponding measured values due to neglect of internal wall cooling. Only at low power conditions, where the errors incurred through neglect of internal wall cooling are partially balanced by the assumption of 100 percent combustion efficiency in the combustion zone, do the measured and calculated wall temperatures roughly coincide.

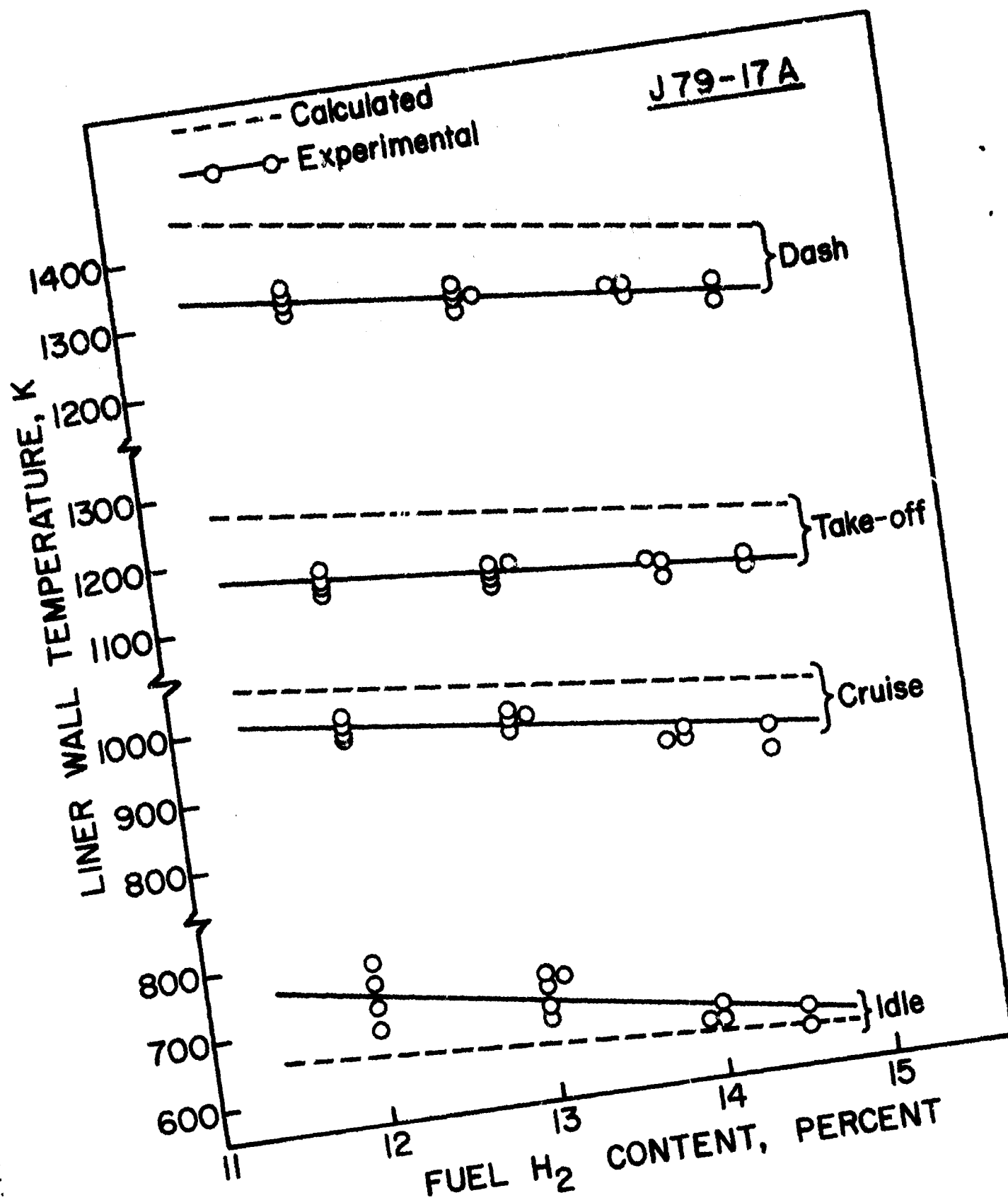


Figure 38. Comparison of Measured and Predicted Values on the Effect of H₂ Content on Liner Temperature for J79-17A Combustor.

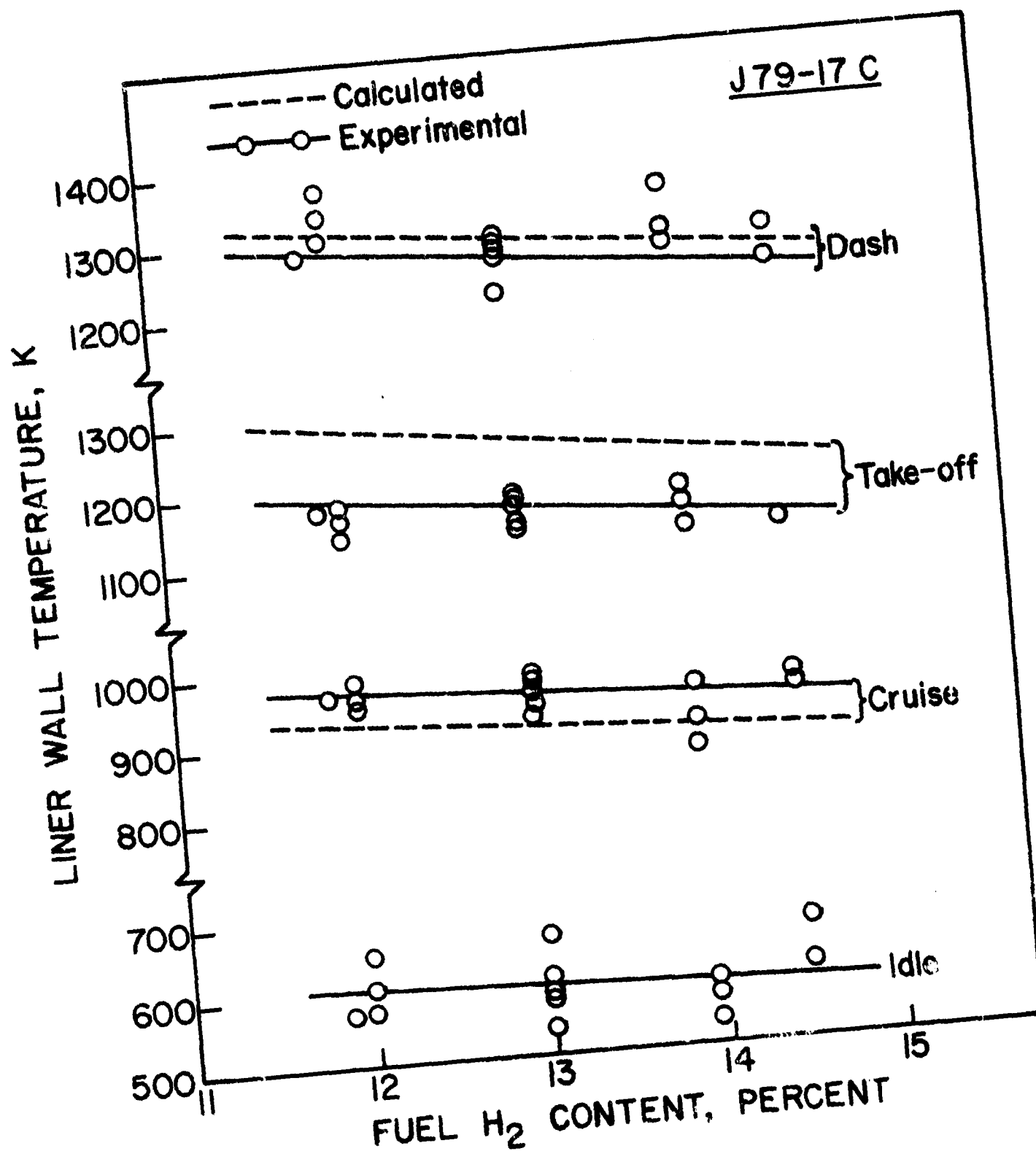


Figure 39. Comparison of Measured and Predicted Values on the Effect of H₂ Content on Liner Temperature for J79-17C Combustor.

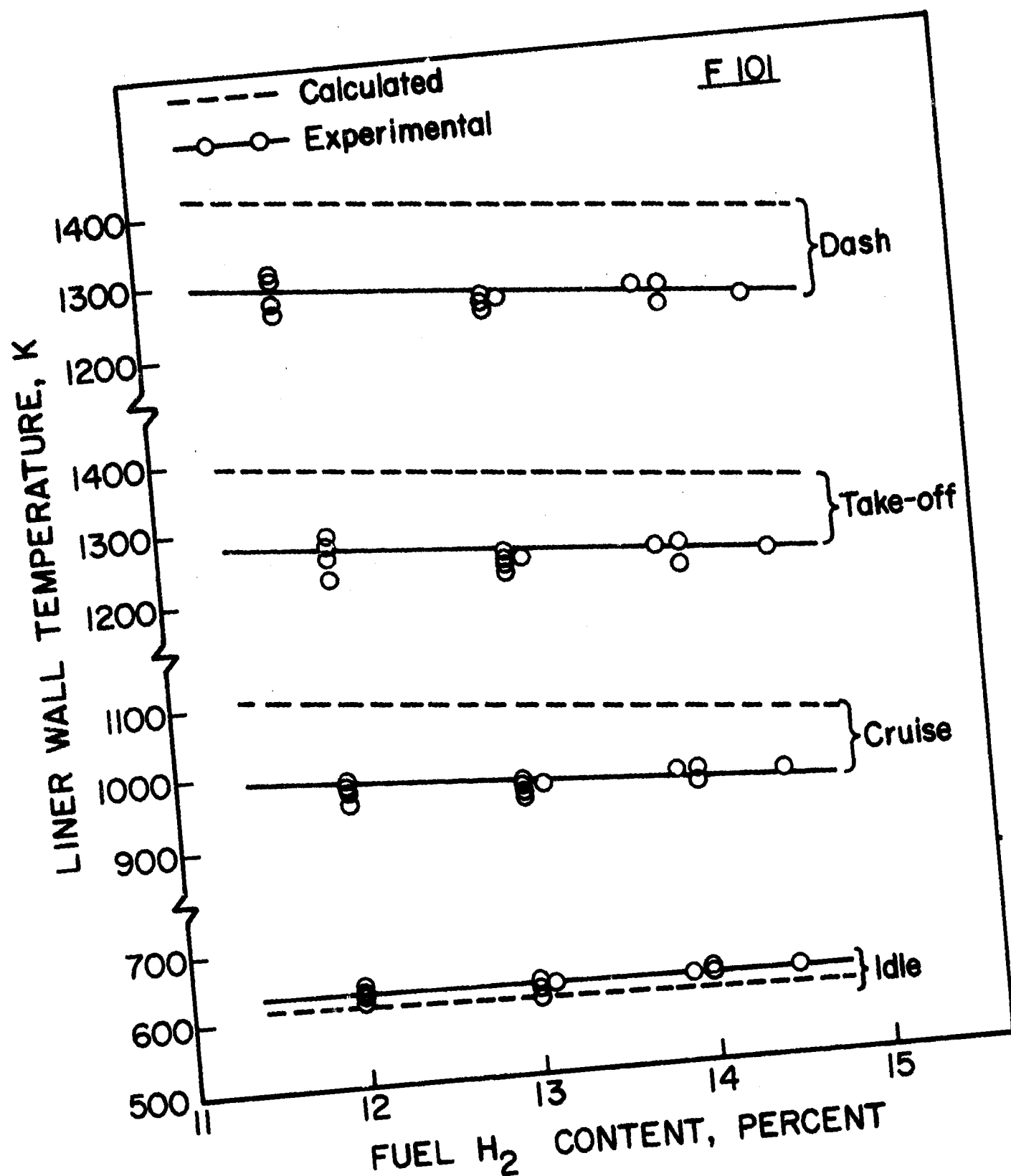


Figure 40. Comparison of Measured and Predicted Values on the Effect of H₂ Content on Liner Temperature for F101 Combustor.

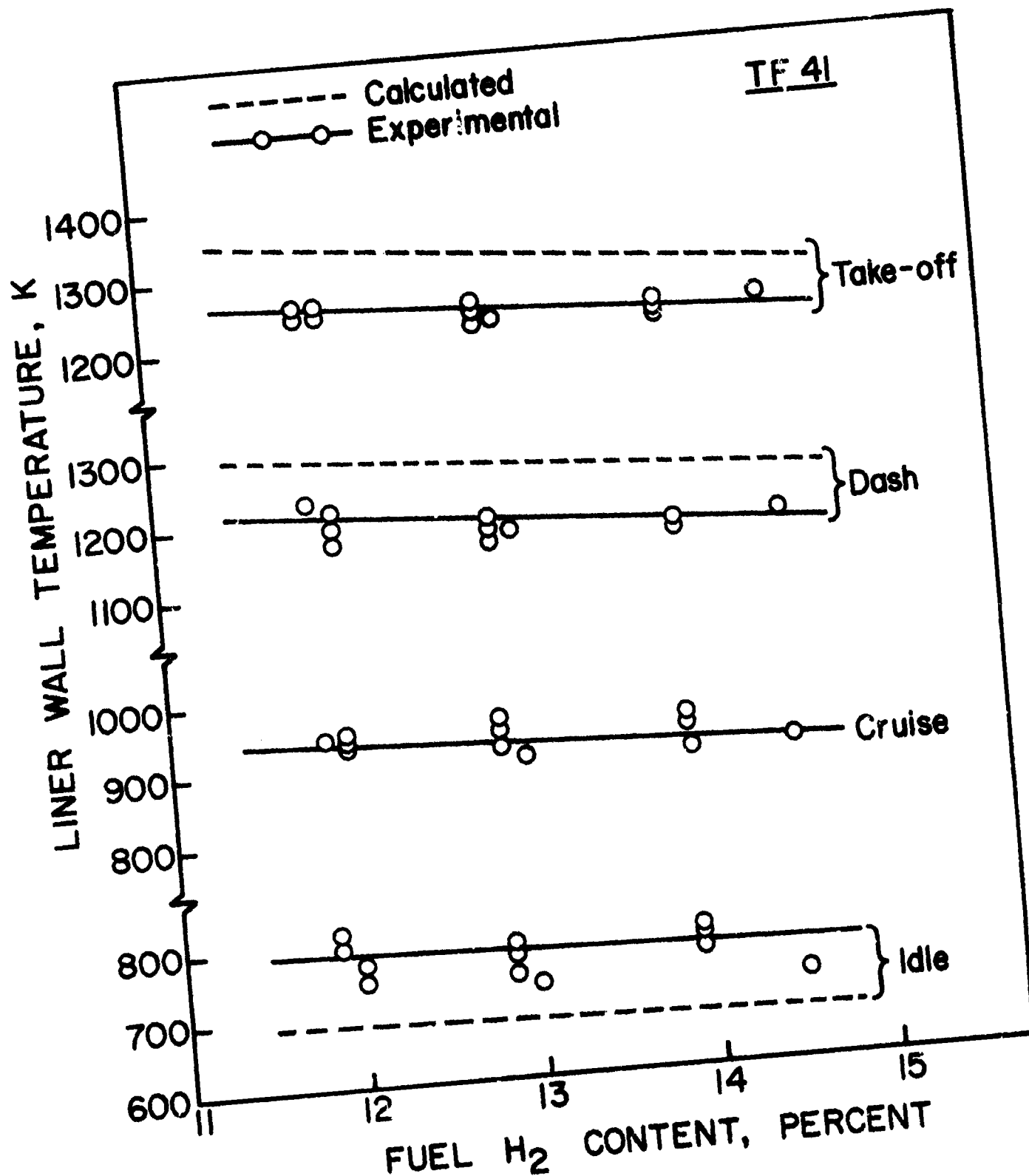


Figure 41. Comparison of Measured and Predicted Values on the Effect of H₂ Content on Liner Temperature for TF41 Combustor.

These factors are not considered too serious in a study that is mainly concerned with fuel type, because they apply with equal force to all fuels. The fact that the measured and calculated values of T_w follow the same trend, as evidenced by Figs. 38 thru 41, tends to support the validity of using the luminosity factor concept as a convenient means for incorporating fuel hydrogen content into the 'standard' equation for flame emissivity. Thus Eq. (21) may be rewritten as

$$\epsilon_g = 1 - \exp \left[- 97440 P_3 (\%H_2)^{-2} (q l_b)^{0.5} T_g^{-1.5} \right] \quad (26)$$

SECTION VII

POLLUTANT EMISSIONS

The pollutant emissions of most concern for the aircraft gas turbine are oxides of nitrogen (NO_x), carbon monoxide (CO), unburned hydrocarbons (UHC), and smoke. The concentration levels of these pollutants can be related directly to the temperature, time, and concentration histories of the combustor. These histories vary from one combustor to another and, for any given combustor, with changes in operating conditions. The nature of pollutant formation is such that the concentrations of carbon monoxide and unburned hydrocarbons are highest at low-power conditions and diminish with increase in power. In contrast, oxides of nitrogen and smoke are fairly insignificant at low power settings and attain maximum values at the highest power condition. The basic causes of these pollutants and the various methods employed to alleviate them have been fully discussed elsewhere [10].

Most modeling of emission characteristics has been concerned with oxides of nitrogen, but efforts have also been made to predict the formation of other pollutant species. To be successful a model must accommodate the complex flow behavior and include a kinetic scheme of the important chemical reactions occurring within the combustor. The kinetics of some relevant combustion processes are, unfortunately, not well understood at the present time, particularly for the production of carbon, carbon monoxide and the hydrocarbon species that are intermediate in

the fuel oxidation process.

The primary requirement for a satisfactory emissions model for gas-turbine combustors is that it should represent an optimum balance between accuracy of representation, utility, ease of use, economy of operation, and capability for further improvement. In recent years, considerable efforts have been directed toward the development of relatively complex mathematical emissions models that can be applied to gas turbines [19-27]. The high cost and complexity of the more sophisticated mathematical models have encouraged the development of semi-empirical models for NO_x and CO emissions. For example, Hung's approach has been used successfully in predicting the influence on NO_x emissions of water injection and wide variations in fuel type [26,27]. Other successful semi-empirical models for predicting emissions have been developed by Fletcher and Heywood [19,28] and by Hammond and Mellor [29,30].

Empirical models can also play an important role in the design and development of low emission combustors. They may serve to reduce the complex problems associated with emissions to forms which are more meaningful and tractable to the combustion engineer who often requires only an insight and a quick estimate of the levels attainable with the design variables at his disposal. They also permit more accurate correlations of emissions for any one specific combustor than can be achieved by the more general analytical models.

1. Oxides of Nitrogen

Lefebvre's semi-empirical model for the prediction of pollutant emissions [9], based on considerations of mixing rates, chemical reaction rates, and combustor residence time, leads to the following expression for NO_x .

$$\text{NO}_x = \frac{9 \times 10^{-8} P_3^{1.25} V_c \exp(0.01 T_{st})}{m_A T_{pz}} \text{ g/kg} \quad (27)$$

Equation (27) demonstrates that the only influence of fuel type on NO_x formation is via the two temperature's terms, T_{pz} and T_{st} . The former is calculated as

$$T_{pz} = T_3 + \Delta T_{pz}$$

where ΔT_{pz} is the temperature rise due to combustion corresponding to the inlet temperature, T_3 , and the primary-zone fuel/air ratio. T_{st} is the stoichiometric flame temperature corresponding to the inlet temperature, T_3 . Equation (27) suggests that, in the combustion of heterogeneous fuel-air mixtures, it is the stoichiometric flame temperature that determines the formation of NO_x . However, for the residence time in the combustion zone, which is also significant to NO_x formation, the appropriate temperature term is the bulk value, T_{pz} , as indicated in the denominator of Eq. (27).

It should be noted that Eq. (27) is suitable for conventional spray combustors only. For lean premix/prevaporize combustors, in which the maximum attainable temperature is T_{pz} ,

it may still be used, provided that T_{pz} is substituted for T_{st} . It should also be noted that predictions of NO_x based on Eq. (27) tend to be too high when the overall combustor air/fuel ratio exceeds a value of around 100. This is because with diminishing fuel/air ratio the flame shrinks back toward the fuel nozzle and no longer occupies the entire combustion volume, V_c . However, this is not considered a serious drawback since, in practice, interest is normally focused on conditions of high fuel/air ratio, where NO_x formation rates attain their highest values.

The excellent correlation of data provided by Eq. (27) is illustrated in Figs. 42 thru 52. These figures include all combustors except the J85 for which the measured values are too low for satisfactory correlation.

2. Carbon Monoxide

For the prediction of CO emissions the relevant expression is [9]

$$CO = \frac{86 \dot{m}_A T_{pz} \exp(-0.00345 T_{pz})}{\left[V_c - 0.55 \times 10^{-6} \frac{f_{pz} \dot{m}_A}{\rho_{pz}} \frac{D_o^2}{\lambda_{eff}} \right] \left[\frac{\Delta P_L}{P_3} \right]^{0.5} P_3^{1.5}} \quad \text{g/kg} \quad (28)$$

As CO takes longer to form than NO_x , the relevant temperature is not the local peak value adjacent to the evaporating fuel drops, but the average value throughout the primary zone, namely T_{pz} . Also, because CO emissions are most important at low pressure conditions, where evaporation rates are relatively slow, it is necessary to reduce the combustion volume, V_c , by the volume

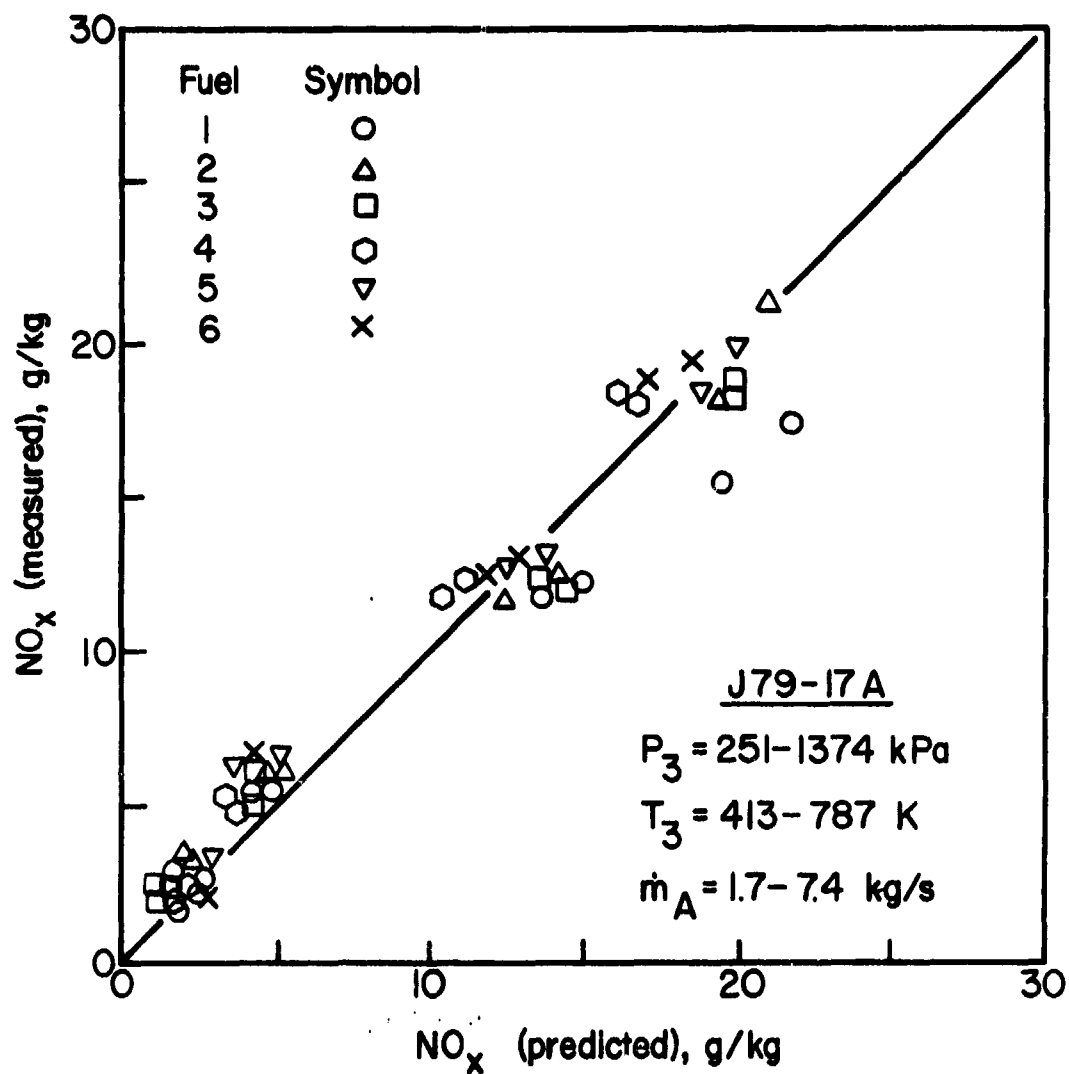


Figure 42. Comparison of Measured and Predicted Values of NO_x Emissions for J79-17A Combustor. (Fuels 1 to 6).^x

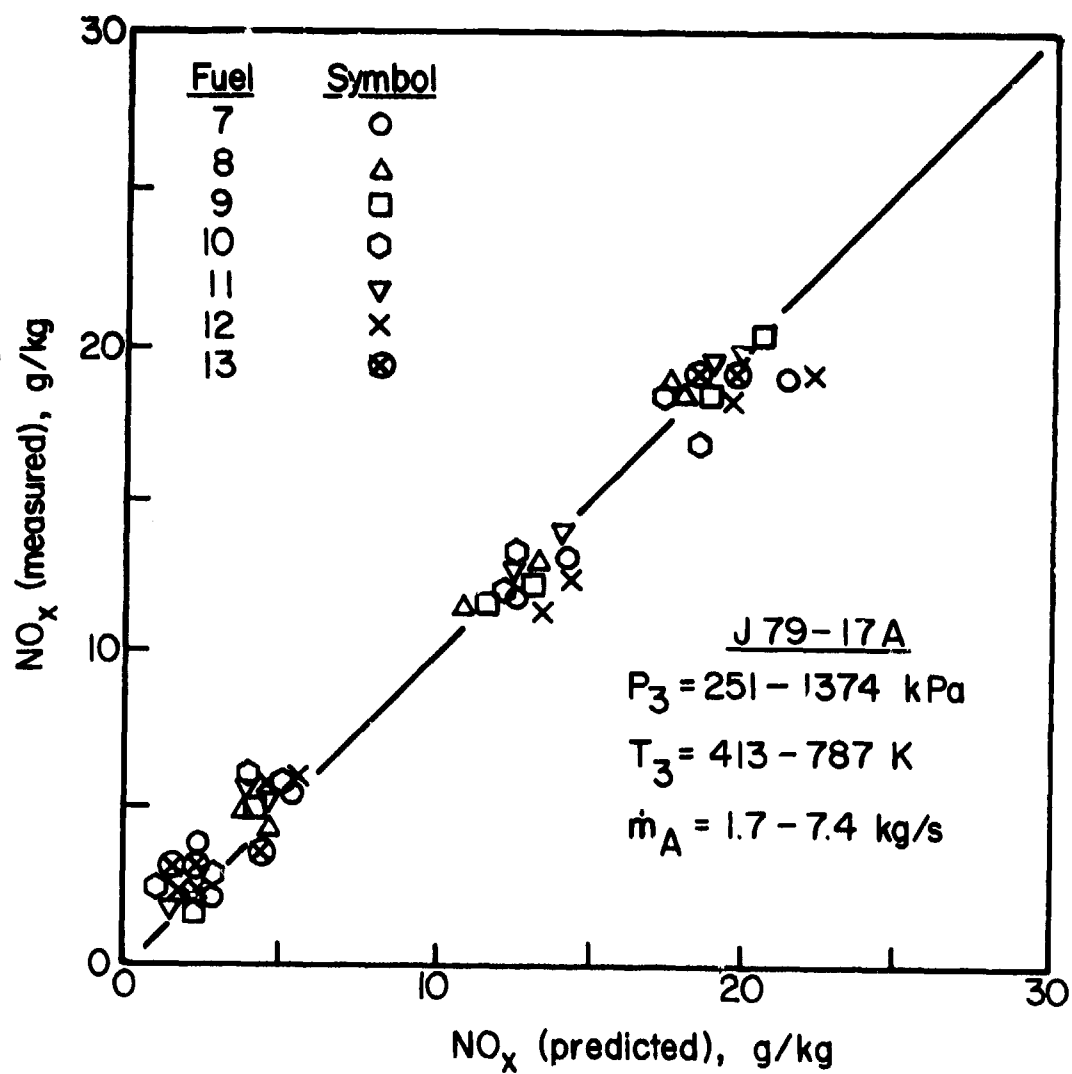


Figure 43. Comparison of Measured and Predicted Values of NO_x Emissions for J79-17A Combustor. (Fuels 7 to 13).^x

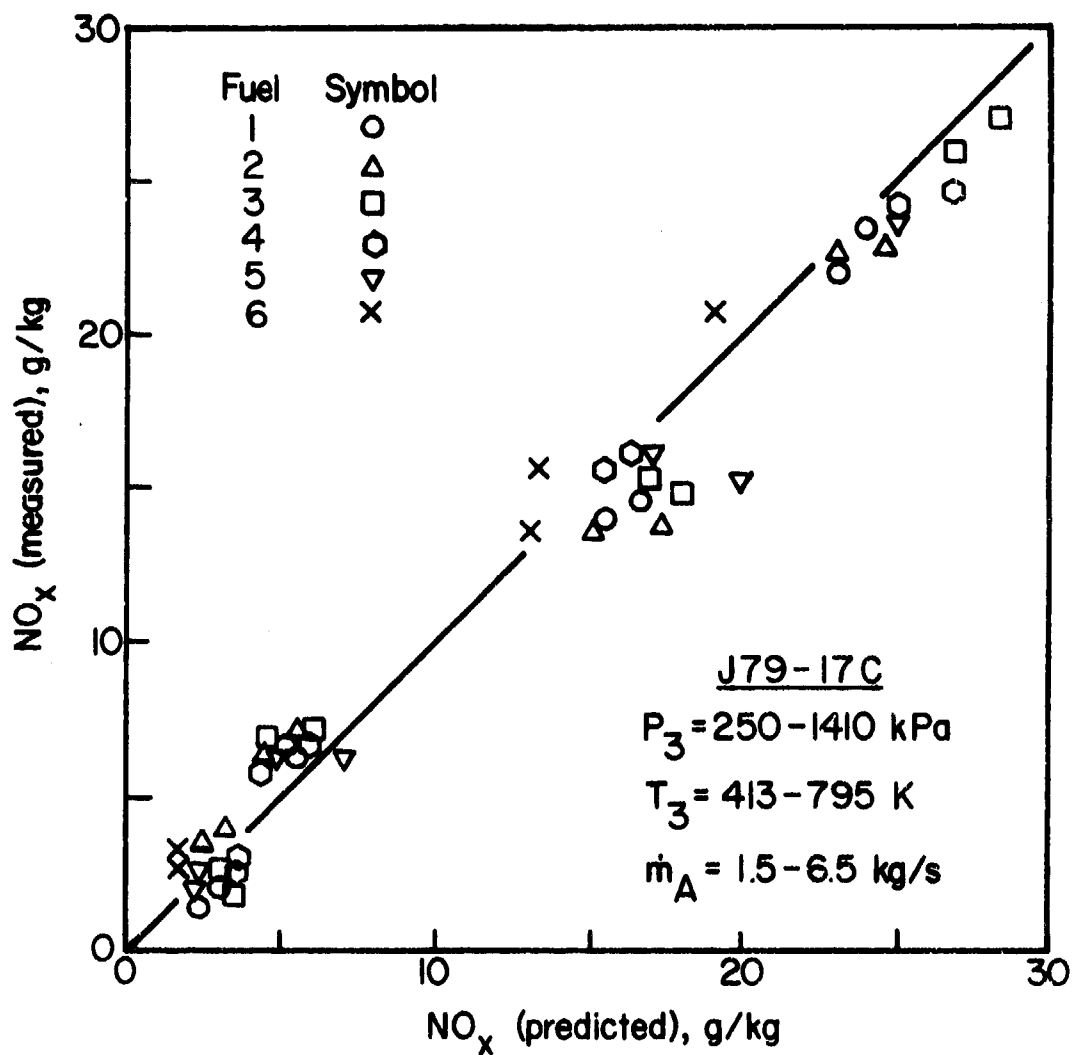


Figure 44. Comparison of Measured and Predicted Values of NO_x Emissions for J79-17C Combustor. (Fuels 1 to 6).^x

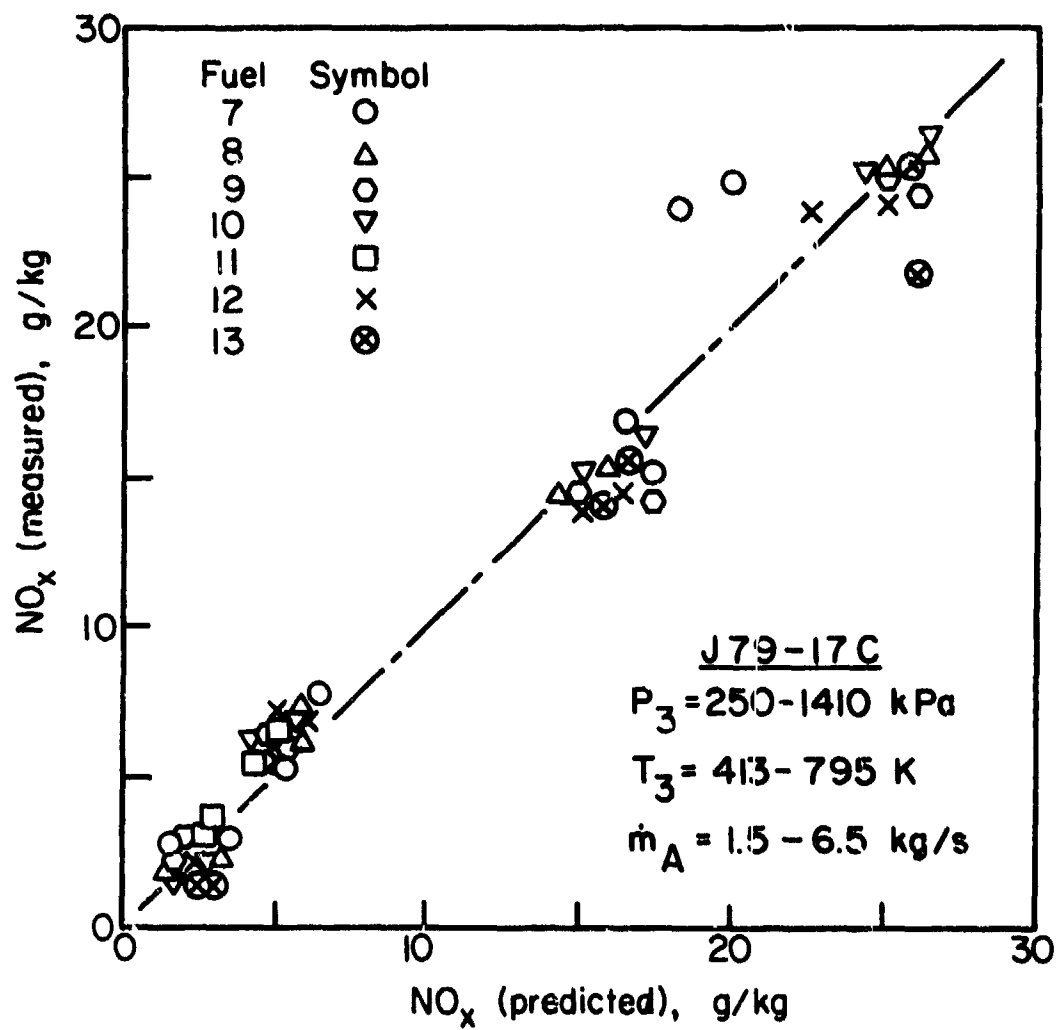


Figure 45. Comparison of Measured and Predicted Values of NO_x Emissions for J79-17C Combustor. (Fuels 7 to 13^{*}).

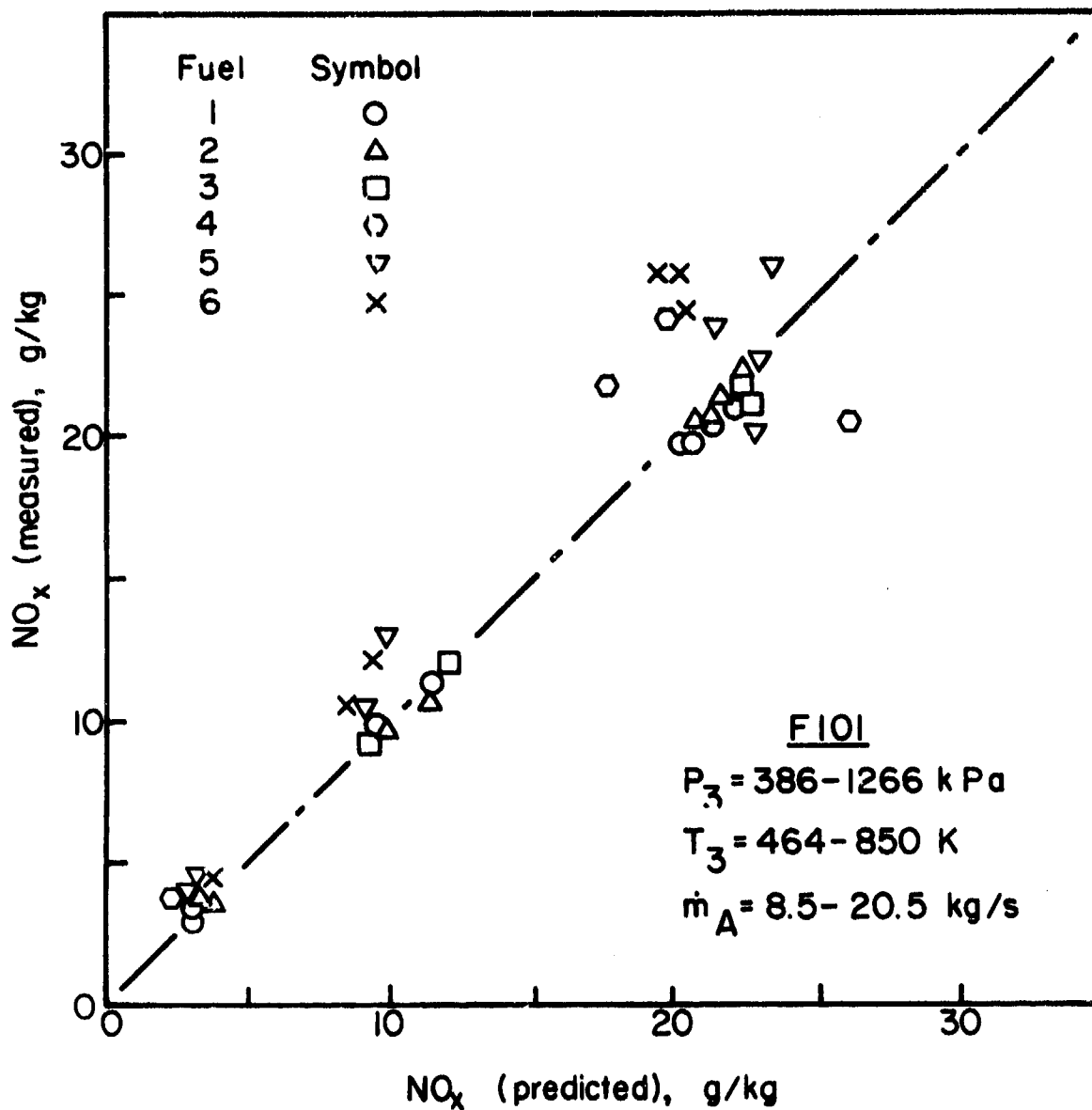


Figure 46. Comparison of Measured and Predicted Values of NO_x Emissions for F101 Combustor. (Fuels 1 to 6).

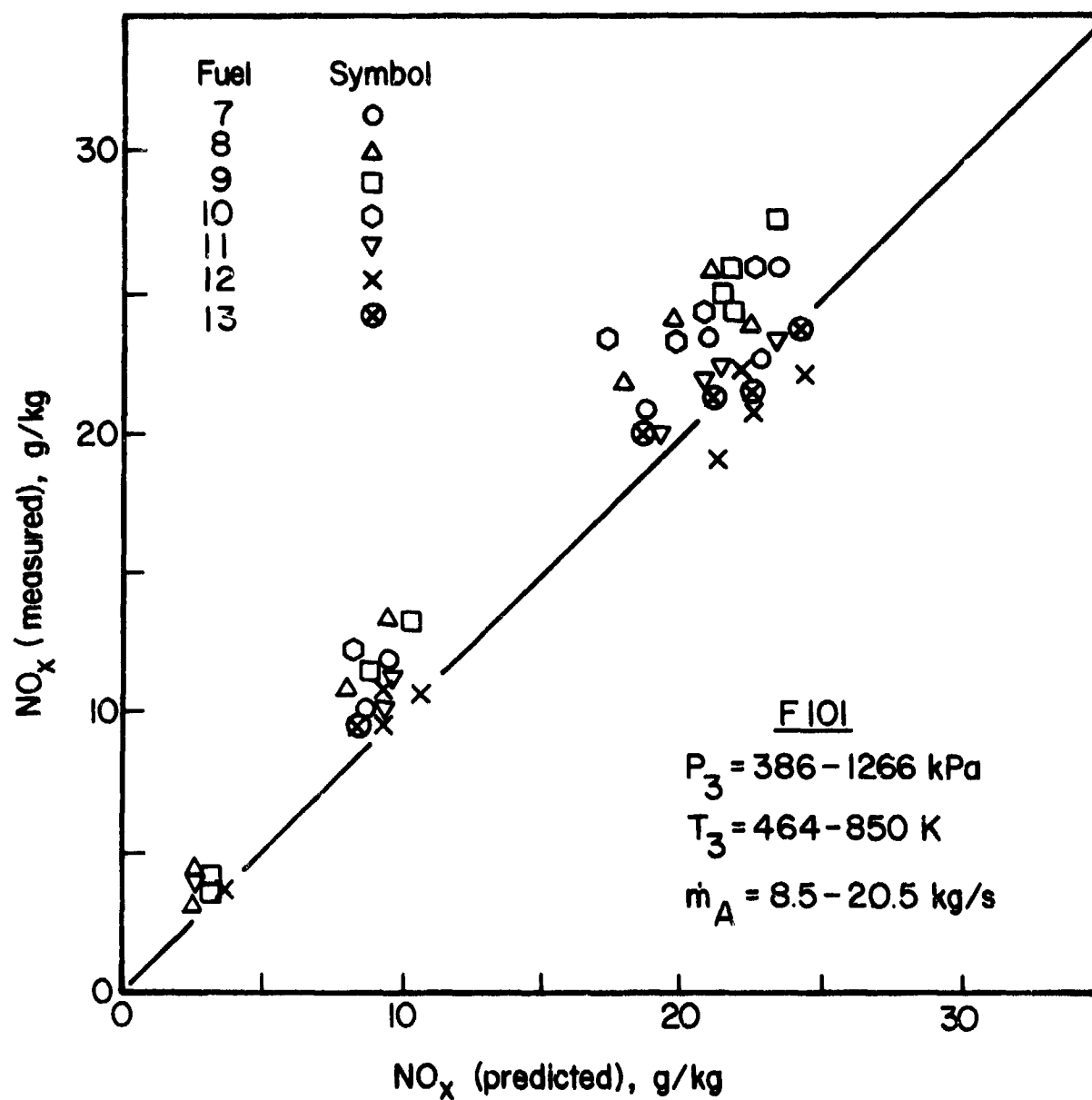


Figure 47. Comparison of Measured and Predicted Values of NO_x Emissions for F101 Combustor. (Fuels 7 to 13).

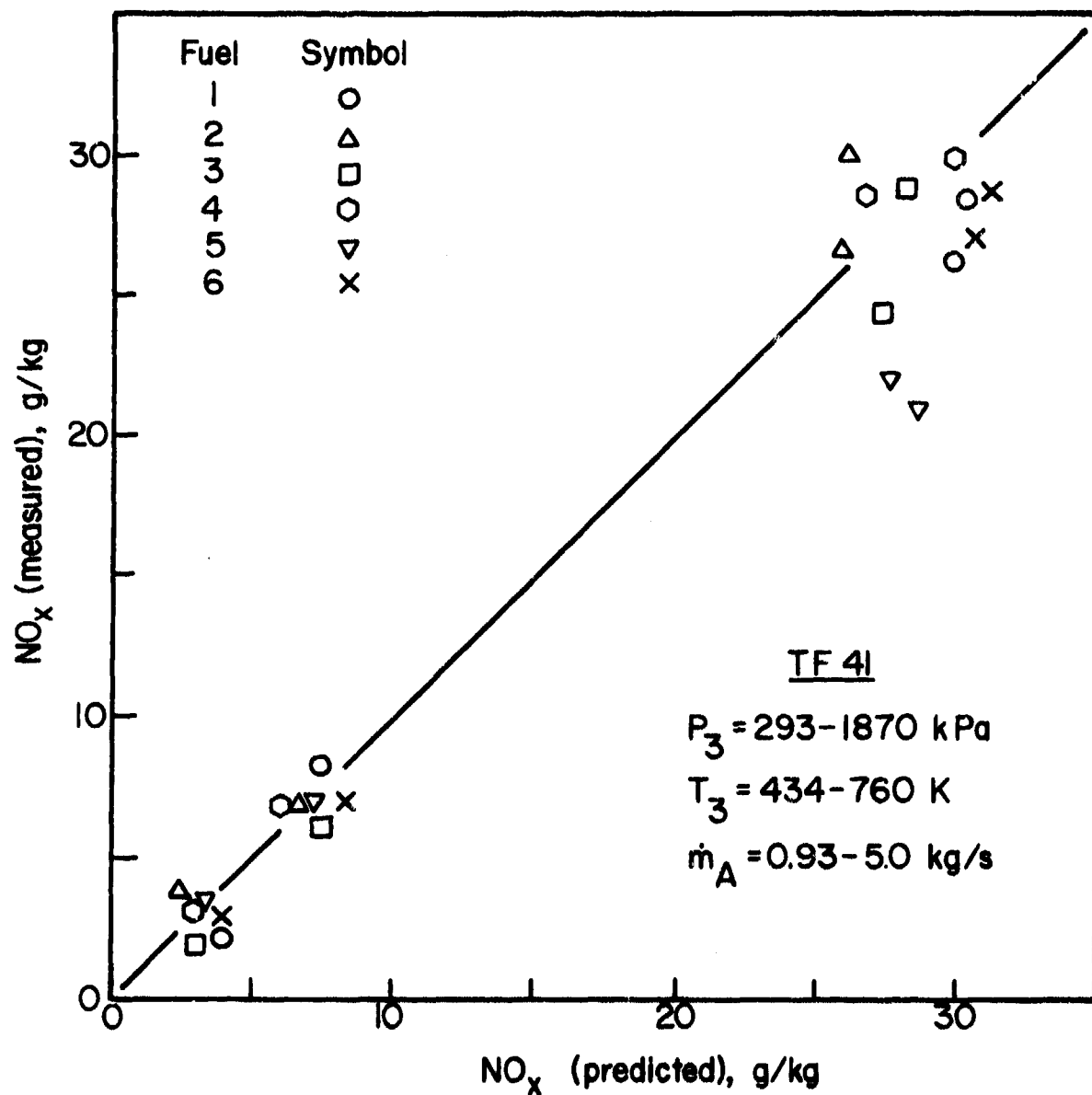


Figure 48. Comparison of Measured and Predicted Values of NO_x Emissions for TF41 Combustor. (Fuels 1 to 6).

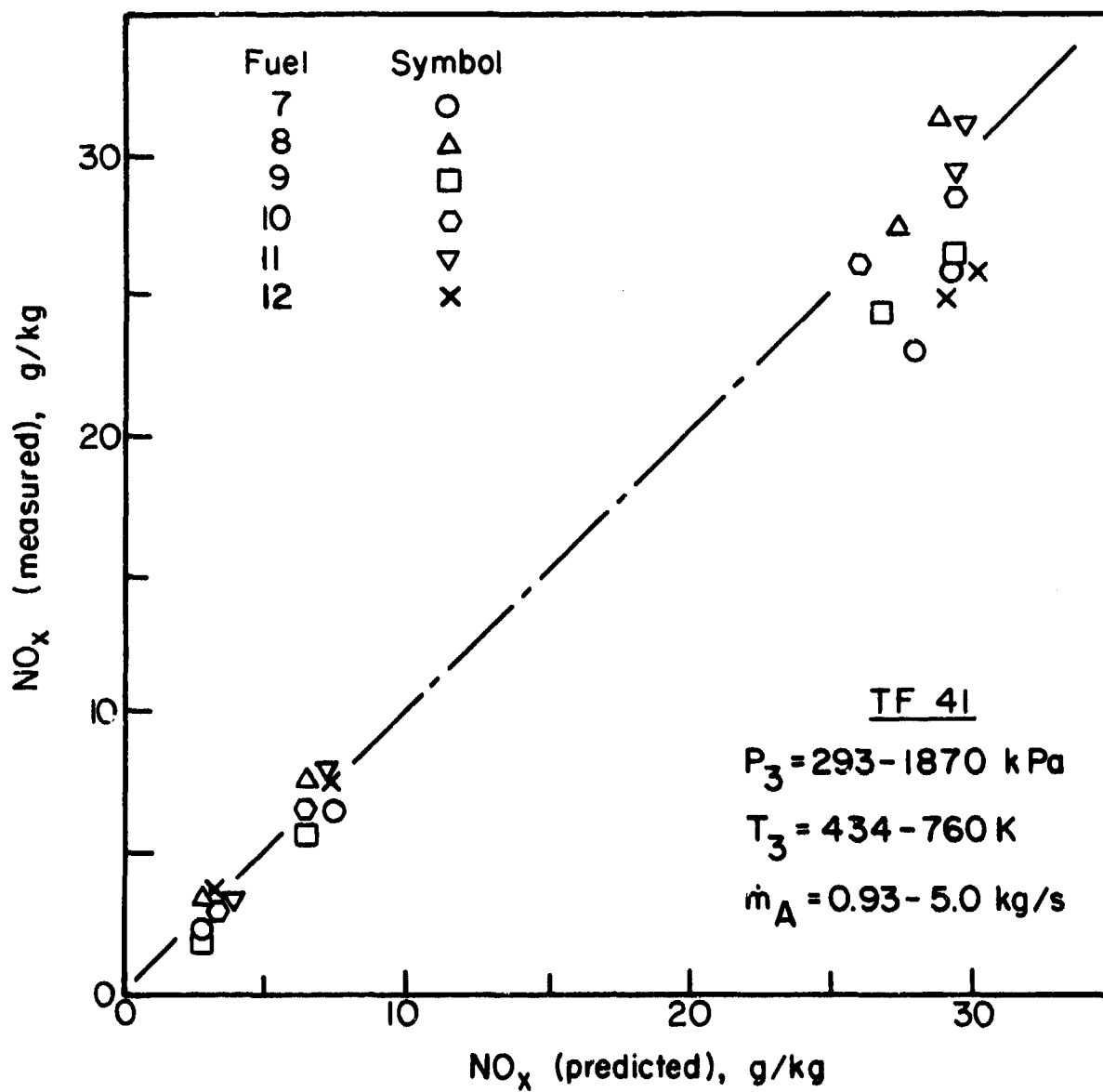


Figure 49. Comparison of Measured and Predicted Values of NO_x Emissions for TF41 Combustor. (Fuels 7 to 12). ^x

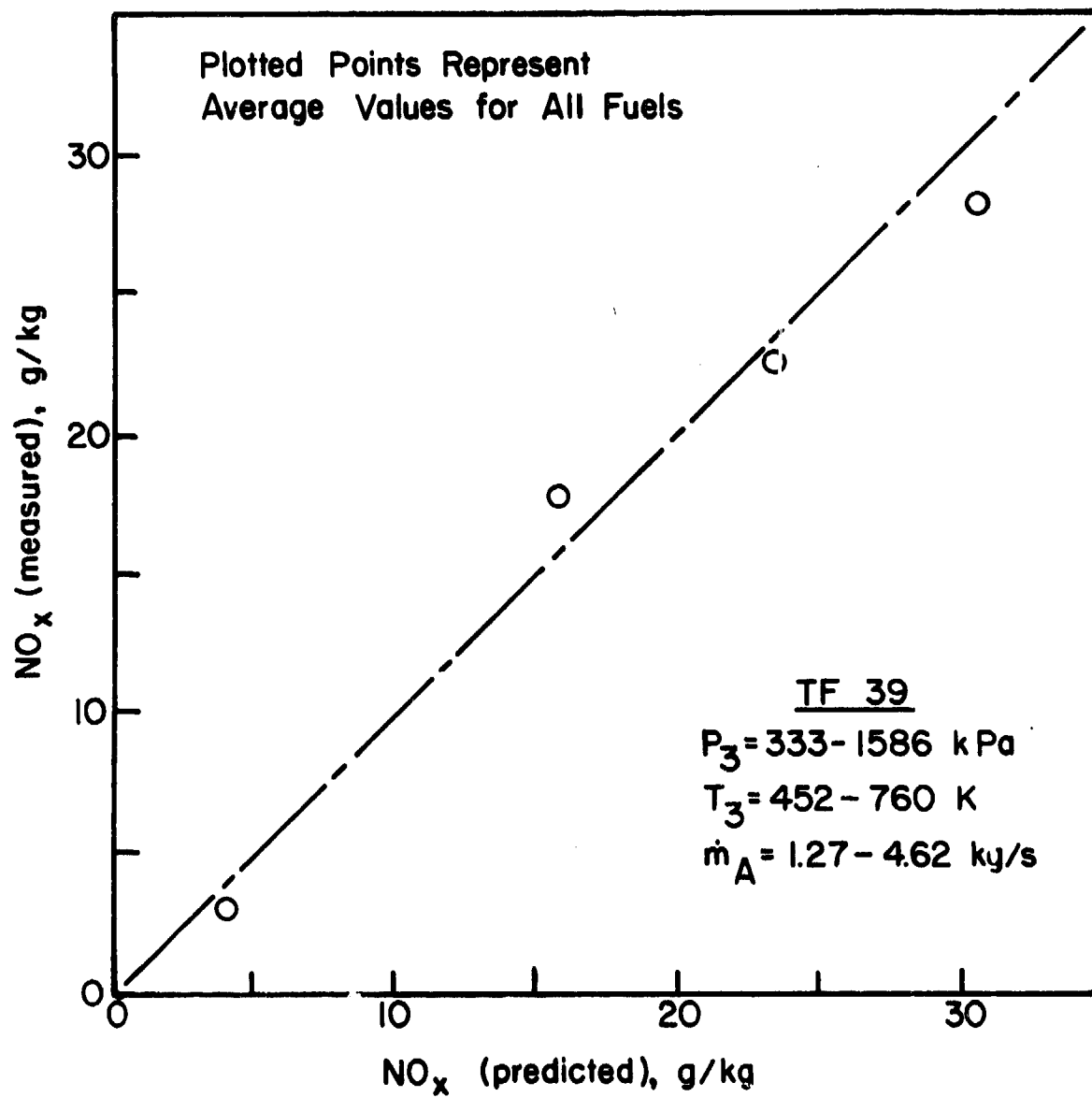


Figure 50. Comparison of Measured and Predicted Values of NO_x Emissions for TF39 Combustor.

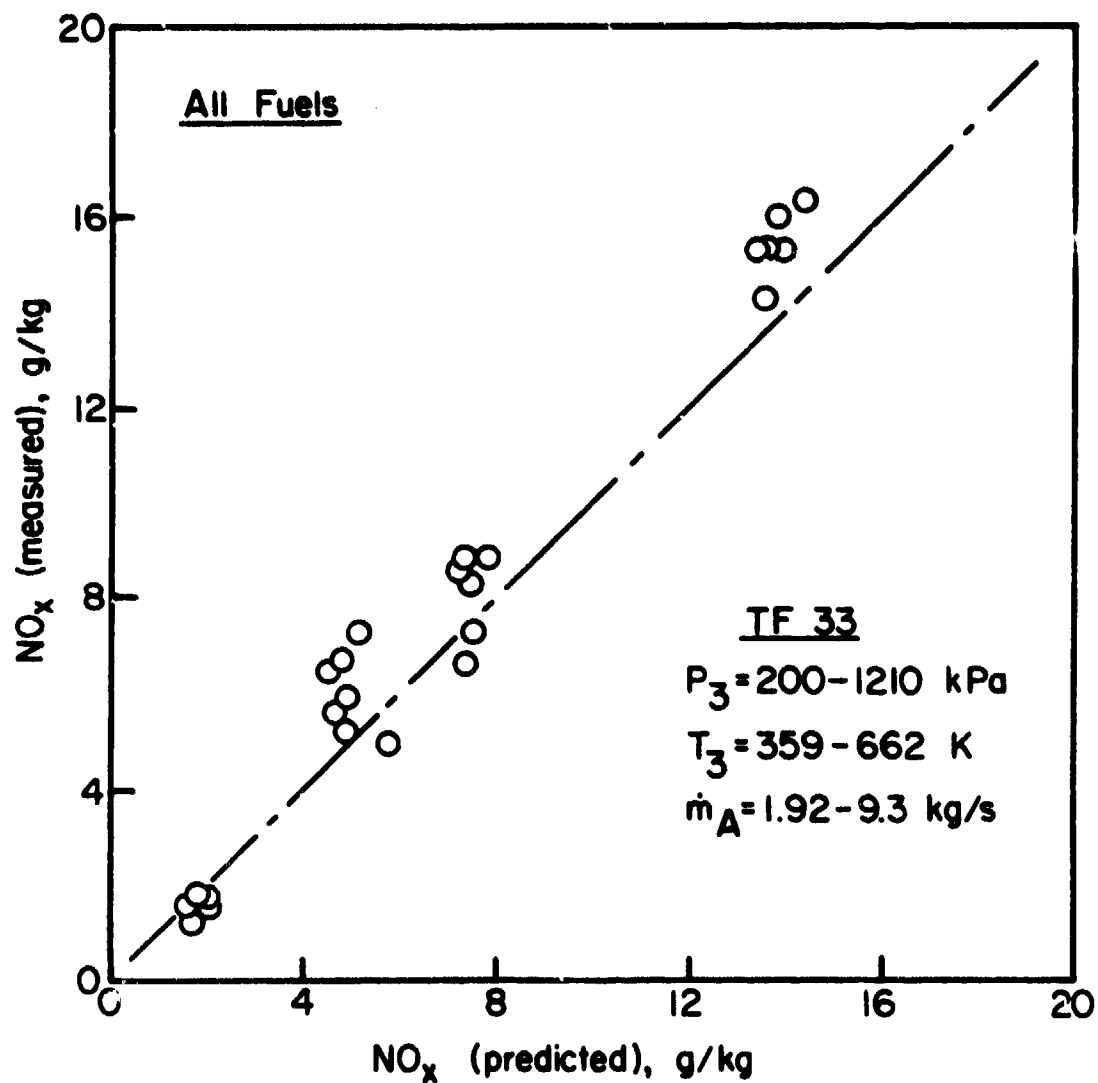


Figure 51. Comparison of Measured and Predicted Values of NO_x Emissions for TF33 Combustor.

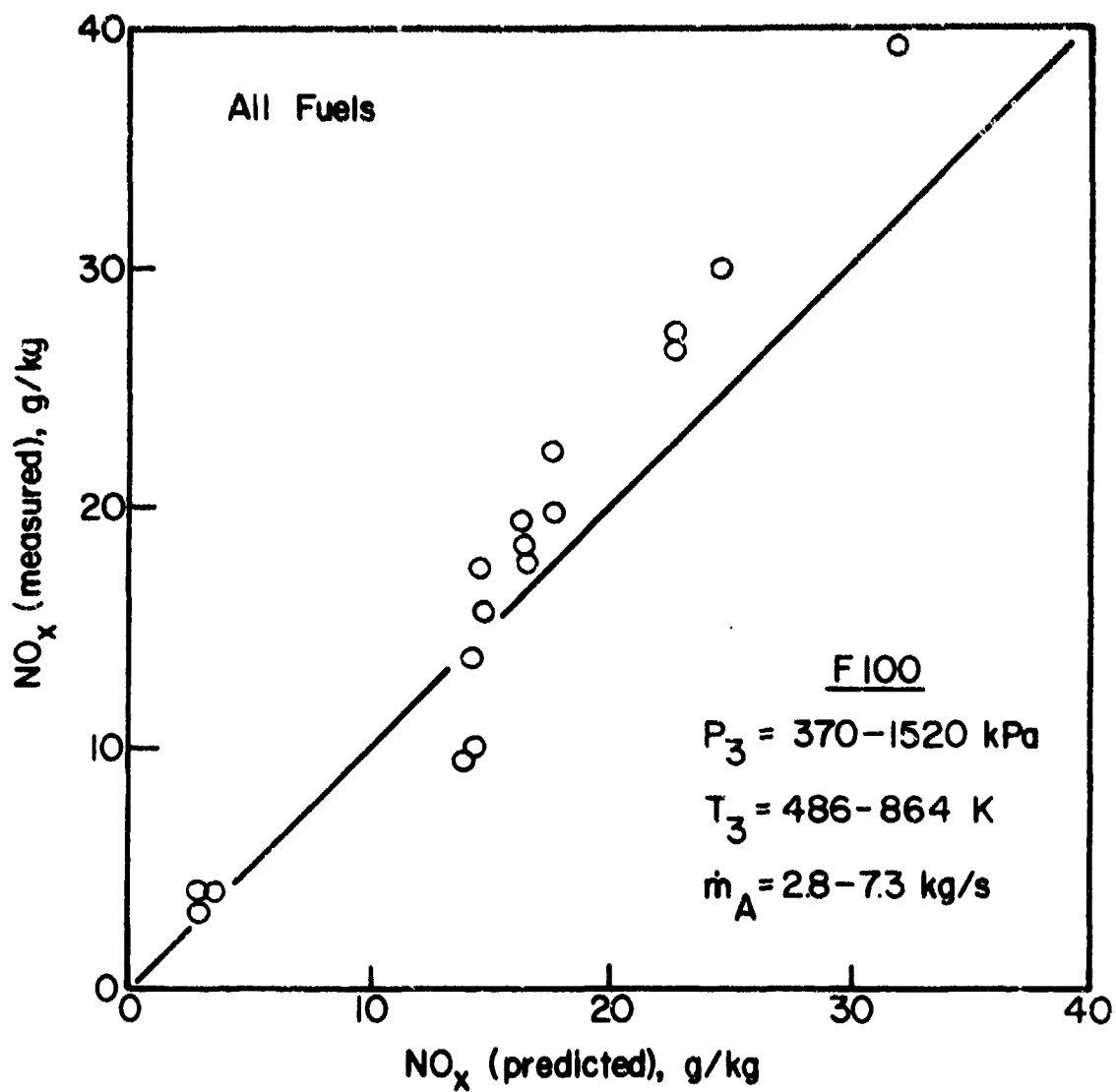


Figure 52. Comparison of Measured and Predicted Values of NO_x Emissions for F100 Combustor.

occupied in fuel evaporation, V_e . This was evaluated [8] as

$$V_e = 0.55 \times 10^{-6} f_{pz} \dot{m}_A D_o^2 / \rho_{pz} \lambda_{eff} \quad (29)$$

The correlations of experimental data achieved with Eq. (28) are illustrated in Figs. 53 thru 57 for the J79-17A, J79-17C, F101, TF41, and F100 combustors, respectively.

It is perhaps worthy of note that although Eqs. (27) and (28) have no strong theoretical foundation, they do embody the main variables of combustor size, pressure loss, flow proportions, and operating conditions of inlet air pressure, temperature, and mass flow rate. The effect of variations in overall combustor fuel/air ratio is also included via its influence on primary-zone temperature. Fuel type affects both flame temperature and mean drop size. For NO_x , drop size is unimportant since at the high pressure conditions where NO_x emissions are most prominent, the fraction of the total combustion volume employed in fuel evaporation is so small that wide variations in fuel drop size have a negligible effect on NO_x . However, at low pressure operation, where CO emissions attain their highest concentrations, a significant proportion of the primary-zone volume is needed to evaporate the fuel. Under these conditions, any factor that influences fuel evaporation rates, such as evaporation constant, or mean drop size, will have a direct effect on the volume available for chemical reaction and, therefore, on the emissions of CO and UHC. Thus, for the correlation of CO data the effects of fuel type cannot be ignored.

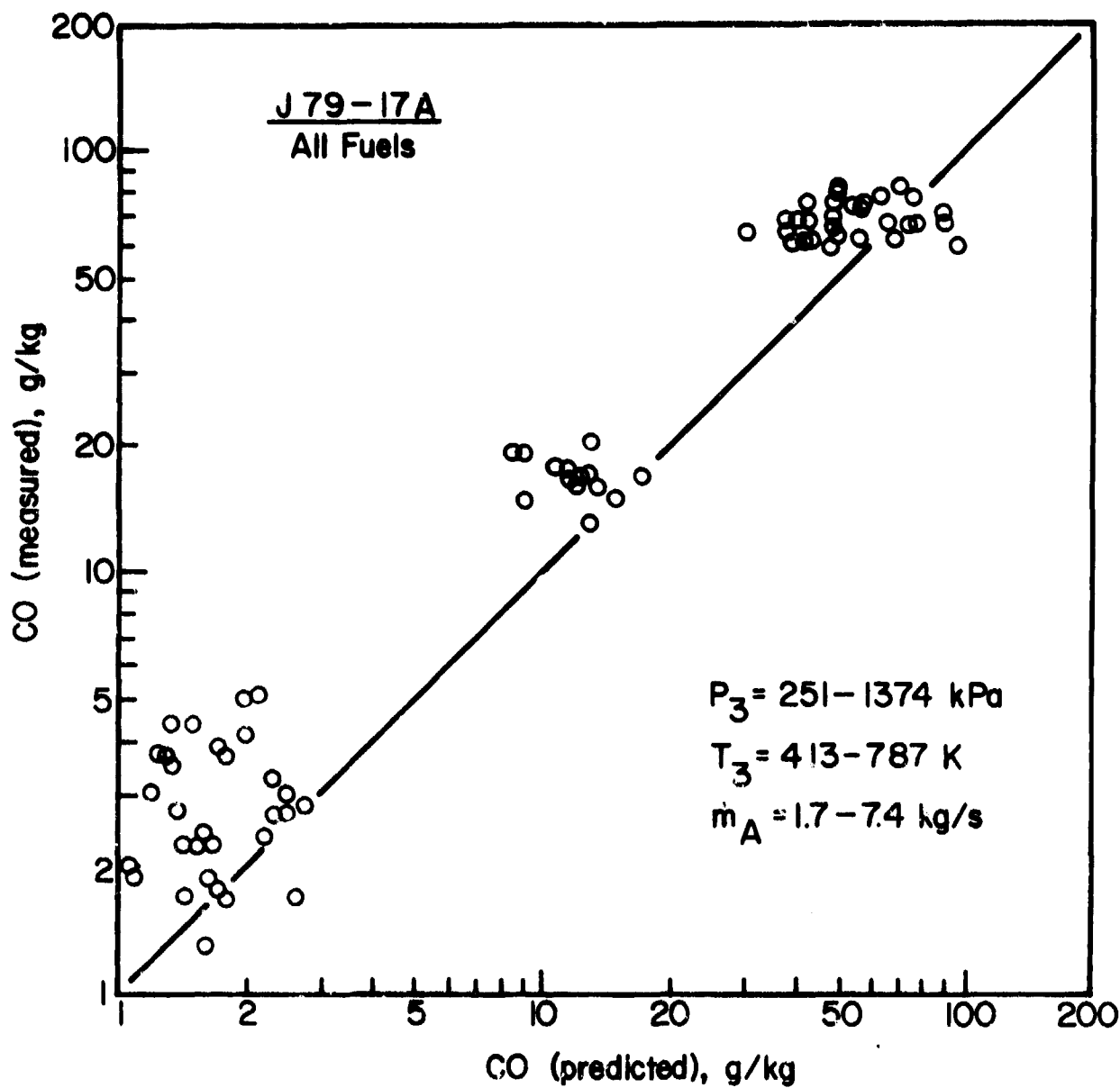


Figure 53. Comparison of Measured and Predicted Values of CO Emissions for J79-17A Combustor.

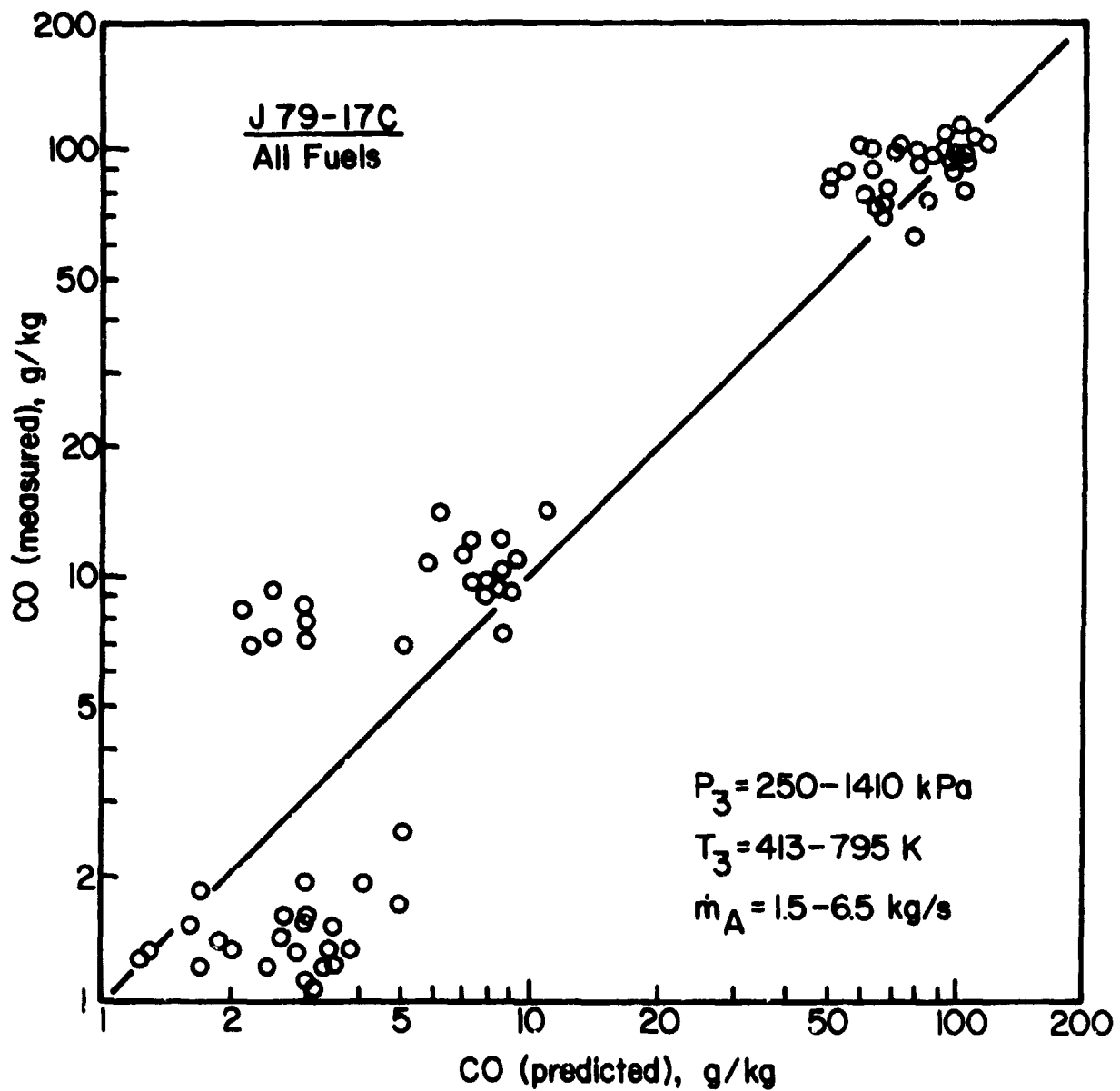


Figure 54. Comparison of Measured and Predicted Values of CO Emissions for J79-17C Combustor.

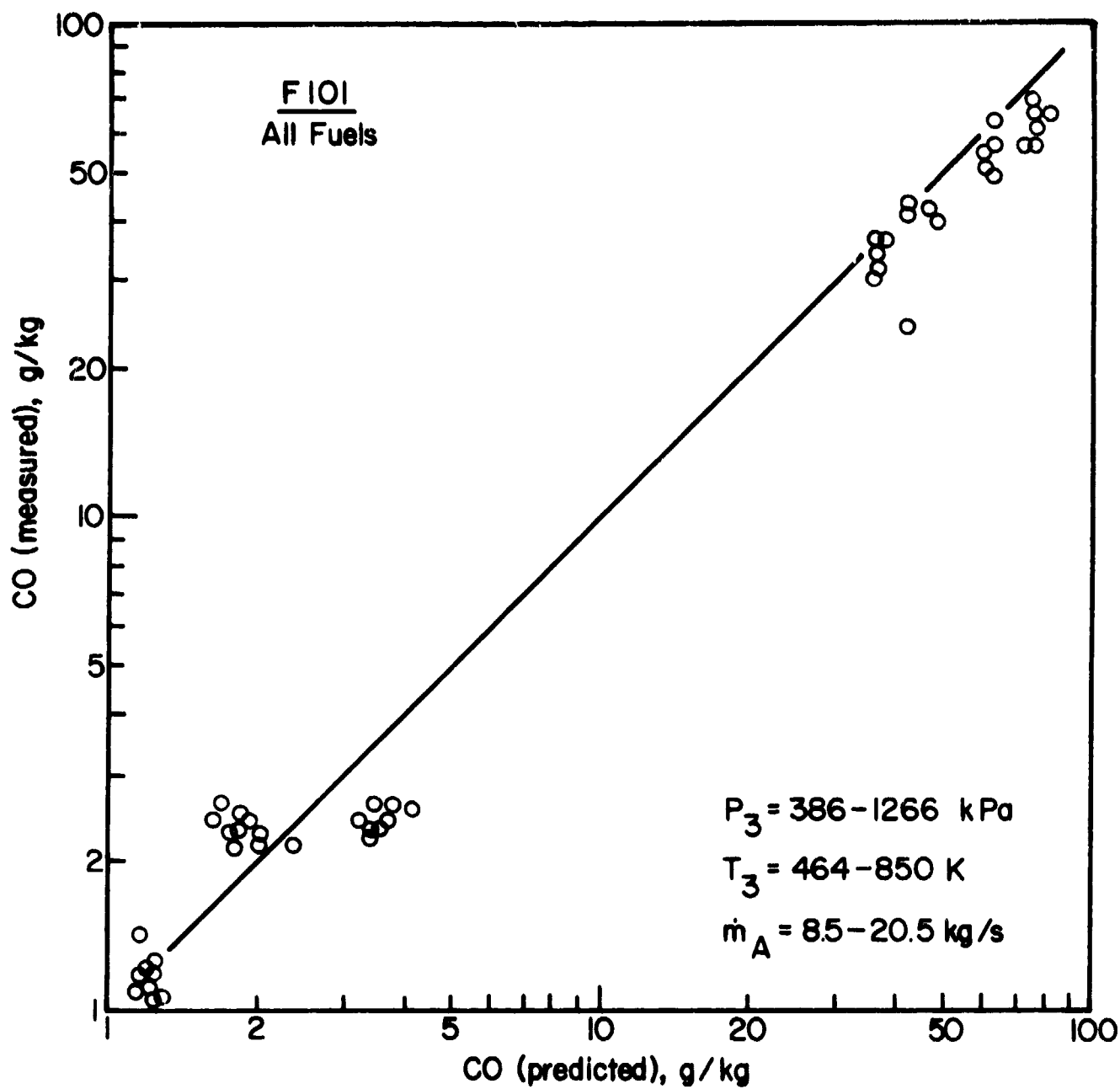


Figure 55. Comparison of Measured and Predicted Values of CO Emissions for F101 Combustor.

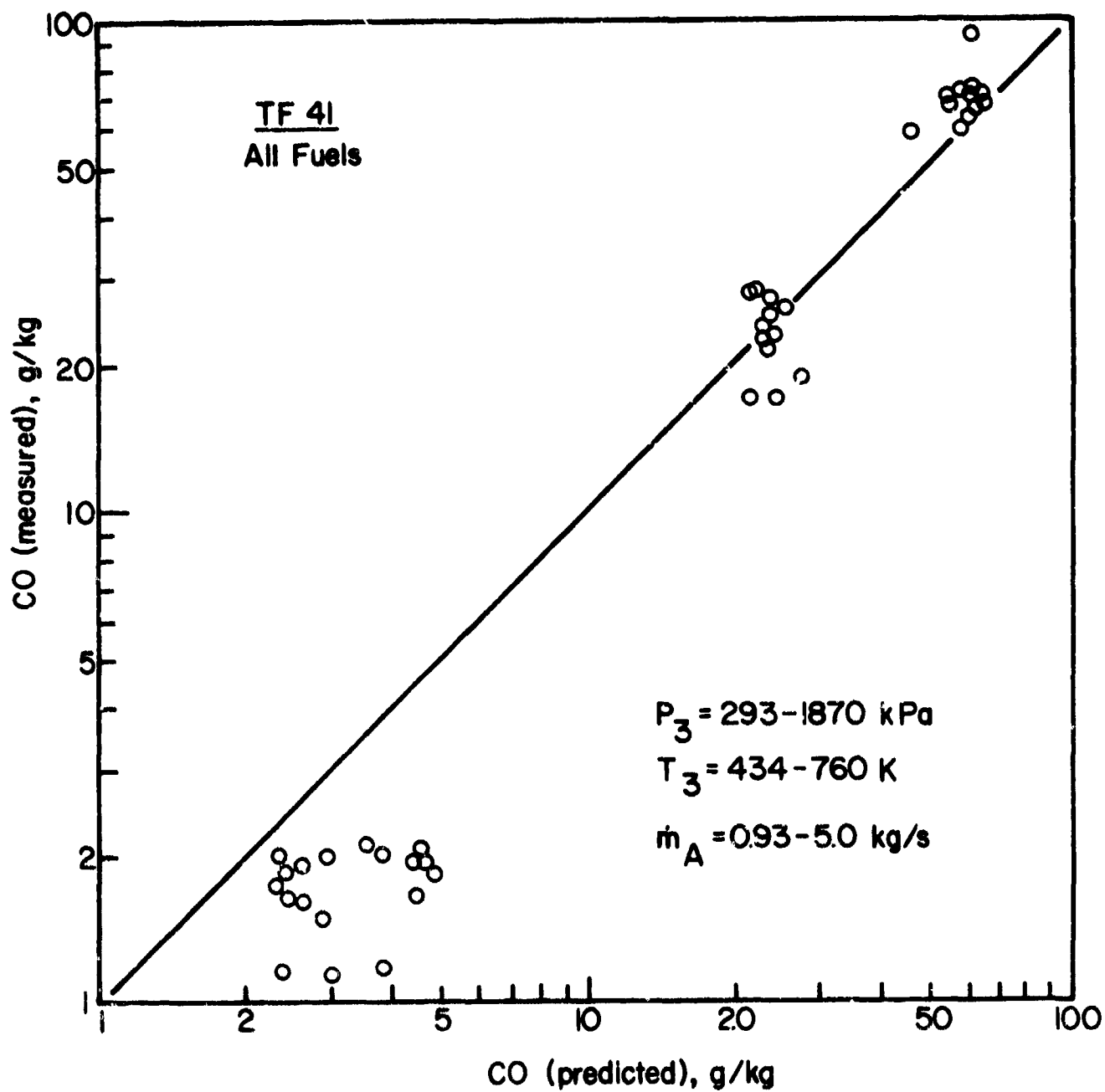


Figure 56. Comparison of Measured and Predicted Values of CO Emissions for TF41 Combustor..

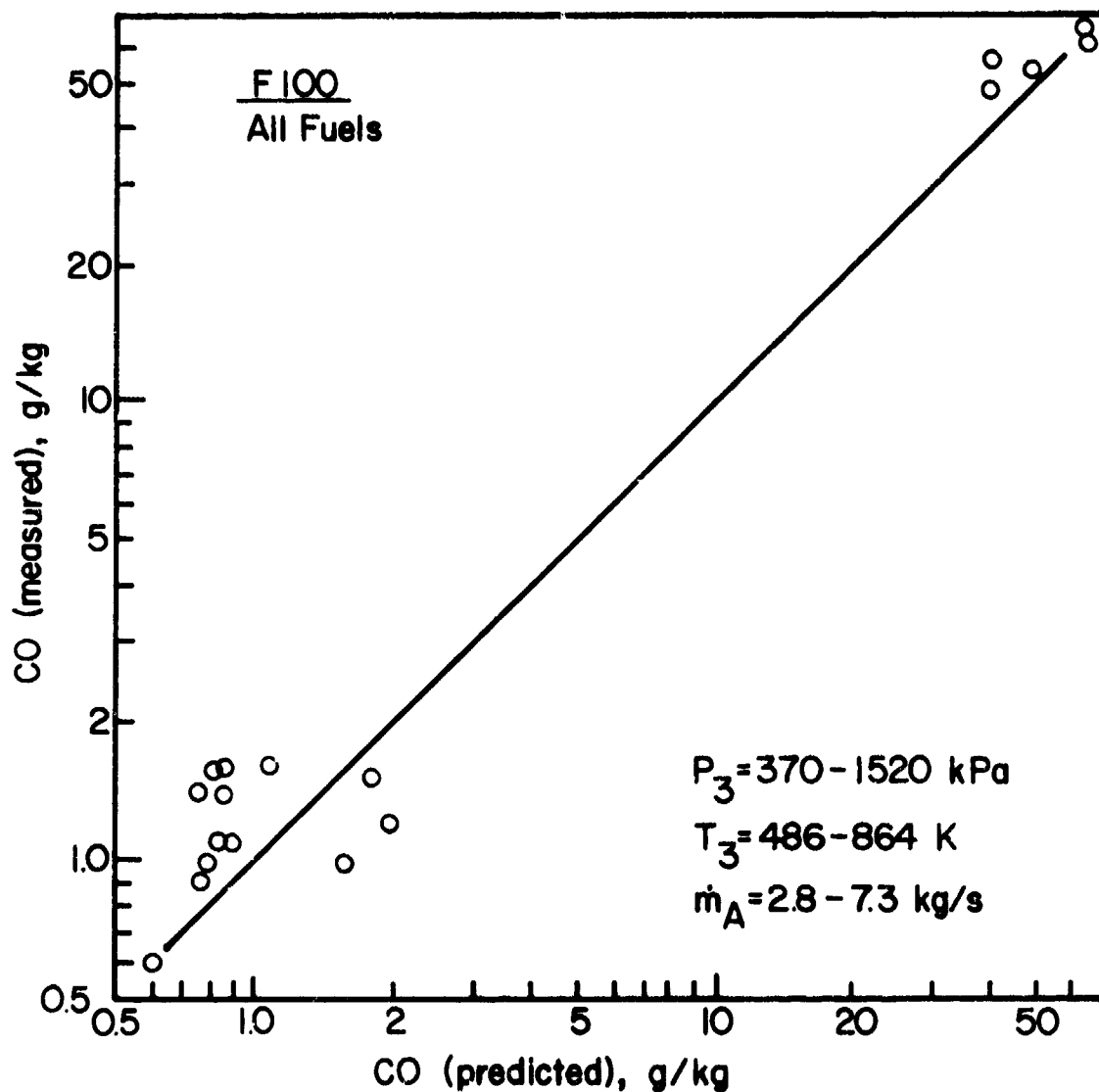


Figure 57. Comparison of Measured and Predicted Values of CO Emissions for F100 Combustor.

3. Unburned Hydrocarbons

Unburned hydrocarbons include fuel that emerges at the combustor exit in the form of droplets or vapor, as well as the products of the thermal degradation of the parent fuel into species of lower molecular weight, such as methane and acetylene. They are normally associated with poor atomization, inadequate burning rates, the chilling effects of film-cooling air, or any combination of these. An increase in engine power setting usually reduces the emission of unburned hydrocarbons, partly through improved fuel atomization but mainly through the effects of higher inlet air pressure and temperature, which together enhance chemical reaction rates in the primary combustion zone. Analysis of the experimental data yields an equation of the form

$$UHC = \frac{11.764 \dot{m}_A T_{pz} \exp(-0.00345 T_{pz})}{\left[V_c - 0.55 \times 10^{-6} \frac{f_{pz} \dot{m}_A}{\rho_{pz}} \frac{D_o^2}{\lambda_{eff}} \right] \left[\frac{\Delta P_L}{P_3} \right] P_3^{2.5}} \text{ g/kg} \quad (30)$$

This equation is very similar to Eq. (28) for the prediction of CO emissions, except for a stronger dependence on liner pressure drop and inlet air pressure. This is perhaps hardly surprising, since the factors that control CO emissions also influence UHC emissions, and in much the same manner.

Due to the well-known difficulties and uncertainties that are normally associated with the measurement of unburned hydrocarbons, close agreement between the predictions of Eq. (30) and the actual measured values can hardly be expected. However,

although Figs. 58 thru 63, which are drawn for the J79-17A, J79-17C, F101, and TF41 combustors, exhibit more scatter than the corresponding figures drawn for NO_x and CO, the correlation achieved is considered fairly satisfactory.

4. Smoke

Exhaust smoke is caused by the production of finely-divided soot particles in fuel-rich regions of the flame and may be generated in any part of the combustion zone where mixing is inadequate. With pressure atomizers, the main soot-forming region lies inside the fuel spray at the center of the combustor. This is the region in which the recirculating burned products move upstream toward the fuel spray, and where local pockets of fuel vapor are enveloped in oxygen-deficient gases at high temperature. In these fuel-rich regions, soot may be produced in considerable quantities.

Most of the soot produced in the primary zone is consumed in the high-temperature regions downstream. Thus from a smoke viewpoint a combustor may be considered as two separate zones. One is the primary zone, which governs the rate of soot formation, and the other is the intermediate zone (and, on modern high temperature engines, the dilution zone also) which determines the rate of soot consumption. The soot concentration actually observed in the exhaust gases is an indication of the dominance of one zone over the other.

Soot is not an equilibrium product of combustion except at

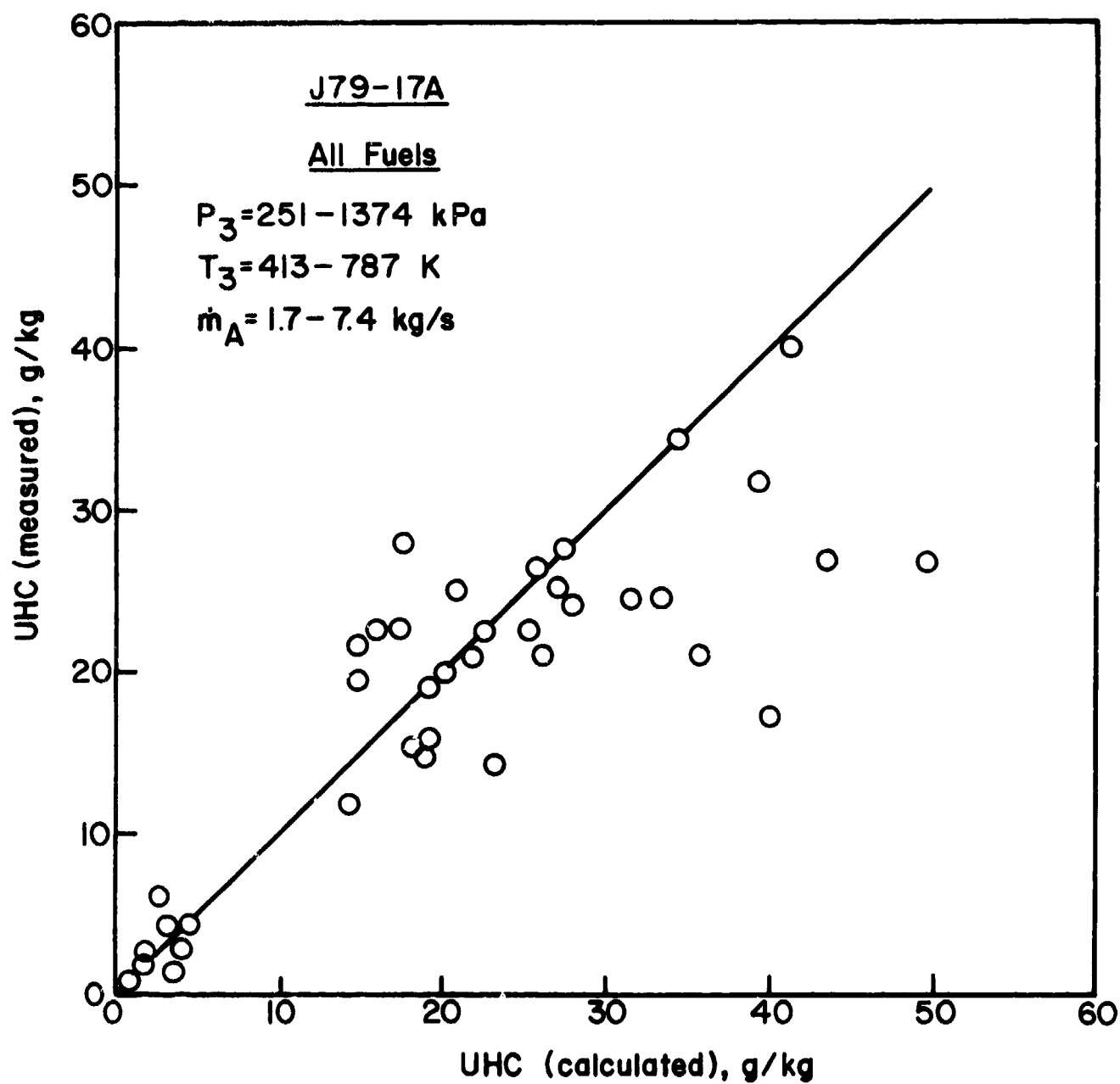


Figure 58. Comparison of Measured and Predicted Values of Unburned Hydrocarbons Emissions for J79-17A Combustor.

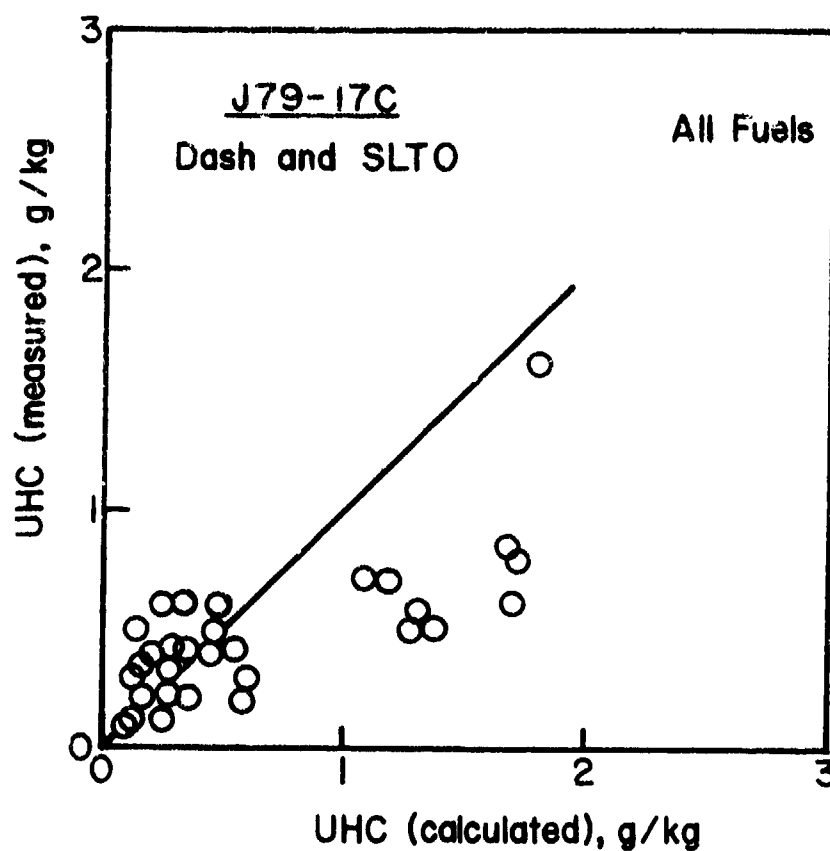


Figure 59. Comparison of Measured and Predicted Values of Unburned Hydrocarbons Emissions for J79-17C Combustor.

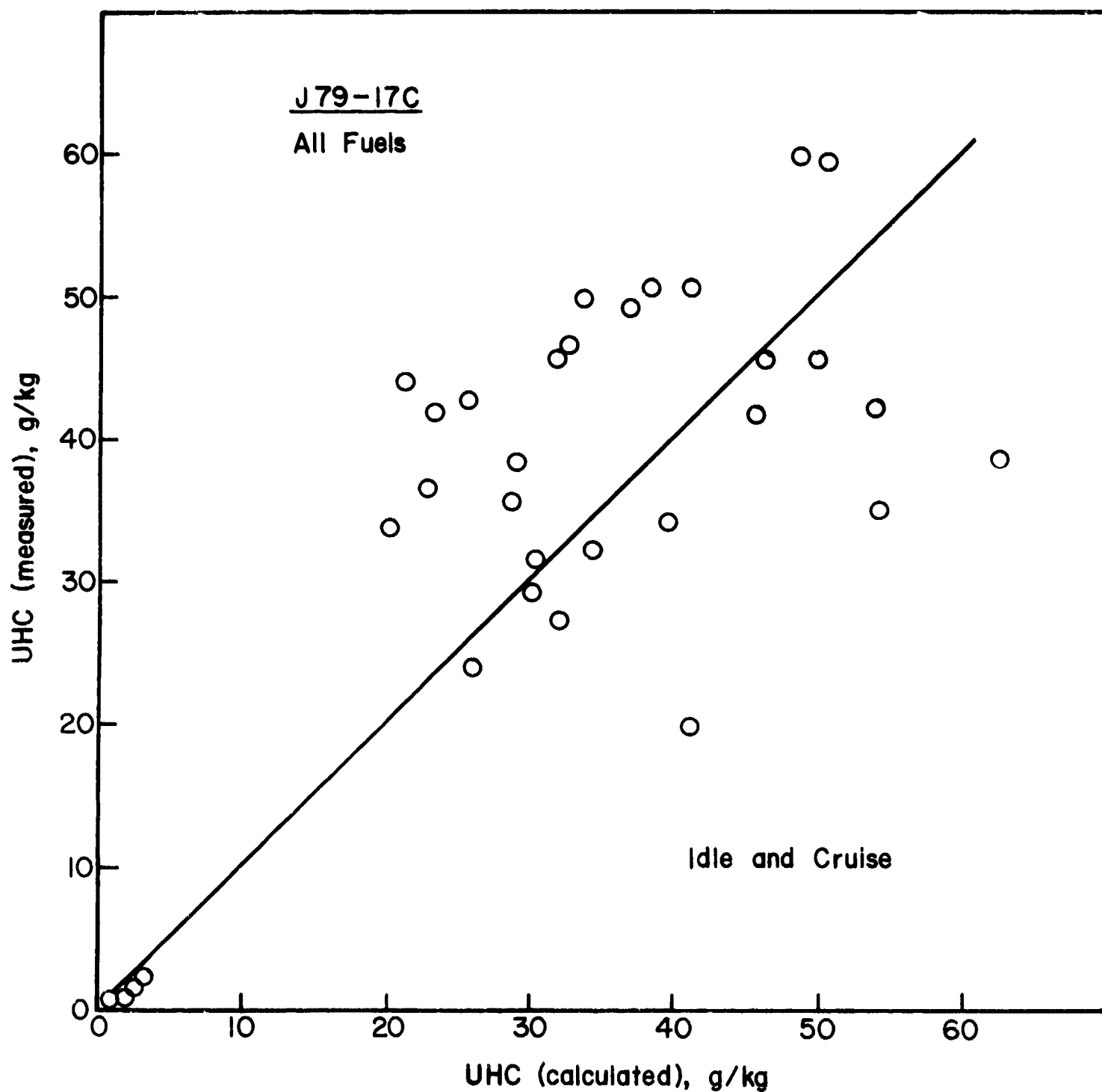


Figure 60. Comparison of Measured and Predicted Values of Unburned Hydrocarbons Emissions for J79-17C Combustor.

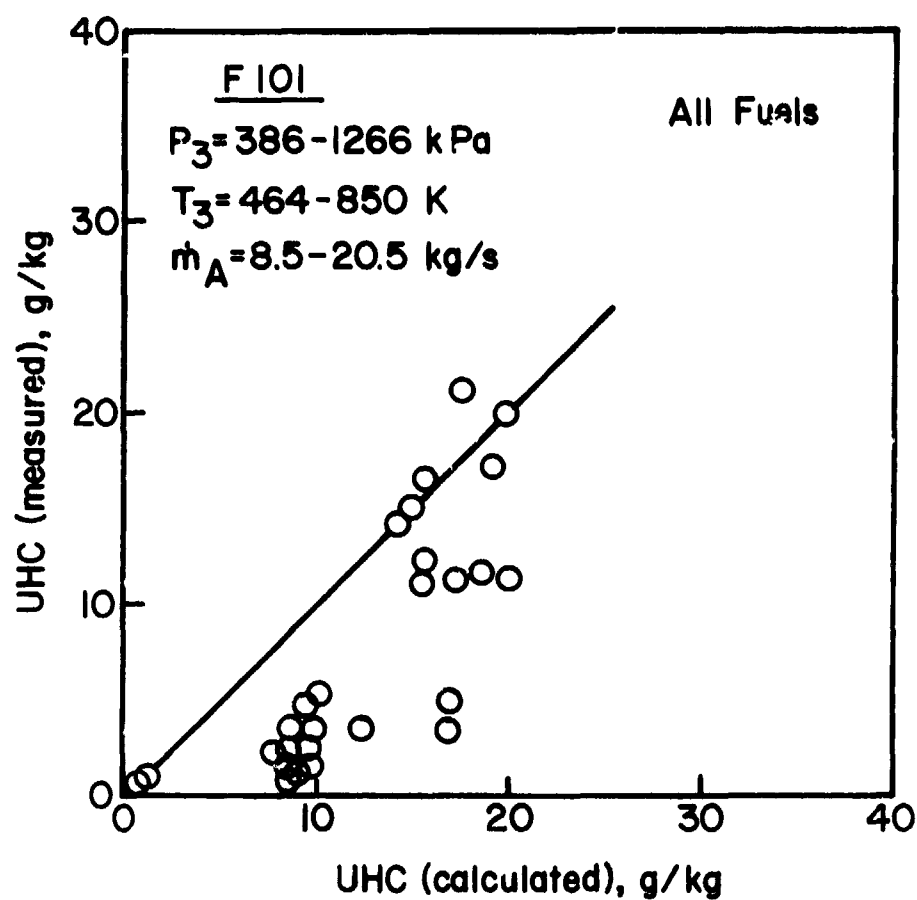


Figure 61. Comparison of Measured and Predicted Values of Unburned Hydrocarbons Emissions for F101 Combustor.

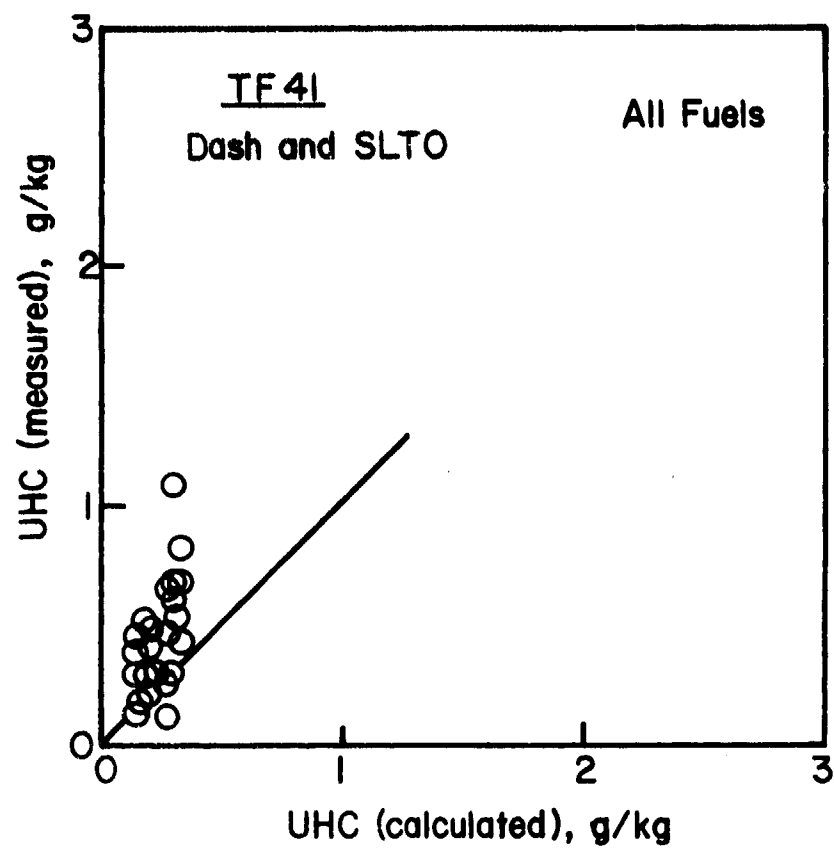


Figure 62. Comparison of Measured and Predicted Values of Unburned Hydrocarbons Emissions for TF41 Combustor.

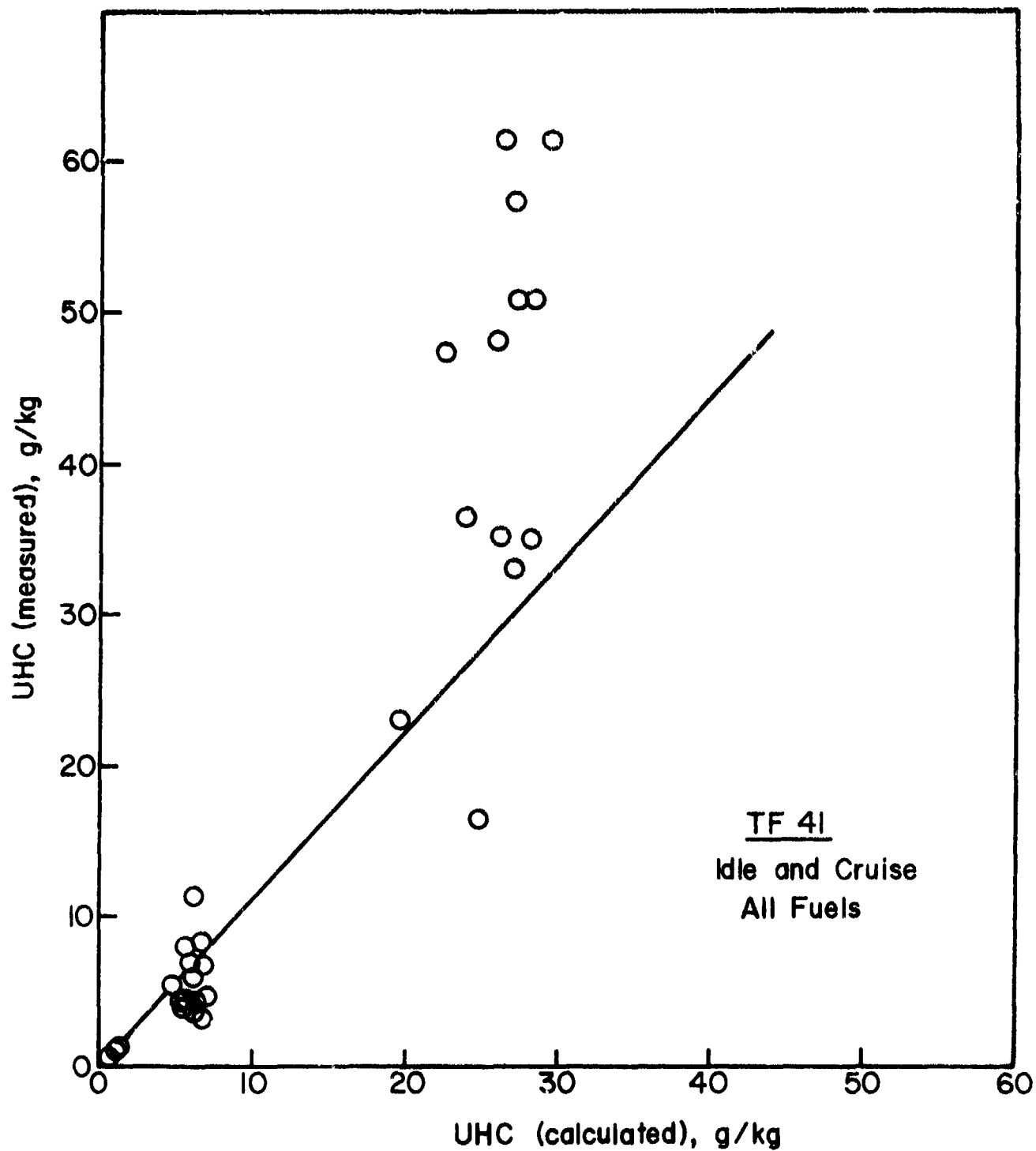


Figure 63. Comparison of Measured and Predicted Values of Unburned Hydrocarbons Emissions for TF41 Combustor.

mixture strengths far richer than those employed in the primary zones of combustors. Thus, it is impossible to predict its rate of formation and final concentration from kinetic or thermodynamic data. In practice, the rate of soot formation tends to be governed more by fuel-spray characteristics and fuel-air mixing than by kinetics.

Many specific mechanistic models for soot formation have been proposed. Current thinking tends to favor the notion that condensed ring aromatic hydrocarbons may produce soot via a different mechanism than do aliphatic hydrocarbons. Aromatic hydrocarbons can produce soot via two mechanisms: (1) condensation of the aromatic rings into a graphite-like structure, or (2) breakup to small hydrocarbon fragments which then polymerize to form larger, hydrogen-deficient molecules which eventually nucleate and produce soot. Based on their shock tube studies, Graham et al. [31,32] concluded that the condensation route is much faster than the fragmentation/polymerization route. According to the condensation-route model, aliphatics produce soot via the fragmentation/polymerization mechanism only. As a result, these hydrocarbons do not form the quantities of soot produced by the aromatics. Indeed, during the fuel-rich combustion of a fuel blend composed of aromatics and aliphatics, the aromatic hydrocarbons would produce the major quantity of soot. Combustion of the aliphatic portions of the fuel would influence temperature and hydrocarbon fragment concentration, but soot formation via fragmentation/polymerization would be minimal.

Experimental data obtained by Blazowski [33] using various blends of iso-octane and toluene fuels were found to be consistent with this model. However, the results of an experimental study by Naegeli and Moses [34] suggest that the picture will be more complicated for fuels with high concentrations of polycyclic aromatics.

For gas turbine combustors the main controlling factors for soot formation and smoke have been determined experimentally as fuel properties, combustion pressure and temperature, fuel/air ratio, atomization quality, and mode of fuel injection [10].

In order to analyze the smoke data contained in references 1 thru 6, the first step must be to convert the quoted smoke numbers (SN) into soot concentrations (X_c) expressed in mg/kg. This conversion was accomplished using the following different factors for different levels of smoke number [35].

SN = 0 to 1	$X_c = 0.1 (SN)$
SN = 1 to 5	$\log X_c = 0.136 (SN) - 1.136$
SN = 5 to 10	$\log X_c = 0.06265 (SN) - 0.769$
SN = 10 to 20	$\log X_c = 0.03187 (SN) - 0.4614$
SN = 20 to 30	$\log X_c = 0.0301 (SN) - 0.426$
SN > 30	$\log X_c = 0.02538 (SN) - 0.2845$

The following equation was then used to convert engine

exhaust soot concentrations into corresponding combustor exit values.

$$X_{c_4} = X_{c_8} \left[\frac{q_4}{q_8} \right] \left[\frac{1 + q_8}{1 + q_4} \right] \quad (31)$$

For the purpose of analysis, it is convenient to consider two separate zones (a) a soot-forming zone, and (b) a soot oxidation zone. The soot concentration measured at the combustor exit represents the difference in effectiveness between these two competing processes. Unfortunately, any attempt to derive suitable expressions to represent rates of soot-formation and soot-oxidation is seriously hampered by lack of knowledge of the basic mechanisms involved, so that in practice there is little alternative except to resort to an empirical approach. Useful guidance is provided by the knowledge gained from past experience in attempting to alleviate the problems of smoke and soot formation in gas turbine combustors. Thus, for example, the work of Holderness and Macfarlane [36] has shown that soot formation increases rapidly with increase in pressure, and is appreciably diminished by increase in AFR. Moreover, sufficient is known to indicate that soot oxidation proceeds most rapidly in regions of high temperature containing excess air. These considerations, in conjunction with analysis of the experimental data, lead to the following expressions for the soot formation and soot oxidation processes.

$$X_f \propto \frac{P_3^2 q_{pz} (18 - \% H_2)^{1.5}}{f_{pz} m_A T_{pz}} \quad (32)$$

$$X_o = \frac{C_3^2 q_{pz} \exp(0.0011T_{sz}) (18 - \%H_2)^{1.5}}{f_{pz} m_A q_{sz} T_{pz}} \quad (33)$$

$$\text{Now } X_c = X_f - X_o$$

Hence,

$$X_c = \frac{C_3^2 q_{pz}}{f_{pz} m_A T_{pz}} \left[1 - \frac{C_4}{q_{sz}} \exp(0.0011T_{sz}) \right] \times [18 - \%H_2]^{1.5} \text{ mg/kg} \quad (34)$$

Application of this equation to the correlation of experimental data on soot concentrations yields results as illustrated in Figs. 64 thru 71. The values of C_3 and C_4 associated with these figures are listed in Table 3. This table shows a large disparity between values of C_3 for different combustors which is not surprising, since C_3 relates to soot formation in the primary zone, and its numerical value will be very dependent on fuel spray characteristics, primary-zone fuel/air ratio, and primary-zone mixing characteristics, all of which vary widely between one combustor to another. This is in marked contrast to the secondary zone where, in the hot gas stream entering this zone, the fuel is fully vaporized, combustion is almost complete, and plug flow of combustion products at fairly uniform conditions of temperature and composition is well established. Thus, for the secondary zone, differences between different combustor types should be appreciably less, and this is confirmed by the lack of marked divergence between the experimentally-derived values of C_4 .

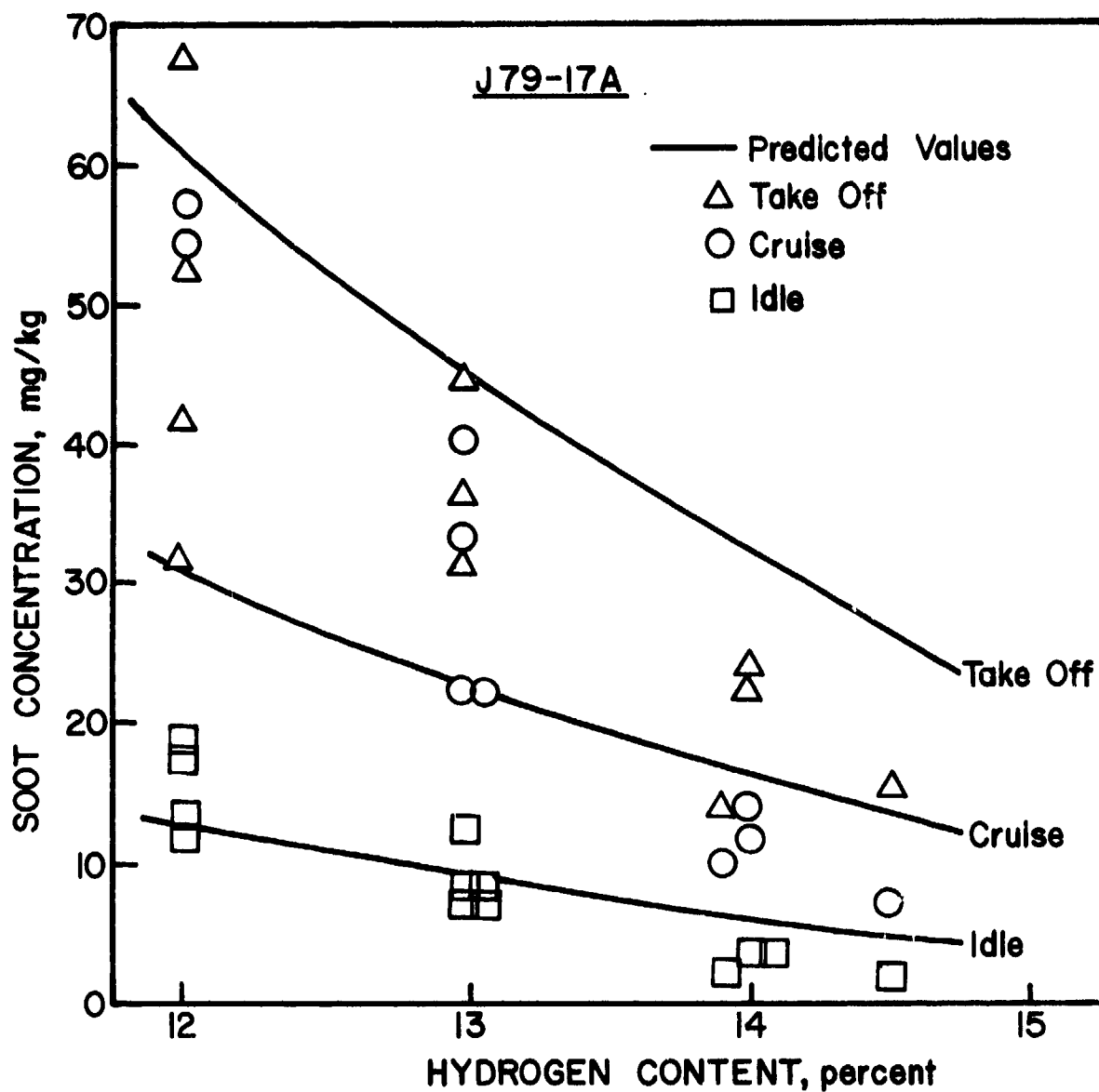


Figure 64. Graphs Illustrating Influence of Hydrogen Content and Engine Operating Conditions on Soot Emissions for J79-17A Combustor.

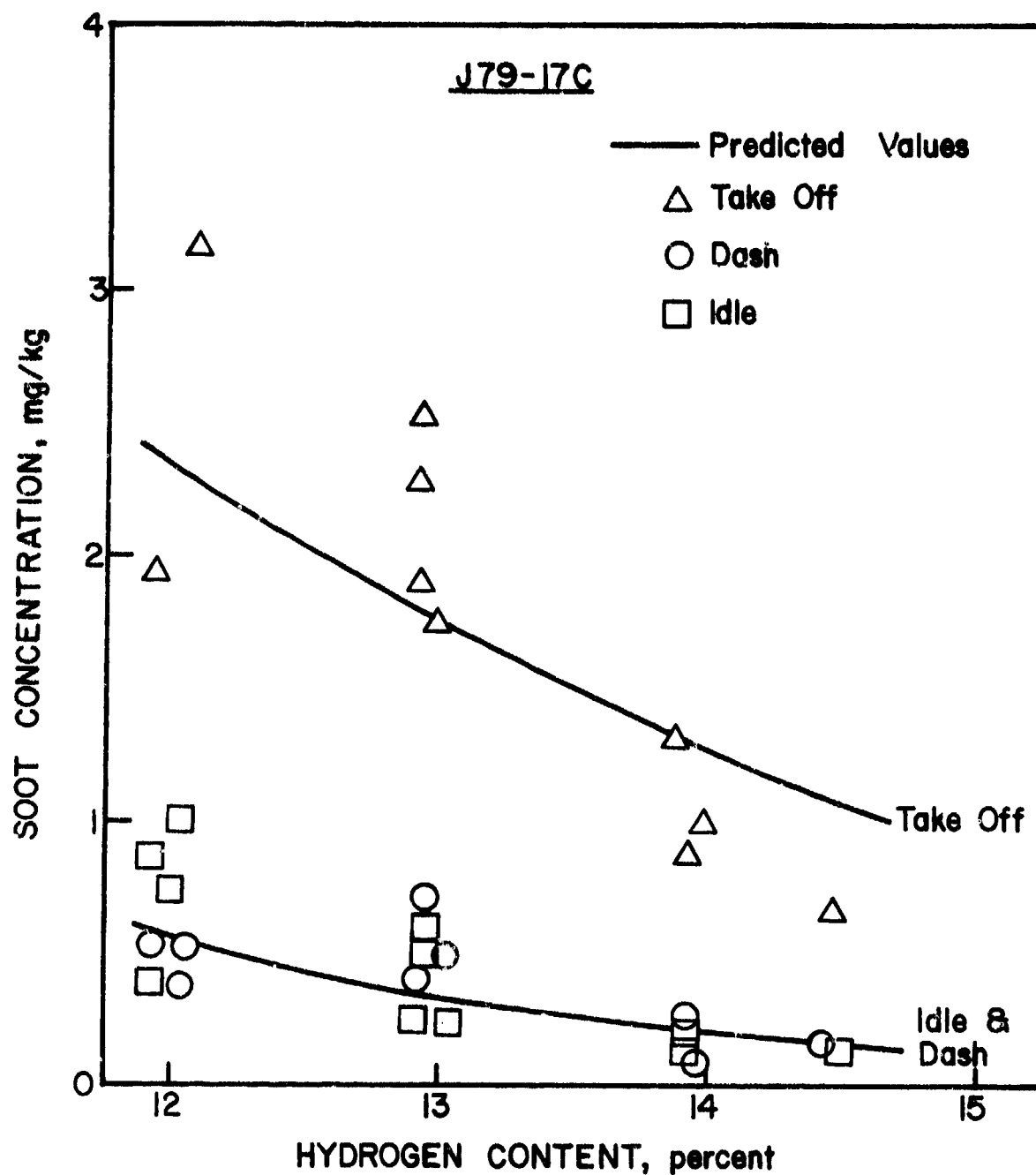


Figure 65. Graphs Illustrating Influence of Hydrogen Content and Engine Operating Conditions on Soot Emissions for J79-17C Combustor.

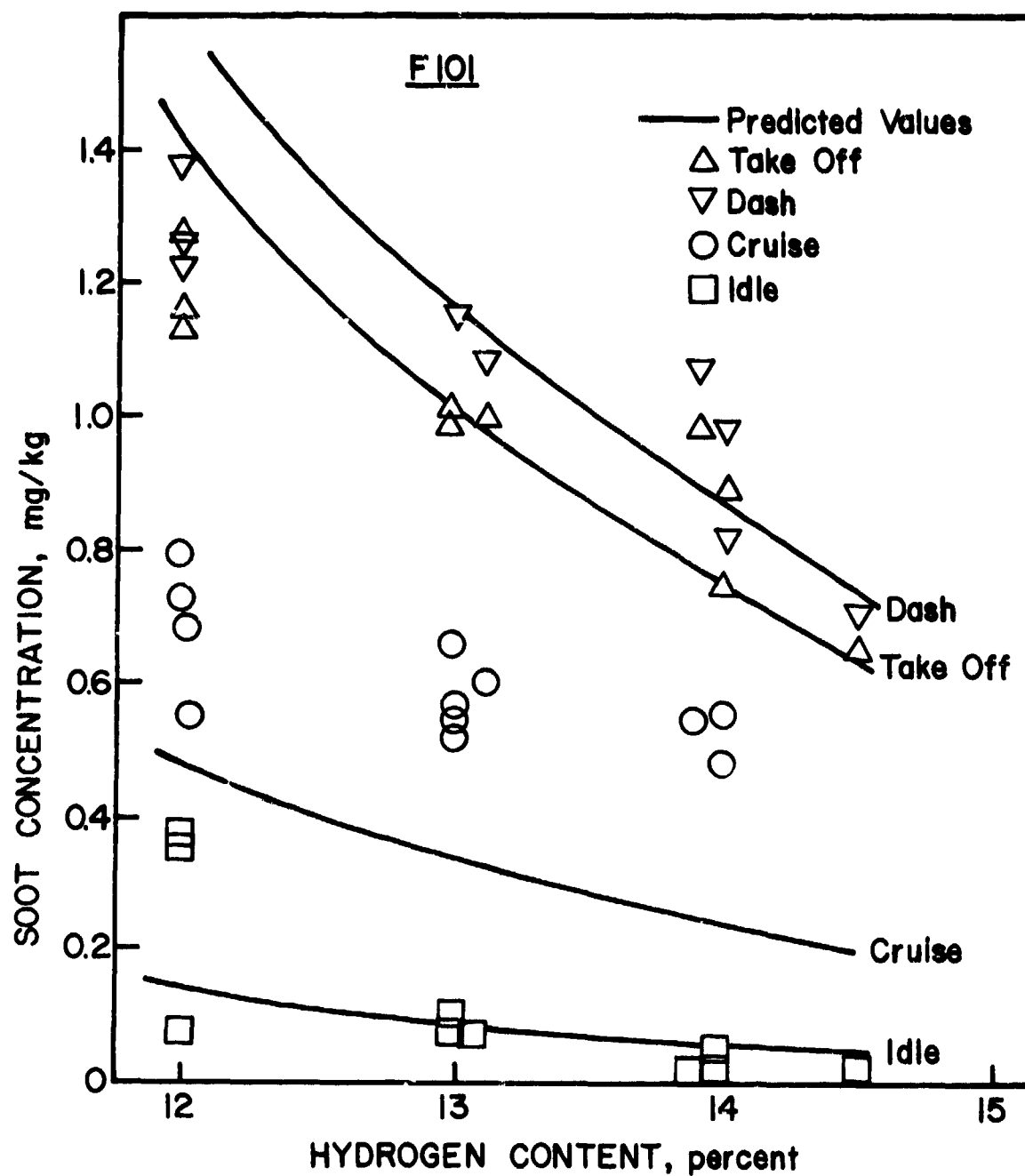


Figure 66. Graphs Illustrating Influence of Hydrocarbon Content and Engine Operating Conditions of Soot Emissions for F101 Combustor.

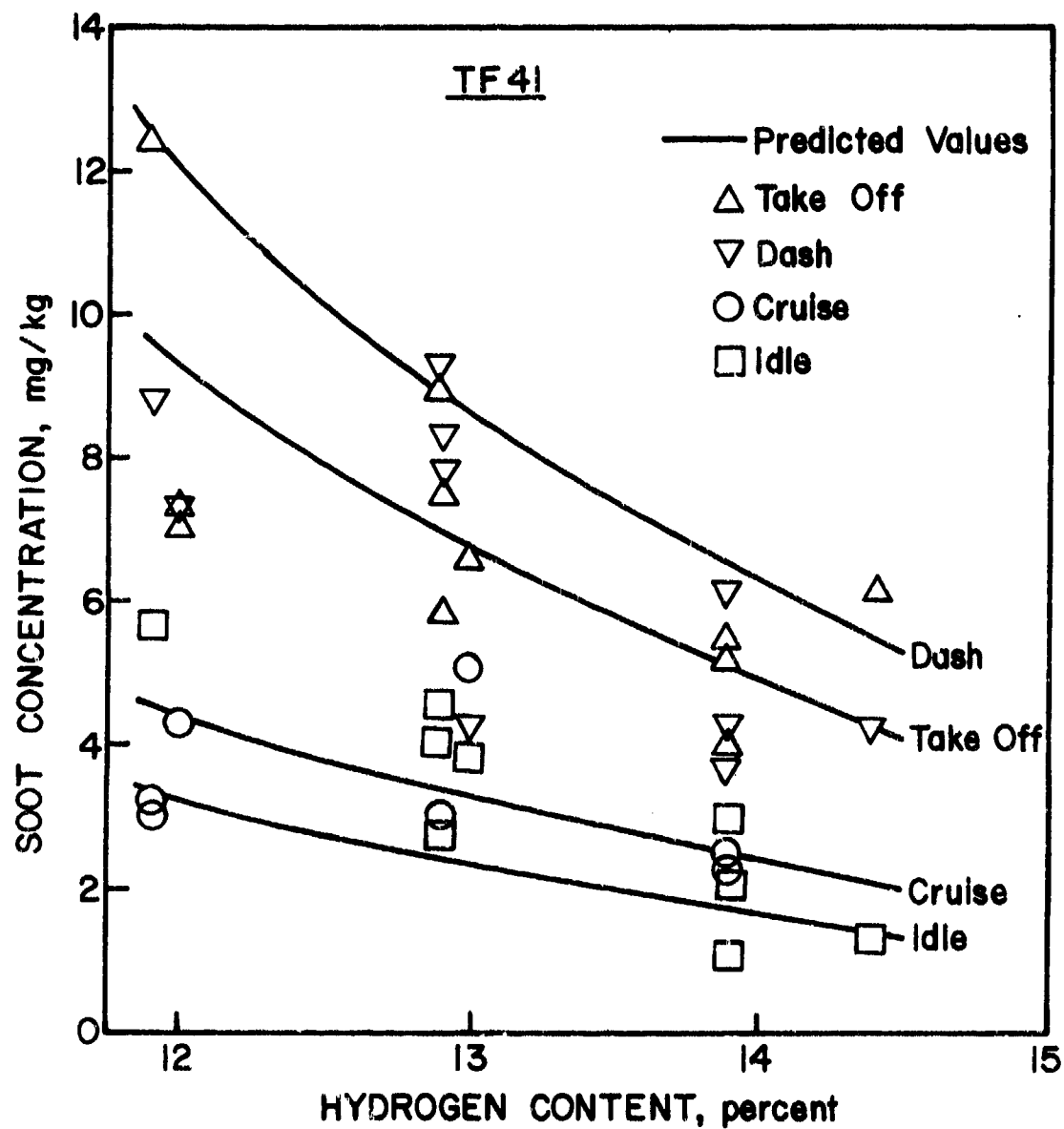


Figure 67. Graphs Illustrating Influence of Hydrogen Content and Engine Operating Conditions on Soot Emissions for TF41 Combustor.

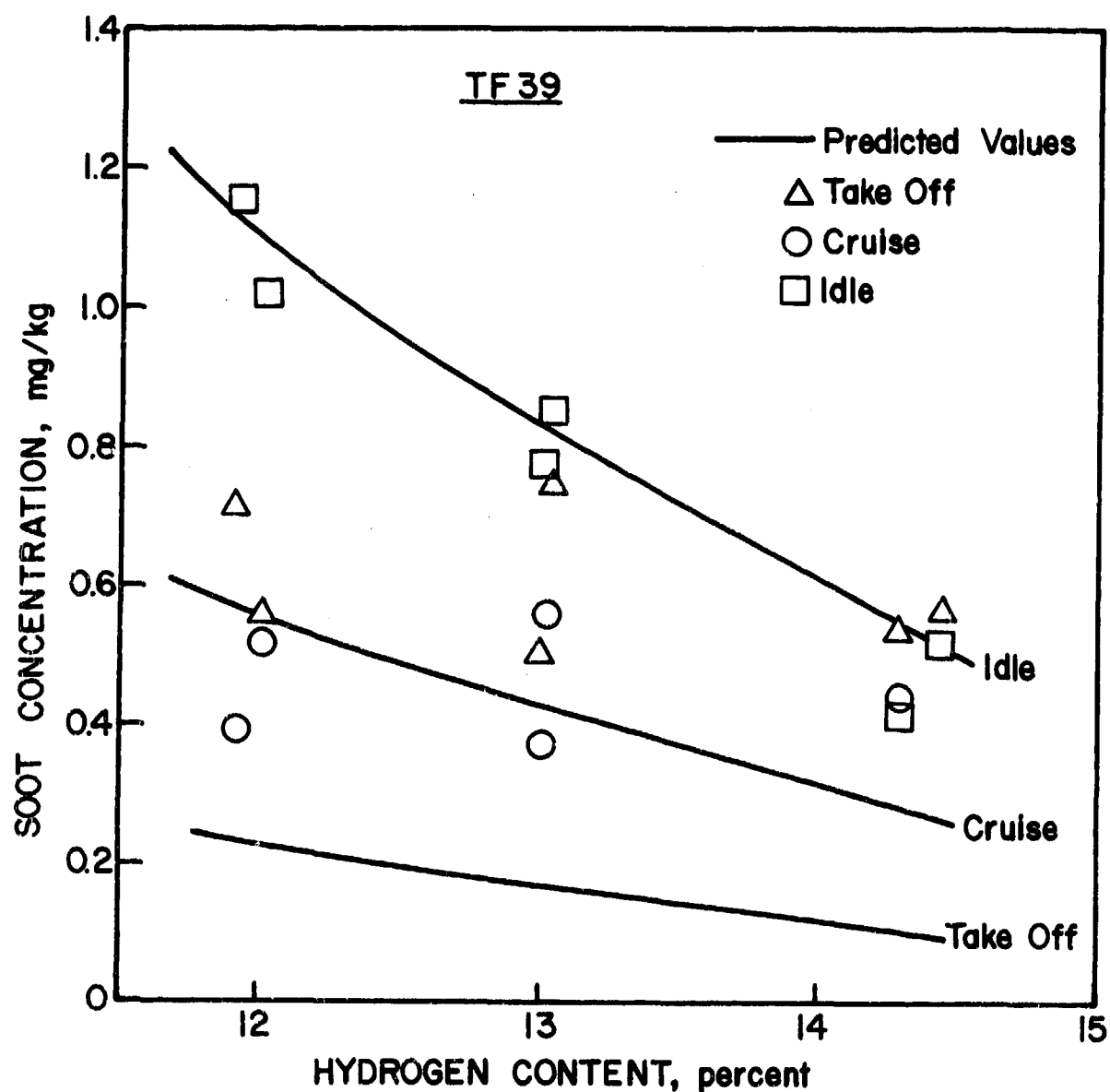


Figure 68. Graphs Illustrating Influence of Hydrogen Content and Engine Operating Conditions on Soot Emissions for TF39 Combustor.

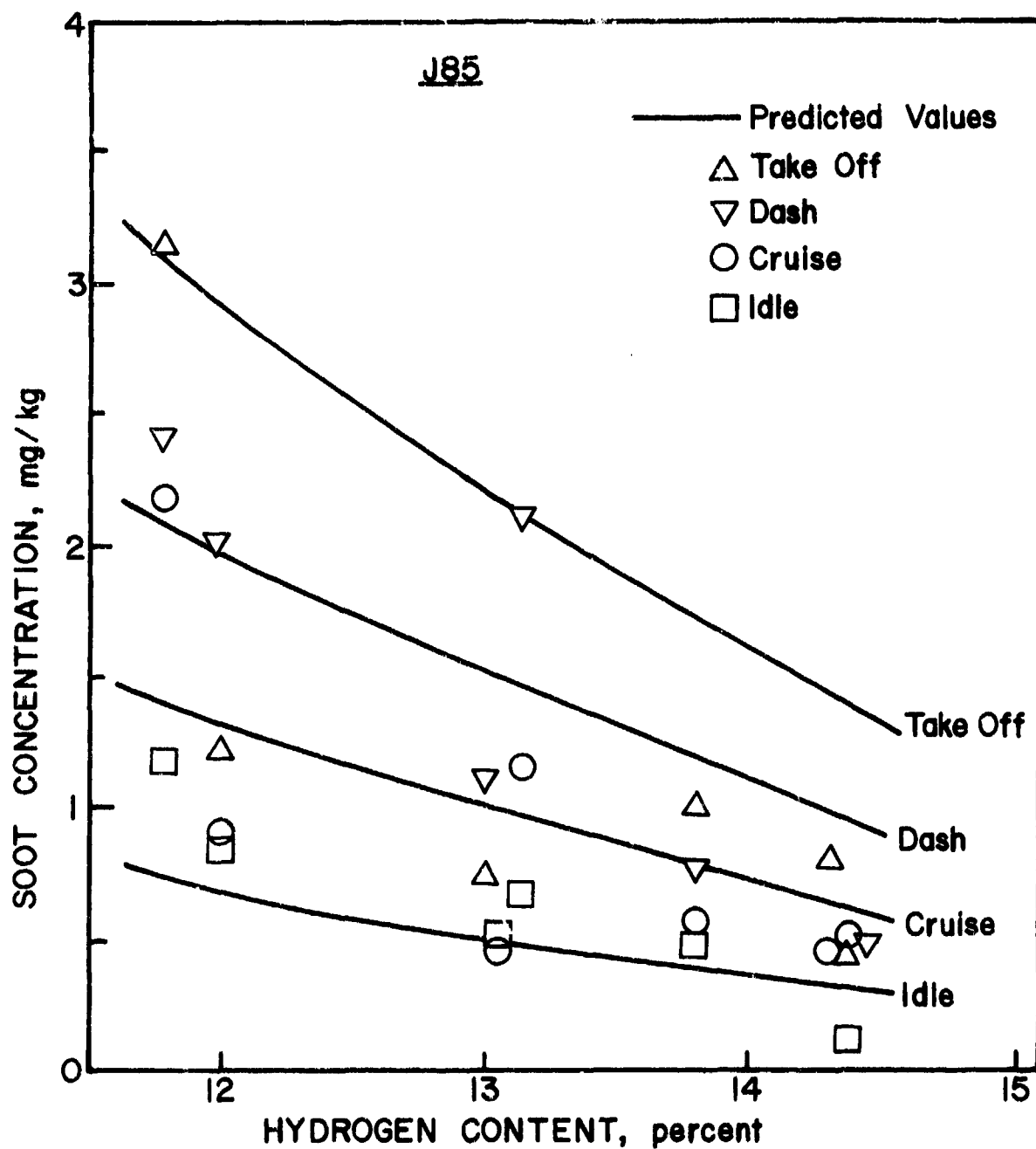


Figure 69. Graphs Illustrating Influence of Hydrogen Content and Engine Operating Conditions on Soot Emissions for J85 Combustor.

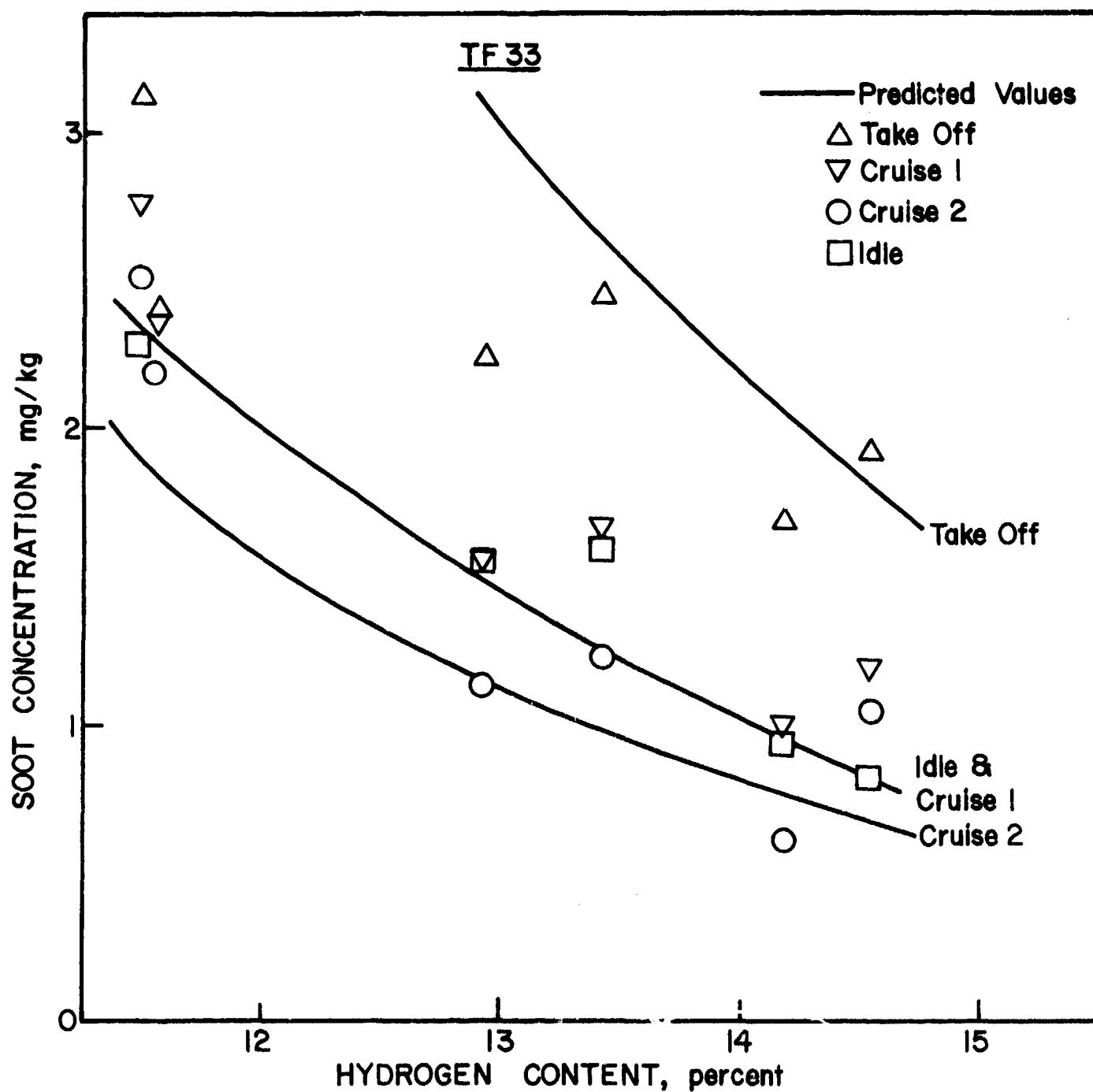


Figure 70. Graphs Illustrating Influence of Hydrogen Content and Engine Operating Conditions on Soot Emissions for TF33 Combustor.

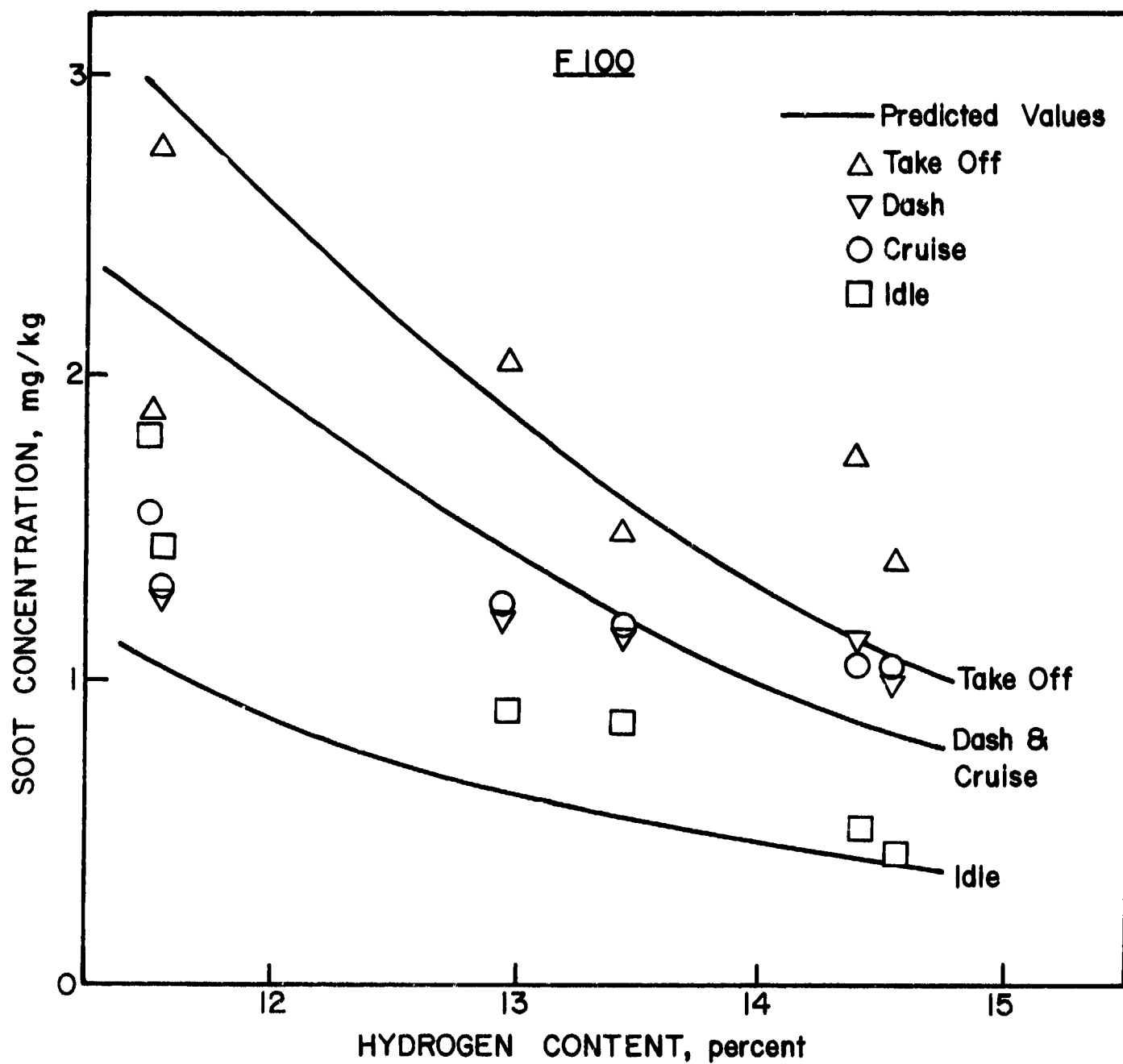


Figure 71. Graphs Illustrating Influence of Hydrogen Content and Engine Operating Conditions on Soot Emissions for F100 Combustor.

Table 3. Values of C_3 and C_4 employed in equation (34).

Engine	C_3	C_4
J79-17A	2.43	0.0046
J79-17C	0.045	0.0042
F101	0.017	0.0020
TF41	0.0785	0.0037
TF39	0.145	0.0044
J85	0.33	0.0038
TF33	1.0	0.0045
F100	0.0375	0.0035

listed in Table 3.

If allowance is made for the difficulties involved in the sampling and measurement of soot concentrations and the poor measurability of fuel aromatics content, the level of agreement between measured and predicted values of soot concentration, as exhibited in Figs. 64 thru 71, is quite reasonable. However, although Eq. (34) predicts quite well the influence of combustor operating conditions on smoke output, and also demonstrates that soot concentrations rise with decreases in hydrogen content of the fuel, it also shows that the extent of this increase varies from one combustor to another in a manner that cannot be predicted a priori. Thus it offers no guidance on the likely smoke emissions to be anticipated from any new type of combustor. Only if the values of C_3 and C_4 were sensibly constant for all combustors would it be reasonable to regard Eq. (34) as completely satisfactory for the prediction of smoke emissions.

Another defect of Eq. (34) is the absence of a term to describe the degree of mixing of fuel and air prior to combustion. This is known to have a strong influence on smoke emissions, for example, the very large difference in smoke output between the J79-17A and J79-17C combustors, as reflected in the large difference in their values of C_3 , is known to be due in large measure to the steps taken to improve the premixing of fuel and air in the latter case. Improvements in the prediction of smoke emissions cannot be expected until more quantitative information on the influences of fuel-air preparation and fuel

chemistry on soot formation becomes available. In the meantime Eq. (34) can provide useful guidance on the effects of changes in fuel type and combustor operating conditions on smoke output. For any given combustor, all that is needed are a few smoke measurements obtained with any fuel at any operating conditions, just in order to establish values of C_3 and C_4 for insertion into Eq. (27). This equation can then be used to estimate smoke levels for other fuels and/or other operating conditions.

It is of interest to note in Eq. (34) that the fuel is represented by its hydrogen content only. This is because hydrogen content was found to provide a slightly better correlation of experimental data than aromatics content. Furthermore, no conclusions could be drawn regarding the relative importance to soot formation and smoke of single-ring and multi-ring aromatics. This is because the data show that replacing single-ring aromatics by multi-ring aromatics increases the level of exhaust smoke in some cases and reduces it in others.

SECTION VIII

PATTERN FACTOR

The attainment of a satisfactory and consistent distribution of temperature in the combustor efflux gases is one of the major objectives of combustor design and development. Experimental investigations into dilution-zone performance carried out on test rigs and actual chambers have provided useful guidance, but trial and error methods are still widely used in developing the temperature-traverse quality of individual combustor designs to a satisfactory standard.

The mixing processes in the dilution zone are affected in a complicated manner by the dimensions, geometry, and pressure drop of the liner, the size, shape and discharge coefficients of the liner holes, the airflow distribution to various zones of the chamber, and the temperature distribution of the hot gases entering the dilution zone. The latter is strongly influenced by fuel spray characteristics such as drop size, spray angle and spray penetration, since these control the pattern of burning and hence the distribution of temperature in the primary-zone gases.

Several parameters have been proposed to describe the temperature distribution in the combustor efflux, the most widely used being the "overall temperature distribution factor" which tends to highlight the maximum temperature found in the traverse and is, therefore, of special importance to the design and durability of nozzle guide vanes. It is normally defined as

$$\text{Pattern factor} = \frac{T_{\max} - T_4}{T_4 - T_3} \quad (35)$$

Of prime importance to pattern factor are liner length, which governs the time and distance that are available for mixing, and the pressure loss factor of the liner which controls the penetration and turbulence of the dilution jets. At low pressures, where evaporation rates are relatively slow, a significant portion of the liner length is occupied by the fuel evaporation process, so that less length is available for mixing. This may be accounted for by reducing the liner length, L_L , by an amount, L_e , in the following equation for pattern factor

$$\frac{T_{\max} - T_4}{T_4 - T_3} = 1 - \exp \left[- Z \left[\frac{\Delta P_L}{q_{\text{ref}}} \right] \left[\frac{L_L - L_e}{D_L} \right] \right]^{-1} \quad (36)$$

where $Z = 0.07$ for tubular liners and 0.05 for annular liners [10].

The evaporation length, L_e , is obtained as the product of evaporation time and the average gas velocity in the predilution zone. In reference 9 it is shown that L_e is given by

$$L_e = 0.33 \times 10^{-6} \dot{m}_A D_o^2 / \rho_g A_L \lambda_{\text{eff}} \quad (37)$$

where ρ_g is the average gas density upstream of the dilution zone. It is calculated at a temperature T_g which is obtained as

$$T_g = T_3 + \Delta T_g$$

where ΔT_g is the temperature rise due to combustion for a fuel/air ratio of $0.6 q_{\text{ov}}$. A_L is the average cross-sectional

area of the liner. It is estimated by dividing the volume of the liner by its maximum length. D_L is the average diameter or height of the liner. For a tubular liner it is readily obtained as $D_L = (4 A_L / \pi)^{0.5}$.

Substitution of L_e from Eq. (37) into Eq. (36) gives

$$\frac{T_{\max} - T_4}{T_4 - T_3} = 1 - \exp \left[- 2 \left[\frac{\Delta P_L}{q_{\text{ref}}} \right] \left[\frac{L_L}{D_L} - \frac{0.33 \times 10^{-6} \dot{m}_A D_o^2}{\rho_g A_L D_L \lambda_{\text{eff}}} \right] \right]^{-1} \quad (38)$$

For the three tubular combustors examined, namely the J79-17A, J79-17C, and TF41, insertion of values for $\Delta P_L / q_{\text{ref}}$ of 14, 15, and 19, respectively into Eq. (38) provides excellent correlations of the experimental data, as illustrated in Figs. 72 thru 74. It is of interest to note that the improvement in pattern factor with increase in engine power, as predicted by Eq. (38), (due to reduction in evaporation time), is fully borne out by the results contained in Figs. 72 thru 74.

The influence of fuel type on pattern factor is manifested through the effects of mean drop size (via viscosity and surface tension) and effective evaporation constant (via T_{bn}) on droplet evaporation time. Over the range of fuels examined, the effect of fuel type on pattern factor is relatively small, at least at high power conditions where the evaporation time is always a small fraction of the total combustor residence time, regardless of fuel type. However, if measurements of pattern factor are conducted at low power conditions, where the evaporation time constitutes a significant proportion of the total residence time,

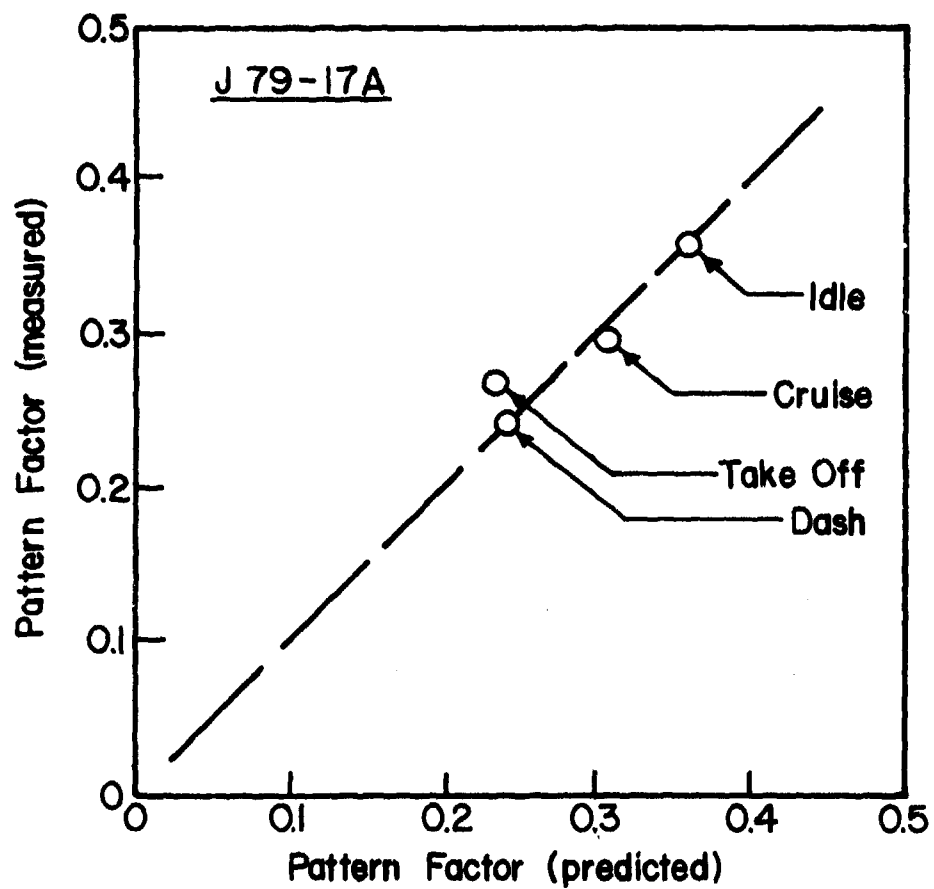


Figure 72. Comparison of Measured and Predicted Values of Pattern Factor for J79-17A Combustor.

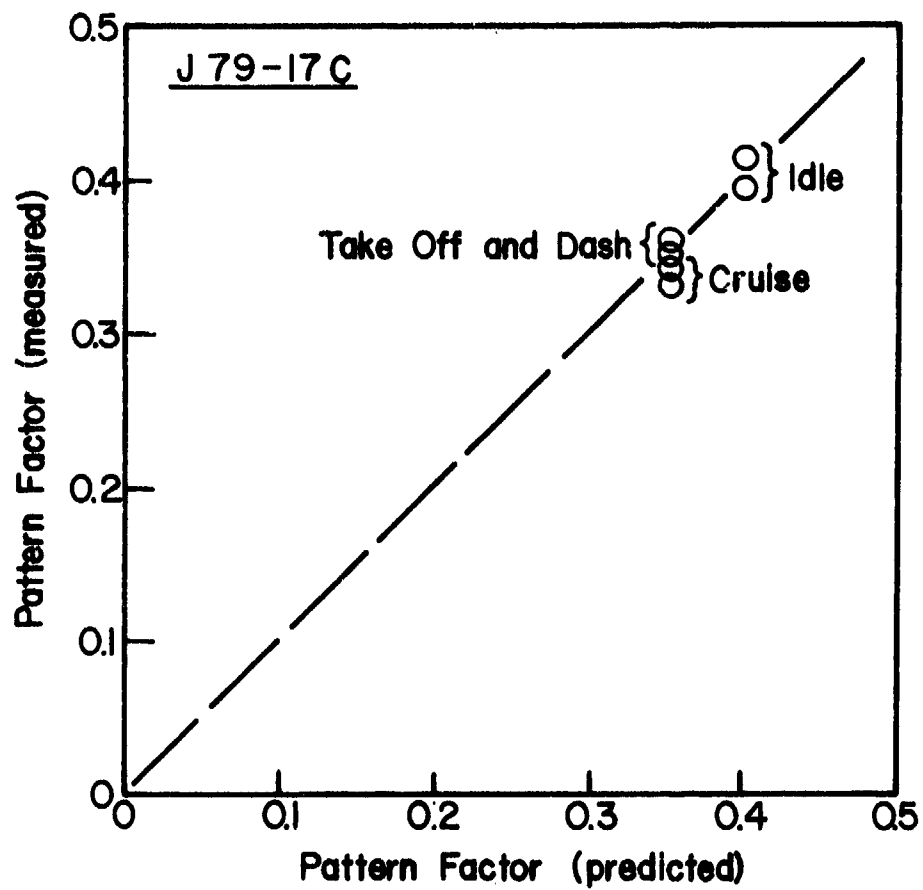


Figure 73. Comparison of Measured and Predicted Values of Pattern Factor for J79-17C Combustor.

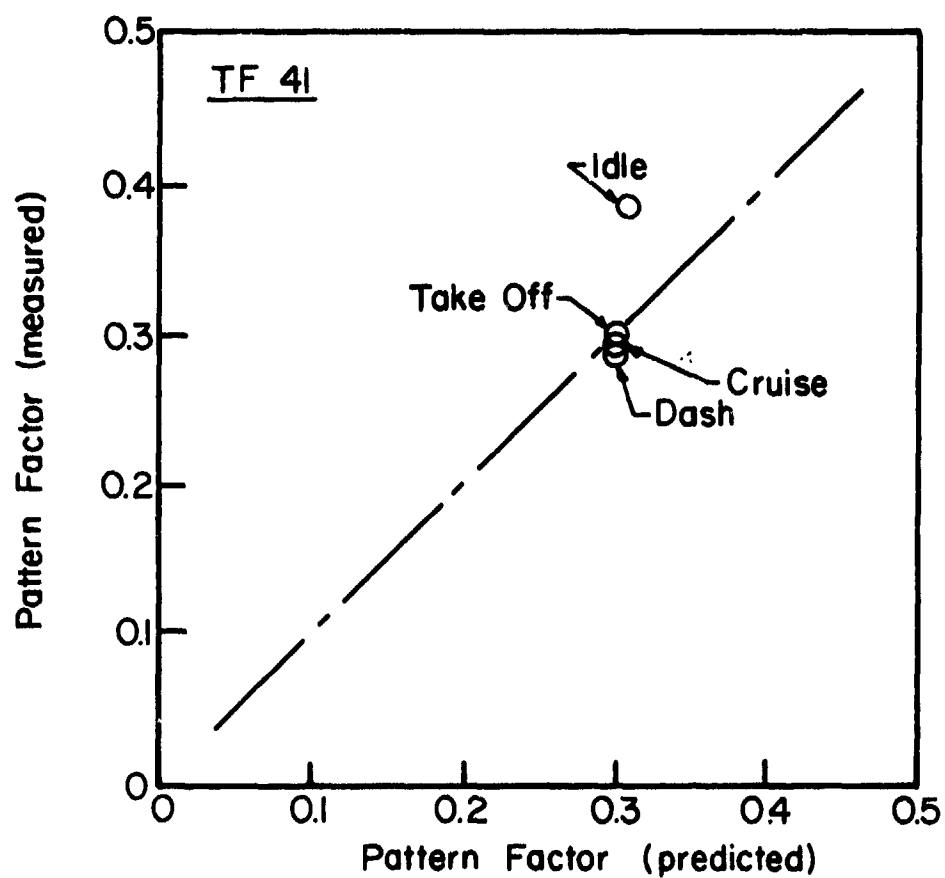


Figure 74. Comparison of Measured and Predicted Values of Pattern Factor for TF41 Combustor.

then a strong effect of fuel type on pattern factor should be expected.

The practical utility of Eq. (38) is that it allows the pattern factor at max power to be predicted from measurements of pattern factor carried out at reduced power, i.e. at cheaper and more convenient test conditions. It also demonstrates, as stated above, that at the highest combustion pressures where heat flux rates to nozzle guide vanes and turbine blades attain their maximum values, the influence of fuel type on pattern factor is negligibly small.

SECTION IX

DISCUSSION AND SUMMARY

Analysis of the key processes occurring within gas turbine combustors, along with examination of the experimental data contained in references 1 thru 6, shows that although the impact of fuel type on combustion performance and liner durability is usually small in comparison with the effects of liner geometry and combustor operating conditions, it is nevertheless of sufficient magnitude to warrant serious consideration. For some performance parameters, such as liner wall temperature and exhaust smoke, it is found that fuel chemistry plays an important role. For others, the effects of fuel type are manifested through the physical properties that govern atomization quality and evaporation rates.

In the following sections the effects of liner size, liner pressure drop, combustor operating conditions, and fuel type on various aspects of combustion performance are reviewed briefly in turn.

1. Combustion Efficiency

From analysis of the experimental data contained in references 1 thru 6 it is found that combustion efficiency is obtained as the product of the θ efficiency, η_{c_θ} , and the evaporation efficiency, η_{c_e} , i.e.

$$\eta_c = \eta_{c_\theta} \times \eta_{c_e} \quad (7)$$

$$\text{where } \eta_{c_\theta} = 1 - \exp \left[\frac{-0.022 p_3^{1.3} V_c \exp(T_c/400)}{f_c \dot{m}_A} \right] \quad (8)$$

$$\text{and } \eta_{c_e} = 1 - \exp \left[\frac{-36 \times 10^3 P_3 V_c \lambda_{eff}}{T_c D_o^2 f_c \dot{m}_A} \right] \quad (9)$$

In common with other loading parameters for the correlation of combustion-efficiency data, Eqs. (8) and (9) show that combustion efficiency is enhanced by increases in gas pressure, inlet air temperature, and combustion volume. Equation (9) also demonstrates the adverse effect of low fuel volatility on combustion efficiency, especially at operating conditions where atomization quality is relatively poor. This, of course, is well known from practical experience, but the main attribute of Eq. (9) lies in the direct quantitative relationships it provides between atomization quality (via SMD), fuel volatility (via λ_{eff}), and combustion efficiency, which allow the effect on combustion efficiency of any change in fuel type or fuel nozzle characteristics to be readily estimated.

2. Lean Blowout

Weak extinction values of fuel/air ratio are obtained as

$$q_{LBO} = A \left[\frac{f_{pz}}{V_c} \right] \left[\frac{\dot{m}_A}{P_3^{1.3} \exp(T_3/300)} \right] \left[\frac{D_o^2}{\lambda_{eff}^{LCV}} \right] \left[\frac{D_o \text{ at } T_F}{D_o \text{ at } 277.5K} \right]^2 \text{ g/kg} \quad (16)$$

In this equation it is of interest to note that the dependence of weak extinction limits on combustor volume and operating conditions is very similar to that for combustion efficiency.

Also in common with combustion efficiency is the slight effect of fuel chemistry (via LCV), whereas physical properties are important due to their influence on D_o and λ_{eff} .

The reasonable degree of similarity between the values Af_{pz} listed in Table 2 for several different types of combustors, suggests that prospects are good for predicting, within close and acceptable limits, the lean blowout limits of future combustor designs. It should also serve to encourage further experimental and analytical efforts in this area.

3. Lean Lightup

The equation for lean lightup fuel/air ratio is almost identical to that for lean blowout fuel/air ratio, except for a slightly stronger dependence on P_3 . We have

$$q_{LLO} = B \left[\frac{f_{pz}}{V_c} \right] \left[\frac{\dot{m}_A}{P_3^{1.5} \exp(T_3/300)} \right] \left[\frac{D_o^2}{\lambda_{eff}^{LCV}} \right] \left[\frac{D_o \text{ at } T_F}{D_o \text{ at } 277.5K} \right]^2 \text{ g/kg} \quad (17)$$

The very satisfactory correlation of ignition data provided by Eq. (17) demonstrates the important role played by the atomization process in providing an adequate concentration of fuel vapor in the spark region. This equation also provides useful quantitative relationships between fuel volatility (B or λ_{eff}), atomization quality (D_o), operating conditions (P_3 , T_3 , and \dot{m}_A), and combustion volume (V_c). Thus, for example, it can be used to estimate the increase in combustor volume and/or improvement in atomization quality needed to recover the loss in altitude relight capability caused by changing the fuel to one of lower

volatility.

Despite the well-known inconsistencies that tend to plague ignition data, the values of Bf_{pz} listed in Table 2 do not exhibit appreciable scatter. In fact, they are consistent to within a few percent for the four combustors featuring pressure atomizers; namely, the J79-17A, J79-17C, TF39, and J85. (Note that although the J79-17C nozzle is a hybrid type, at lightup most of the fuel issues from the primary which is a pressure swirl atomizer). These results may be regarded therefore as representing useful progress towards establishing accurate prediction formulae for lean lightoff limits.

4. Liner Wall Temperature

The most important factor governing liner wall temperature is the combustor inlet temperature, T_3 . Inlet pressure is also significant due to its influence on the concentration of soot particles in the flame, and hence on the magnitude of the luminous radiation flux to the liner wall. At max power conditions, where liner wall temperatures are of most concern, evaporation rates are so high that the physical properties of the fuel appear to have a negligible influence on T_w . Chemical effects are also quite small, as shown in Figs. 38 thru 41. However, even small increases in maximum values of liner wall temperature can seriously curtail liner life. Thus, for the range of fuels covered in this investigation, fuel type must be considered of significance to liner durability.

In the calculation of liner wall temperatures, the effect of fuel type can be accommodated quite conveniently by introducing the fuel hydrogen content into the existing equation for gas emissivity. This approach leads to the following equation for ϵ_g .

$$\epsilon_g = 1 - \exp \left[- 97440 P_3 (\%H_2)^{-2} (q_{1b})^{0.5} T_g^{-1.5} \right] \quad (26)$$

5. NO_x Emissions

It is found that NO_x emissions are very dependent on combustor operating conditions, and also on the size of the combustion zone which governs the time available for NO_x formation. The key factor controlling NO_x is the stoichiometric flame temperature which, in turn, is almost solely dependent on combustor inlet temperature. As far as fuel type is concerned, physical properties are of little consequence except at low power conditions where NO_x emissions are always quite small due to the correspondingly low values of T_{st} . Fuel chemistry also has little influence on NO_x because it affects only slightly the values of bulk gas temperature and stoichiometric flame temperature in the following equation for NO_x.

$$NO_x = \frac{9 \times 10^{-8} P_3^{1.25} V_c \exp(0.01 T_{st})}{m_A T_{pz}} \text{ g/kg} \quad (27)$$

6. CO Emissions

These are correlated by the expression: -

$$CO = \frac{86 m_A T_{pz} \exp(-0.00345 T_{pz})}{\left[V_c - 0.55 \times 10^{-6} \frac{f_{pz} m_A}{\rho_{pz}} \frac{D_o^2}{\lambda_{eff}} \right] \left[\frac{\Delta P_L}{P_3} \right]^{0.5} P_3^{1.5}} \text{ g/kg} \quad (28)$$

Combustor size and operating conditions also play a prominent role in determining the level of CO emissions. Special importance is attached to inlet temperature and primary-zone fuel/air ratio, due to their combined effect in resolving the primary-zone temperature. As in the case of NO_x emissions, the influence of fuel chemistry is small and is manifested through slight variations in T_{pz} with changes in lower calorific value. However, since CO emissions attain their maximum values at low power conditions, where a significant proportion of the total residence time in the combustion zone is occupied by the evaporation process, the influence of those physical properties which affect evaporation rates becomes important.

7. Unburned Hydrocarbons

It is found that the factors which govern CO emissions also influence UHC emissions, and in much the same manner, except for a slightly higher dependence on inlet air pressure and liner wall pressure drop. We have

$$\text{UHC} = \frac{11,764 \dot{m}_A T_{pz} \exp(-0.00345 T_{pz})}{\left[v_c - 0.55 \times 10^{-6} \frac{f_{pz} \dot{m}_A}{\rho_{pz}} \frac{D_o^2}{\lambda_{eff}} \right] \left[\frac{\Delta P_L}{P_3} \right] P_3^{2.5}} \text{ g/kg} \quad (30)$$

8. Smoke

Of all the parameters studied, smoke emissions is the one that is most affected by changes in fuel type. The physical properties of the fuel are important insofar as they influence the mean drop size in the spray and the penetration of the spray across the combustion zone. Spray penetration is of considerable

importance from a smoke viewpoint because inadequate penetration leads to enhanced fuel enrichment of the soot-forming regions just downstream of the fuel injector. Smoke emissions are also strongly dependent on engine operating conditions and primary-zone fuel/air ratio, as indicated by the following equation for exhaust soot concentration.

$$X_c = \frac{C_3 P_{3pz}^2}{f_{pz} m_A T_{pz}} \left[1 - \frac{C_4}{q_{sz}} \exp(0.0011 T_{sz}) \right] [18 - \%H_2]^{1.5} \text{ mg/kg} \quad (34)$$

Although the correlations achieved, as illustrated in Figs. 64 thru 71, show appreciable scatter, it is considered that Eq. (34) could prove very useful for predicting the effects of changes in operating conditions and fuel type on exhaust smoke levels.

9. Pattern Factor

This is described with good accuracy by the following equation

$$\frac{T_{\max} - T_4}{T_4 - T_3} = 1 - \exp \left[- Z \left[\frac{\Delta P_L}{q_{\text{ref}}} \right] \left[\frac{L_L}{D_L} - \frac{0.33 \times 10^{-6} m_{A D_o}^2}{\rho_g A_L D_L \lambda_{\text{eff}}} \right] \right]^{-1} \quad (38)$$

where appropriate values of Z are 0.070 and 0.050 for tubo-annular and annular combustors, respectively. The above equation shows that the main parameters controlling pattern factor are the pressure drop across the liner wall and the liner L/D ratio. It also takes into account the influence of evaporation time in reducing the time available for mixing within the liner. At the high pressure conditions where pattern factor is of most concern, the evaporation time is always quite short in comparison to the

total residence time of the combustor, and so the dependence of pattern factor on fuel type is fairly small.

At lower power settings, the evaporation time increases due to increase in D_0 and reduction in λ_{eff} . This produces a deterioration in pattern factor as indicated by Eq. (38) and also by Figs. 72 thru 74, which demonstrate for all engines that pattern factor at idle is distinctly worse than at take-off. These considerations highlight the importance of measuring pattern factor only at the correct combustor inlet conditions corresponding to engine operation at max power. Tests carried out at lower pressure levels give values that are overpessimistic. Also, they show a dependence of pattern factor on fuel type which greatly exaggerates the dependence actually observed at high pressures.

SECTION X

CONCLUSIONS

1. The fuels' physical properties that govern atomization quality and evaporation rates strongly affect combustion efficiency, weak extinction limits, and lean lightoff limits. The influence of fuel chemistry on these performance parameters is quite small and stems from the effects of slight variations in lower calorific value on combustion temperature.
2. For any given combustor and fuel type, Eq. (7) enables values of combustion efficiency to be calculated a priori at any stipulated combustor operating conditions.
3. The effects of changes in fuel type, liner airflow distribution, and engine operating conditions on lean blowout and lean lightup limits may be estimated with good accuracy from Eqs. (16) and (17), respectively.
4. Liner wall temperatures are controlled mainly by combustor operating conditions and combustor design, with fuel effects playing a minor role. However, since in modern high pressure ratio engines the combustor is called upon to perform satisfactorily for long periods at extreme conditions on current fuels, it follows that any factor, however secondary, that creates a more adverse combustion environment, will have a large and disproportionate effect on combustion performance and liner durability.

Analysis of the experimental data, which cover a range of

fuel types from JP4 to DF2, shows that fuel chemistry, as indicated by hydrogen content, has a significant effect on flame emissivity, flame radiation, and liner wall temperature.

5. The influence of fuel chemistry on the emissions of carbon monoxide, unburned hydrocarbons, and oxides of nitrogen is quite small. The fuels' physical qualities affect the exhaust gas concentrations of both carbon monoxide and unburned hydrocarbons at low power settings where fuel evaporation rates are relatively low. However, at the high power conditions where the emissions of carbon monoxide and unburned hydrocarbons become negligibly small, the influence of physical properties on these emissions is negligibly small.
6. Smoke emissions are strongly dependent on combustion pressure, primary-zone fuel/air ratio, and the mode of fuel injection (dual-orifice or airblast). Fuel chemistry, as indicated by hydrogen content, is also important. The data contained in references 1 thru 6 do not support the notion that multi-ring aromatics exhibit stronger smoking tendencies than single-ring aromatics.
7. Fuel chemistry has no direct influence on pattern factor. However, physical properties have an effect that is appreciable at low power conditions but which diminishes in importance with increase in engine power, becoming very small at the highest power setting, where the durability of

hot section components is a major concern.

8. Values of pattern factor measured at convenient low power conditions, may be inserted into Eq. (38) and used to predict the pattern factor attainable at max. power conditions.

SECTION XI

REFERENCES

1. Gleason, C. C., T. L. Oller, M. W. Shayeson and D. W. Bahr, Evaluation of Fuel Character Effects on J79 Engine Combustion System, AFAPL-TR-2018, June 1979.
2. Gleason, C. C., T. L. Oller, M. W. Shayeson and D. W. Bahr, Evaluation of Fuel Character Effects on F101 Engine Combustor System, AFAPL-TR-79-2018, June 1979.
3. Vogel, R. E., D. L. Troth and A. J. Verdouw, Fuel Character Effects on Current High Pressure Ratio, Can-Type Turbine Combustion Systems, AFAPL-TR-79-2072, April 1980.
4. Gleason, C. C., T. L. Oller, M. W. Shayeson and M. J. Kenworthy, Evaluation of Fuel Character Effects on J79 Smokeless Combustor, AFWAL-TR-80-2092, November 1980.
5. Oller, T. L., C. C. Gleason, M. J. Kenworthy, J. D. Cohen, and D. W. Bahr, Fuel Mainburner/Turbine Effects, AFWAL-TR-81-2100, May 1982.
6. Russel, P. L., Fuel Mainburner/Turbine Effects, AFWAL-TR-81-2081, Sept. 1982.

7. Lefebvre, A. H., Fuel Effects on Gas Turbine Combustion, AFWAL-TR-83-2004, 1984.
8. Lefebvre, A. H., Fuel Effects on Gas Turbine Combustion-Ignition, Stability, and Combustion Efficiency presented at 29th ASME International Gas Turbine Conference, Amsterdam, June 1984. To be published in ASME J. Eng. Power.
9. Lefebvre, A. H., Fuel Effects on Gas Turbine Combustion-Liner Temperature, Pattern Factor and Pollutant Emissions, AIAA Journal of Aircraft, Vol. 21, No. 11, pp. 887-898, November 1984.
10. Lefebvre, A. H., Gas Turbine Combustion, McGraw Hill, 1983.
11. Dobbins, R. A., L. Crocco, and I. Glassman, Measurement of Mean Particle Sizes of Sprays from Diffractively Scattered Light, AIAA J., Vol. 1, no. 8, pp. 1882-1886, 1963.

12. Lorenzetto, G. E., and
A. H. Lefebvre,
Measurements of Drop Size on
a Plain Jet Airblast Atomizer,
AIAA J., vol. 15. no. 7, pp.
1006-1010, 1977.
13. Roberts, J. M. and
M. J. Webb,
Measurement of Droplet Size
for Wide Range Particle Dis-
tribution, AIAA J., vol. 2,
no. 3, pp. 583-585, 1964.
14. Chin, J. S. and
A. H. Lefebvre,
Effective Values of Evapora-
tion Constant for Hydrocarbon
Fuel Drops, Proceedings of
the Twentieth Automotive
Technology Development Con-
tractors Coordination Meeting,
pp. 325-331, 1983.
15. Ballal, D. R. and
A. H. Lefebvre,
Weak Extinction Limits of Tur-
bulent Flowing Mixtures, Trans.
ASME. J. Eng. Power, Vol. 101,
No. 3, pp. 343-348, 1979.
16. Lefebvre, A. H.,
An Evaporation Model for
Quenching Distance and Mini-
mum Ignition Energy in Liquid
Fuel Sprays, Paper presented
at Fall Meeting of Combustion
Institute (Eastern Section),
1977.

17. Ballal, D. R. and
A. H. Lefebvre,
General Model of Spark Ignition for Gaseous and Liquid Fuel/Air Mixtures, Eighteenth Symposium (International) on Combustion, pp. 1737-1746, 1981.
18. Lefebvre, A. H. and
M. V. Herbert,
Heat-Transfer Processes in Gas-Turbine Combustion Chambers, Proc. Inst. Mech. Engrs., Vol. 174, No. 12, pp. 463-473, 1960.
19. Fletcher, R. S. and
J. B. Heywood,
A Model for Nitric Oxide Emissions from Aircraft Gas Turbine Engines, AIAA Paper No. 71-123.
20. Mosier, S. A. and
R. Roberts,
Development and Verification of an Analytical Model for Predicting Emissions from Gas Turbine Engine Combustors during Low Power Operation, AGARD CP-125, 1973.
21. Roberts, R., L. D. Aceto,
R. Kollrack, D. P. Teixeira
An Analytical Model for Nitric Oxide Formation in a Gas Tur-

- and J. M. Bonnell,
bine Combustor, AIAA Journal,
Vol. 10, No. 6, pp. 820-826,
1972.
22. Mador, R. J. and
R. Roberts,
A Pollutant Emission Prediction Model for Gas Turbine Combustors, AIAA Paper No. 74-1113, 1974.
23. Edelman, R., and
C. Economos,
A Mathematical Model for the Jet Engine Combustion Pollutant Emissions AIAA Paper No. 71-74, 1971.
24. Swithenbank, J.,
A. Turan, and P. G. Felton,
Three-Dimensional, Two Phase Mathematical Modeling of Gas Turbine Combustors, Gas Turbine Combustor Design Problems, Hemisphere, pp. 249-314, 1980.
25. Pratt, D. T.,
Coalescence/Dispersion Modeling of Gas Turbine Combustors, Gas Turbine Combustor Design Problems, Hemisphere, pp. 315-330, 1980.
26. Hung, W. S. Y.,
Accurate Method of Predicting the Effect of Humidity on Injected Water on NO_x

- Emissions from Industrial Gas
Turbines, ASME Paper No.
74-WA/GT-6, 1974.
27. Hung, W. S. Y., An Experimentally Verified
 No_x Emission Model for
 Gas Turbine Combustors, ASME
 Paper No. 75-GT-71, 1975.
28. Fletcher, R. S., The Control of Oxides of
 R. D. Siegel and Nitrogen Emissions from Air-
 E. K. Bastress, craft Gas Turbine Engines,
 NREC 1162, FAA-RD-71-111,
 Vols I, II, and III,
 Northern Research and
 Engineering Corp.,
 Cambridge, MA, 1971.
29. Hammond, D. C. (Jr.) Analytical Predictions of
 and A. M. Mellor, Emissions from and within an
 Allison J-33 Combustor, Combustion
 Science and Technology,
 Vol. 6, No. 5, pp. 279-286, 1973.
30. Mellor, A. M., Semi-Empirical Correlations
 for Gas Turbine Emissions,
 Ignition, and Flame Stabiliza-
 tion, Prog. Energy Combust.
 Sci., Vol. 6, pp. 347-358, 1981.

31. Graham, S. C.,
J. B. Homer and
J. L. J. Rosenfeld,
The Formation and Coagulation
of Soot Aerosols Generated by
the Pyrolysis of Aromatic
Hydrocarbons, Proc. Roy. Soc.
London A, Vol. 344, pp.
259-285, 1978.
32. Graham, S. C.,
J. B. Homer and
J. L. J. Rosenfeld,
The Formation and Coagulation
of Soot Aerosols, Int. Shock
Tube Symposium, 10th Proceedings,
pp. 621-631, July 1975.
33. Blazowski, W. S.,
Dependence of Soot Production
on Fuel Blend Characteristics
and Combustion Conditions, J.
Eng. Power, Vol. 102, pp.
403-408, April 1980.
34. Naegeli, D. W. and
C. A. Moses,
Effect of Fuel Molecular
Structure on Soot Formation
in Gas Turbine Engines, ASME
Gas Turbine Conference, New
Orleans, Paper 80-GT-62.
35. Shaffernocker, W. M.
and Stanforth, C. M.,
Smoke Measurement Techniques,
SAE Paper C80346, 1968.
36. Holderness, F. H. and
J. J. Macfarlane,
Soot Formation in Rich Kero-
sine Flames at High Pressure,

Paper No. 18, Atmospheric
Pollution by Aircraft Engines,
AGARD CP-125, Advisory Group
for Aerospace Research and
Development, 1973.

LIST OF SYMBOLS

A, B	constants in Eqs. (16) and (17), respectively
A_{an}	combustor annulus area, m^2
A_L	liner cross-sectional area, m^2
C_1	heat flux from combustion gases to liner by convection, W/m^2
C_2	heat flux from liner wall to annulus air by convection, W/m^2
C_3, C_4	constants in Eq. (34)
D_{an}	hydraulic mean diameter of combustor annulus, m
D_h	hydraulic mean diameter of atomizer air duct at exit plane, μm
D_L	liner diameter or height, m
D_o	initial mean drop size of fuel spray, μm
D_p	atomizer prefilmer diameter, m
f_c	fraction of total combustor air employed in combustion
f_{pz}	fraction of total combustor air employed in primary-zone combustion
f_f	fraction of fuel vaporized within combustion zone
k	thermal conductivity, J/ms K
L	length, or luminosity factor
L_c	length of combustion zone, m
L_e	liner length employed in fuel evaporation, m
L_L	total liner length, m
LCV	lower calorific value of fuel, MJ/kg
l_b	mean beam length of radiation path, m
m	mass flow rate, kg/s

n	reaction order
P	pressure, kPa
ΔP	pressure differential, kPa
$(\Delta P_L/P_3)$	liner pressure drop as percentage of P_3
q	fuel/air ratio
q_c	fuel/air ratio in combustion zone
q_{ov}	combustor overall fuel/air ratio
q_{ref}	reference dynamic head, kPa
q_{LBO}	fuel/air ratio at lean blowout, g fuel/kg air
q_{LLO}	fuel/air ratio at lean lightup, g fuel/kg air
R_1	radiation heat flux from combustion gases to liner wall, W/m^2
R_2	radiation heat flux from liner to casing, W/m^2
SMD	Sauter mean diameter of fuel spray, μm
SN	smoke number
T	temperature, K
T_{bn}	boiling temperature at normal atmospheric pressure, K
ΔT	temperature rise, K
U	velocity, m/s
V_c	total combustion zone volume (=predilution zone volume), m^3
V_e	evaporation volume, m^3
V_{pz}	primary zone volume, m^3
X_c	soot concentration, mg/kg gas
Z	constant in Eq. (38)
ϵ	emissivity
σ	Stefan-Boltzmann constant ($5.67 \times 10^{-8} W/m^2 K$), or surface tension, kg/s^2

μ	dynamic viscosity, kg/ms
ν	kinematic viscosity, m^2/s
λ_{eff}	effective value of evaporation constant, mm^2/s
η_c	combustion efficiency
$\eta_{c\theta}$	combustion efficiency based on chemical kinetics
η_{ce}	combustion efficiency based on fuel evaporation
ρ	density, kg/m^3

Subscripts

A	air
F	fuel
g	gas
ad	adiabatic value
st	stoichiometric value
c	combustion zone value
an	annulus value
pz	primary zone value
sz	secondary zone value
max	maximum value
w	wall value
3	combustor inlet value
4	combustor outlet value
8	engine discharge value
L	liner value